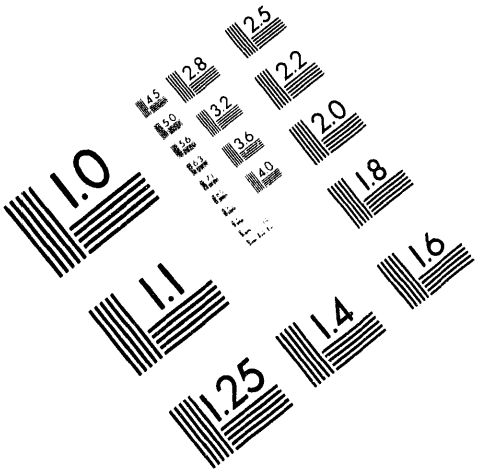

Association for Information and Image Management
1100 Wayne Avenue, Suite 1100
Silver Spring, Maryland 20910
301/587-8202

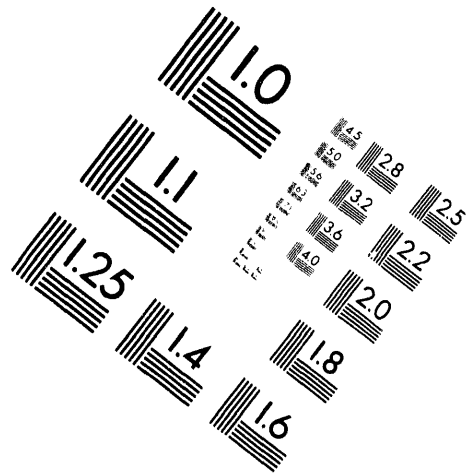

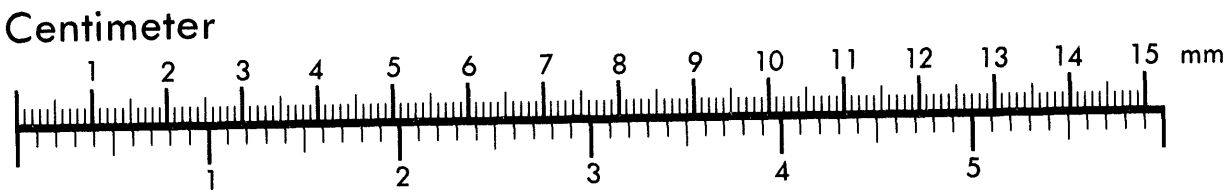

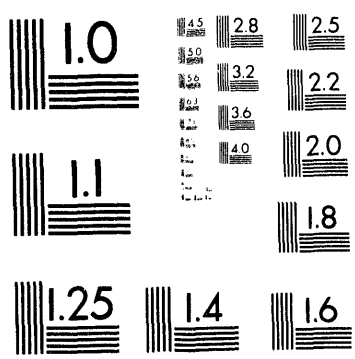

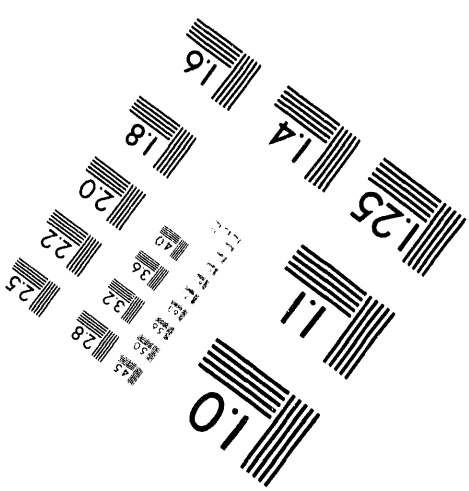

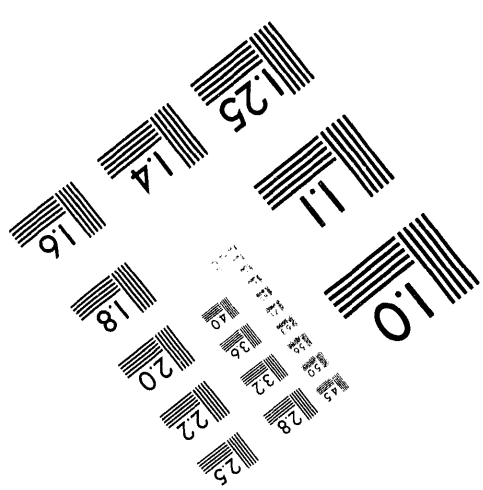

MANUFACTURED TO AIIM STANDARDS
BY APPLIED IMAGE, INC.

1 of 1

DOE/MWIP-15

Surrogate Formulations for Thermal Treatment of Low-Level Mixed Waste, Part I: Radiological Surrogates

TTP OR132015
B&R Code EW4020

J. A. D. Stockdale
W. D. Bostick
D. P. Hoffman
Martin Marietta Energy Systems, Inc.
Oak Ridge, Tennessee

Hom-Ti Lee
Oak Ridge Associated Universities
Oak Ridge, Tennessee
under subcontract 19KAGB85Z

Prepared for the
Mixed Waste Integrated Program
U.S. DEPARTMENT OF ENERGY
Office of Technology Development
Washington, D.C. 20585

January 1994

Prepared by
OAK RIDGE K-25 SITE
Oak Ridge, Tennessee 37831-7274
managed by
MARTIN MARIETTA ENERGY SYSTEMS, INC.
for the
U.S. DEPARTMENT OF ENERGY
under contract DE-AC05-84OR21400

CONTENTS

FIGURES

TABLES

ABBREVIATIONS AND ACRONYMS

DOE	U.S. Department of Energy
EPA	U.S. Environmental Protection Agency
IRF	Incinerator Research Facility
IWGFR	International Working Group on Fast Reactors
K	degrees kelvin
LLNL	Lawrence Livermore National Laboratory
MWIP	Mixed Waste Integrated Program
PCB	polychlorinated biphenyl
PVC	polyvinyl chloride
RCRA	Resource Conservation and Recovery Act of 1976
SCWO	supercritical water oxidation process
YAG	yttrium-aluminum-garnet (laser)

ACKNOWLEDGMENTS

The authors thank W. D. Bond, T. C. Ho, J. R. Peterson, and J. M. Leitnaker for their careful reading of this manuscript and their suggestions. We thank J. Chiang for providing Table 6. We are also indebted to J. Shor, G. D. Del Cul, and J. Ferrada for information and suggestions. We wish especially to thank B. Ebbinghaus and O. Krikorian for communicating their data on the oxyhydroxides of uranium and plutonium before publication.

EXECUTIVE SUMMARY

The evaluation and comparison of proposed thermal treatment systems for mixed wastes can be expedited by tests in which the radioactive components of the wastes are replaced by surrogate materials chosen to mimic, as far as is possible, the chemical and physical properties of the radioactive materials of concern. In this work, sponsored by the Mixed Waste Integrated Project of the U.S. Department of Energy, we have examined reported experience with such surrogates and suggest a simplified standard list of materials for use in tests of thermal treatment systems.

The chief radioactive nuclides of concern in the treatment of mixed wastes are ^{239}Pu, ^{238}U, ^{235}U, ^{137}Cs, ^{103}Ru, ^{99}Tc, and ^{90}Sr. These nuclides are largely by-products of uranium enrichment, reactor fuel reprocessing, and weapons program activities. Cs, Ru, and Sr all have stable isotopes that can be used as perfect surrogates for the radioactive forms. Technetium exists only in radioactive form, as do plutonium and uranium. If we wish to preclude radioactive contamination of the thermal treatment system under trial burn, surrogate elements must be chosen for these three. For technetium, we suggest the use of natural ruthenium, and for both plutonium and uranium, we recommend cerium. The seven radionuclides listed can therefore be simulated by a surrogate package containing stable isotopes of ruthenium, strontium, cesium, and cerium.

1. INTRODUCTION

The various U.S. Department of Energy (DOE) research and development sites have accumulated quantities of waste that contain both radioactive elements and other toxic compounds such as hazardous organics and toxic metals, as well as other more innocuous materials. These wastes are known as "mixed wastes." DOE's EM-50 "Mixed Waste Integrated Program" (MWIP) seeks a rationale for safe treatment or disposal of this mixed waste.

An ultimate aim of the waste disposal process is to release the host organization from the expensive responsibilities of containing and safely storing the waste. The disposal of radioactive and toxic substances is regulated by federal and state laws and must be carried out in accordance with these legal requirements. The requirements for ultimate disposal of certain wastes are still in the process of being formulated. This is particularly the case for high-level radioactive waste.

Existing mixed wastes are in various forms.[1] The containment of these wastes is a dynamic situation, with many wastes stored in metal drums or tanks that may be subject to corrosion. While the legal situation for ultimate disposal evolves, it is prudent to consider means for reducing the volume of stored mixed waste and the risk associated with storing it. To be useful, treatment processes need to meet certain requirements as well as comply with legal emission limits.

The treatment system must be an economic one. That is, a system that adds to the ultimate cost of disposal is pointless. A system that succeeds in transforming toxic waste to a "safer" form is not necessarily desirable if its cost exceeds the total life cycle cost of safely storing the existing waste. Treatment systems generally aim at retaining and encapsulating long-lived radioactive elements in a physically stable glassy matrix that meets the leach tests mandated for long-term storage of such material by the regulations of the U.S. Environmental Protection Agency (EPA). If mixed wastes contain valuable metals, it may be desirable to provide means for their recovery as an integral part of the treatment process.

2. THERMAL TREATMENT

Thermal treatment involves heating mixed wastes in an attempt to reduce their volume, to bind and enhance retention of toxic substances, and possibly to recover valuable resources. Frequently, the heating is accompanied by chemical reactions, such as oxidation, which may result in the destruction of toxic organic compounds. Less desirable outcomes such as the generation of nitrogen oxides or the conversion of toxic inorganic materials to more volatile forms may also occur. In addition, complications can arise when the waste containers are themselves directly involved in the reaction processes. For instance, uranium-iron eutectic mixtures formed by the melting of steel containers could result in uranium vapor pressures different from those over the pure metal.

A number of thermal treatment systems are in active development. They include microwave and Joule-heating systems, rotary-kiln and fluidized-bed reactors, and fixed-hearth and centrifugal plasma-arc systems.[2] Within each of these categories, individual systems can vary widely from one another in the range of operating conditions in the primary combustion chamber, and in the nature of the air pollution control systems required to ensure compliance with the legally regulated emission limits. Systems can often be operated in either a reducing or an oxidizing mode, and several key temperatures may need to be considered within a single system. The internal temperature of a plasma arc can be as high as 10,000–15,000 K, though the melt temperature in the primary chamber is usually ~ 1500 K.[3] Temperatures in fluidized-bed and rotary-kiln incinerators are likely to be in the 1000–1500 K region.[4] Examples of thermal treatment systems include the Toxic Substances Control Act (TSCA) rotary-kiln incinerator at the Oak Ridge, Tennessee, K-25 Site, DOE's only permitted system for burning of organic mixed wastes;[5] the fluidized-bed incinerator at the Rocky Flats Plant in Colorado;[6] the fixed-hearth plasma-arc system at the Retech, Inc., facility in Ukiah, California;[7] and the centrifugal plasma-arc systems in Butte, Montana, and Basel, Switzerland.[8]

3. SURROGATE WASTE PACKAGES

Thermal treatment systems larger than lab scale represent major investments. Both to protect this investment and to ensure that emissions during the testing phase do not exceed mandated levels, it is desirable to use simulated waste packages that mimic, as closely as possible, the physical and chemical properties of the actual wastes. These "surrogate" waste packages should be of minimum toxicity, inexpensive, easily handled and fed to the system, and composed of ingredients that are readily obtainable and easily mixed. In addition, the ingredients should not react with one another in unforeseen ways, should be conveniently detectable, and should not alter flame temperatures or other operating conditions from those expected under actual treatment conditions. Last, the composition of the surrogate should be kept as simple as is consistent with the demands of the testing. Testing protocols must ensure minimum variation between surrogate feeds so that there is consistency within a series of tests on a specific thermal treatment system and consistency between tests on different systems.

3.1 REQUIREMENTS FOR ACCEPTABLE SURROGATES

Unfortunately, the surrogate requirements discussed in Sect. 3 are difficult to meet, even at the elemental level, except in the special case of certain radioactive nuclides of concern, where stable isotopes of the same element can provide a perfect surrogate. Examples of nuclides for which stable isotopes are available are ^{137}Cs, ^{90}Sr, and ^{131}I. Different elements have uniquely different chemical and physical properties, so for complete accuracy there can be no substitutions. The situation is further complicated by the degree of complexity likely to be encountered under actual treatment conditions, where many substances are present and the reaction conditions vary from point to point within the primary reaction chamber. A substance that is an excellent surrogate choice at one temperature may not mimic the chemical or physical properties of the waste at another. We have used an approach involving a chemical database and thermodynamic equilibrium calculations in which the Gibbs free energy of the system is minimized at a specific temperature. We have compared elements of most concern from the radioactive viewpoint with possible surrogate elements under simplified reaction conditions where thermodynamic equilibrium is assumed. While this is a reasonable first approach, many uncertainties exist. Actual thermal treatment conditions are expected to be very dynamic. Even if the feed is constant, thermodynamic equilibrium is only a limit, and may or may not be a good approximation depending on the nature of the reactions taking place and their rates. Reaction kinetics and particle formation within the primary chamber may be extremely important. A further difficulty involves the range of temperatures to be considered. Information on temperature distributions within incineration systems is scanty. For a system such as the plasma-arc, in which temperatures within the arc itself are known to be extremely high (10,000–15,000 K), we do not know what temperature is applicable to the primary burn: that is, to the volume in which the initial waste feed is being vaporized. Most likely it is high, but not as high as the arc temperature itself. In our comparisons, temperatures up to 5000 K have been considered. This is a reasonable but conservative approach since other thermal treatment systems such as the rotary kiln and fluidized bed operate at burn temperatures in the 1000–1500 K range. It should be noted that thermodynamic data for temperatures above ~2000 K are in short supply for many compounds. Predictions for higher temperatures, such as those shown in the higher-

temperature phase stability diagrams provided in the Appendix (Figs. 1-25 and 29-31), usually rely upon extrapolations.

In either the fixed-hearth or centrifugal plasma-arc geometry, the melt is exposed periodically to the plasma torch. On casting and solidification, the melt becomes the stable matrix binding the metallic isotopes of concern. The temperature cycling of the melt itself may therefore be important since the melt may also contribute significantly to the emissions from the primary chamber.

3.2 RADIOISOTOPES

The radioisotopes of chief interest are shown in Table 1, together with some potential surrogates. The radioisotopes ^{238}U, ^{235}U, and ^{239}Pu in DOE wastes are largely by-products of uranium enrichment, reactor fuel reprocessing, and weapons program activities. The fission products ^{99}Tc, ^{90}Sr, ^{103}Ru, and ^{137}Cs are long-lived isotopes from fission reactor fuel reprocessing. They are important because their radioactive half-lives are long and their atomic weights are located near the two chief fission yield peaks. They also have biological significance. Cesium is similar to sodium and potassium, and strontium is a "bone seeker" similar to calcium. Cesium, strontium, and ruthenium all have stable isotopes that can be used as perfect surrogates for the radioactive forms. Technetium exists only in radioactive form, as do plutonium and uranium. If we wish to preclude radioactive contamination of the thermal treatment system under trial burn, surrogate elements must be chosen for these three.

Table 1. Radiological/fission product surrogates

Radioisotope	Surrogate	Surrogate qualities
$^{238}U/^{235}U$	Mo	Ubiquitous; models volatility of oxides
	Pr	Unique, fluorescent; models volatility
^{99}Tc	Mn	Ubiquitous, similar chemistry; models volatility
	Re	Unique, similar chemistry; volatility uncertain
	Ru	Unique; models volatility
^{137}Cs	Natural Cs	Nonradioactive, nonhazardous
^{90}Sr	Natural Sr	Nonradioactive, nonhazardous
^{239}Pu	Ce	Unique; models volatility
^{103}Ru	Natural Ru	Unique; doubles as ^{99}Tc surrogate

Table 2 is taken from the report *Development and Use of Sintered Metal Filters with Fluidized Bed and Spray Calcination of Simulated High-Level Waste* by W. J. Bjorklund.[9] Bjorkland's report describes work done at Pacific Northwest Laboratories in Richland, Washington, in the mid 1970s. It is considered here as a good example of previous use of surrogates for radioactive materials. It also includes some discussion of surrogates for

radioactive Rb, Y, Re, Rh, and Pd and for the transuranics Np, Am, and Cm. We will not be concerned with these elements in the present report. Comments on surrogate cost are prominent in Table 2. We will return to this issue in Sect. 3.9.

Table 2. Chemical stand-ins used to simulate nonradioactive high-level waste

Waste constituent to be substituted	Reason for substitution	Substitute used[a]
Rb	Expense	K
Y and Re	Expensive to simulate fission product spectrum	Commercially available rare earth mixtures
Tc	No nonradioactive isotopes	Mo
Ru	Expense	Fe
Rh	Expense	Co
Pd	Expense	Ni
Cs[b]	Expense	K
U, Np, Pu, Am, and Cm	No nonradioactive isotopes	Rare earths

[a] Substitutes shown are those that have been used in the Waste Fixation Program at Pacific Northwest Laboratory.
[b] Substituted in engineering-scale tests only.

3.3 HSC CHEMISTRY AND PHASE STABILITY DIAGRAMS

The program HSC Chemistry®,[10] contains a large chemical database and algorithms for calculations of reaction outcomes, heat and material balances, equilibrium compositions, phase stability diagrams, and electrochemical equilibria. The title "HSC" stands for enthalpy (H), entropy (S), and heat capacity (C). The programs and database have been developed and improved during a period of 10 years by Antti Roine and collaborators at Outokumpu Research Oy in Finland. The version used here is the latest, Version 1.10 for Windows, dated January 1, 1993. We have used HSC Chemistry extensively in this report. It appears to be the most accessible of a number of available programs including the excellent F*A*C*T package available through the McGill University Computing Center.[11] We have obtained equivalent results using F*A*C*T and HSC for several calculations when input data and databases were the same. All calculations within either program yield thermodynamic equilibrium outcomes. HSC contains two databases, labeled "main" and "own." The user will normally add new or updated information, in the prescribed H, S, C format for a given temperature, to the "own" database. The program allots this precedence over information from the "main" database but searches both for all relevant input to a given calculation.

In searching for suitable surrogates for Tc, U, and Pu, we have generated phase stability diagrams for these elements and potential surrogates over the temperature range 1000–5000 K. Phase stability diagrams are convenient tools for general comparisons of chemical properties at temperatures likely to be encountered in thermal treatment of wastes. The phase stability diagrams generated by HSC Chemistry are two-dimensional plots for a specified reaction temperature that show the predicted main condensed chemical phases for the element in question as functions of the pressure (in atmospheres) of two reaction partners. In our work, we selected the reaction partners oxygen and chlorine, and oxygen and hydrogen. Most incinerator burns of mixed waste are expected to contain a certain fraction of halogen-containing material, such as polychlorinated biphenyls (PCBs), polyvinyl chloride (PVC), or the like, so the oxygen-chlorine case is an important one. Some incinerator systems contain large quantities of material that strongly binds halogens. This is the case in the Rocky Flats fluidized-bed incinerator, which contains a bed of sodium carbonate that will rapidly bind chlorine. In this case, the oxyhydroxides of refractory metals such as uranium and plutonium are thought to be the most volatile compounds at certain temperatures.[12] For this reason we have also run phase stability diagrams for the oxygen-hydrogen case if data are available. The axes of the diagrams generated for this report cover a much larger range than is employed in thermal treatment. Rather than narrow these ranges, we have retained, in most cases, the default HSC diagrams to illustrate chemical similarity over a wide parameter range.

For many elements, diagrams were generated for 1000, 2000, and 5000 K. For Tc, U, and Pu and for the most likely surrogate choices, phase stability diagrams were generated for 1000, 2000, 3000, 4000, and 5000 K. The candidate surrogates chosen for comparison are essentially based on choices that seemed reasonable from the periodic table. The elements of the lanthanide series are formed by successive filling of the inner 4f orbitals, while the actinides are formed by the filling of the 5f orbitals. The lanthanides thus show many chemical and physical similarities to the actinides, so we have concentrated on them in the search for surrogates for plutonium and uranium, while also including diagrams on the refractory metals molybdenum and tungsten for comparison with uranium. We generated Ru, Re, and Mn phase stability diagrams for comparison with Tc (stable Ru is likely to be present already as a surrogate for ^{103}Ru), and in line with Table 2, we have also considered Mo.

We emphasize that the nature of the calculated phase stability diagrams and the accuracy of comparisons drawn from them depend on the accuracy and comprehensiveness of the database. In addition, the species shown in the HSC phase stability diagrams are those for the condensed phase only. In the thermal treatment context, these diagrams are most relevant to predictions of the nature of the melt and to the composition of ash and other residuals rather than to the nature and composition of volatile emissions. In selecting surrogates, both residuals and volatile emissions are important. In Sect. 3.7 we discuss the question of volatility in more detail before turning to a final suggested list of surrogates.

3.4 SURROGATES FOR ^{99}Tc

Looking at the oxygen-chlorine phase stability diagrams for Tc (Figs. 1a-1e), and comparing them with those for Ru (Figs. 2a-2e), Re (Figs. 3a-3e), and Mn (Figs. 4a-4c), we can make the following comments:

- Tc_2O_7 is likely to be the dominant phase for reasonable oxygen concentrations and low chlorine concentrations.
- As the chlorine concentration increases, $TcCl_5$ will become increasingly important. The database contains no information on oxychlorides, which may also be important.
- The phase stability diagrams for Ru, Re, and Mn all show similarities to those for Tc. Ruthenium metal vapor is a more dominant phase at high temperatures than is the case for Tc or the others. At temperatures near 2000 K, rhenium is probably the best overall surrogate match to technetium. At higher temperatures, near 5000 K, ruthenium and rhenium each have advantages. If the quantity of oxygen and chlorine is relatively low in the burn, it is possible that the metal vapor phase would be dominant for technetium and ruthenium but that rhenium would be in oxide form (Re_2O_7). Manganese appears to be the worst overall match; though, for a reasonable range of operating conditions, particularly with low chlorine, a combination of manganese oxides would track Tc_2O_7 fairly well.
- Overall, rhenium appears to be the best match to the properties of technetium. However, if stable isotopes of ruthenium are added to any surrogate mixture as a surrogate for ^{103}Ru, it is probably desirable in the interest of simplicity to use stable ruthenium as the surrogate of choice for technetium also.
- The database contains no information on hydrides and oxyhydrides of Tc, Ru, Re, or Mn.

Table 2 suggests the use of molybdenum as a surrogate for technetium. If we compare Figs. 1a-1e for the Tc-O_2-Cl_2 system with Figs. 25a-25e for Mo-O_2-Cl_2, we see that data on technetium oxychlorides are lacking in the HSC database. Apart from this, similarities exist in the two sequences, with the oxides Tc_2O_7 and MoO_3 probably playing a dominant role. If molybdenum were chosen as a surrogate for uranium, perhaps an argument could be made for including it as the surrogate also for technetium. In Sect. 3.6, we argue against the selection of either tungsten or molybdenum as a surrogate for U based on the apparent comparative importance of the oxychloride phases for tungsten and molybdenum at higher temperatures, relative to the situation for uranium. Because of this, and because of the lack of oxychloride information for technetium, making a good comparison with molybdenum is difficult. Thus, using natural ruthenium as a surrogate for both ruthenium and technetium seems preferable to adding molybdenum as a surrogate for Tc. However, this situation could be influenced by cost considerations because molybdenum is much less expensive than ruthenium. Rhenium is an order of magnitude even more expensive. Later in this report, Sect. 3.9 and Table 6 provide some information on the cost issue.

3.5 SURROGATES FOR ^{239}Pu

The lanthanides have properties similar to those of the actinides in many ways. Bates has briefly discussed surrogates for U, Pu, and Am: "While there are no perfect surrogates for

these radionuclides, cerium is generally the most conservative (best simulates their behavior). Other less conservative surrogates of plutonium, in the degree of similarity to plutonium are: neodymium > lanthanum > praseodymium > gadolinium > ytterbium > dysprosium > erbium > europium > terbium > lutetium > samarium."[13] Cerium has been recently used as a surrogate for plutonium in waste treatment investigations employing the supercritical water oxidation process (SCWO). This study was performed at the Idaho National Engineering Laboratory by Shapiro, Garcia, and Bella.[14] Though their work applies to a much lower temperature regime than that encountered in most thermal treatment systems, we mention it here because it lends further credibility to the use of cerium as a surrogate for plutonium. Shapiro, Garcia, and Bella[14] concluded that cerium could be considered a reasonable surrogate for plutonium bearing in mind the following points:

- Cerium exhibits a similar chemistry in that much of its aqueous solution chemistry is similar to that of plutonium.
- Cerium exhibits an oxidation state different from that of plutonium, so it is not directly analogous.
- Cerium potentially can form the strongly oxidizing ceric ion in the SCWO process and enhance rapid corrosion of the reactor.
- Some of cerium's atomic characteristics do not perfectly match those of plutonium, though they are closer than those of other available surrogates.

Cerium has recently been used as a surrogate for plutonium to study various electrorefining parameters.[15] In this context, a comparative study of the physical and chemical properties of cerium and plutonium was carried out by Raraz, Mishra, and Averill.[16] They concluded, "The prominent similarities include the electronic structure, specific heat, standard electrode potential, electrical resistivity, thermodynamic stability of chlorides and oxychlorides, and volume expansion upon solidification. Melting and boiling points, thermal conductivity, density, viscosity, atomic weight, heat of fusion and coefficient of thermal expansion are the prominent dissimilarities that are likely to affect the electro-refining process."

Zirconium can also be an excellent surrogate for plutonium in the low-temperature range when water is present.[17] It readily hydrolyzes to form polymeric species containing both oxo- and hydroxy groups, just as plutonium does.

Figures 5a–5e are phase stability diagrams for the plutonium-oxygen-chlorine system, and Figs. 6a–6e are diagrams for the plutonium-oxygen-hydrogen system. Figures 7a–7e and 8a–8e correspondingly describe the cerium-oxygen-chlorine and cerium-oxygen-hydrogen systems from 1000 to 5000 K. It can be seen that a good match exists between oxygen-chlorine data for plutonium and cerium, with the exception that the oxychloride phase is missing in the cerium data. Polycrystalline CeOCl has recently been prepared by Del Cul in connection with Raman and luminescence studies of lanthanide oxyhalides,[18] but the thermodynamic data necessary for its inclusion in the HSC database have yet to be obtained. In the plutonium diagrams, the oxychloride phase becomes less important as the temperature increases. Its absence in the cerium output does not significantly change the fact that, on the basis of these diagrams, cerium appears to be an excellent surrogate for plutonium for most operating conditions.

The oxygen-hydrogen diagrams for plutonium and cerium are also essentially similar if allowance is made for the absence of the oxyhydroxide phase from the cerium database. This information has only recently become available for plutonium (and for uranium) due to the experiments of Krikorian and Ebbinghaus and their coworkers at LLNL.[19] These experiments were performed in support of the fluidized-bed incinerator at the Rocky Flats Plant. As mentioned previously, the Rocky Flats system contains sodium carbonate particles in the bed, resulting in low effective halogen concentrations. Under these circumstances, the oxyhydroxides are thought to be the most volatile compounds. In comparing the plutonium and cerium diagrams, allowance also needs to be made for the fact that PuH_2 and PuH_3 both appear, whereas only CeH_2 is shown. This also may be a deficiency of the database. Clearly, additional experimental data on cerium in connection with the oxyhydroxide, hydride, and oxychloride phases would be valuable. Nevertheless, cerium does appear to be a reasonable surrogate for plutonium.

For completeness, Figs. 9–21 show phase stability diagrams for the remaining lanthanides, Nd, La, Pr, Gd, Yb, Dy, Er, Eu, Tb, and Sm. For Nd, La, and Pr, the database contains some information on hydrides, so in these cases oxygen-hydrogen phase stability diagrams are included. Praseodymium and europium are perhaps more interesting to consider as components of a surrogate package than are the other lanthanides, with the exception of cerium, since europium fluoresces in the red and praseodymium in the green when exposed to ultraviolet light.[18] Use of one or both of these materials might permit easy tracking of "hold up" material in thermal treatment systems. The praseodymium phase stability diagrams, Figs. 13a–13e and 14a-14e, are very similar to those of cerium, and with the same provisos with respect to oxyhydroxide, hydride, and oxychloride data, are also similar to plutonium. A good case might thus be made for addition of praseodymium to a surrogate package provided that costs are not too high. Since observed fluorescence intensities for samples, taken say from the primary chamber after a trial burn, will depend both upon the praseodymium density and upon the nature of the sample (its transparency and the form of the bound praseodymium), a rational approach may be to include praseodymium together with cerium in one or two pretests to check the feasibility of the technique. Reference 18 presents a diagram of the "free" ion energy levels of the trivalent lanthanides. With ultraviolet excitation, say from the third harmonic of a pulsed yttrium-aluminum-garnet (YAG) laser (335 nm) or N_2 laser (337 nm), or from a mercury-xenon or mercury arc (various filtered wavelengths <400 nm), efficient conversion within the matrix to the characteristic atomic emissions is expected.[20] For praseodymium, the emission of interest is in a band from 454 to 476 nm, and for europium, it is in a band from ~ 670 to 780 nm.[21] We have recently attempted to observe green fluorescence from both black Pr_6O_{11} powder and pale green PrO_2 powder irradiated with near ultraviolet light (~ 250–390 nm) from a mercury arc and with 266-nm pulsed YAG fourth-harmonic laser light. We were unable to see any visible green fluorescence. The nature of the sample may be important, or perhaps observations more sensitive than those by the unaided eye are needed.

3.6 SURROGATES FOR URANIUM

Figures 22a–22e and 23a–23e are phase stability diagrams for the uranium-oxygen-chlorine and uranium-oxygen-hydrogen systems, respectively. The uranium oxyhydroxide data

supplied with the HSC Chemistry program have been updated by new measurements kindly supplied by the LLNL group.[19,22] When the uranium phase stability diagrams are compared with those for cerium (Figs. 7 and 8), qualitative similarities are evident. Differences also occur in that uranium shows a number of chlorides, whereas cerium shows only one; the oxychloride phase is absent in cerium as noted in Sect. 3.5. This phase appears to be relatively unimportant in uranium. The database contains no information on cerium oxyhydroxide.

Both molybdenum and tungsten have been suggested as surrogates for uranium. As metals, they are even more refractory than uranium. Figures 24 and 25 show phase stability diagrams for tungsten and molybdenum. These diagrams clearly show a major difference from those for uranium in that the oxychloride phase becomes dominant for both tungsten and molybdenum as the temperature increases. This is not the case for uranium, and suggests that tungsten or molybdenum may be a poor surrogate choice for uranium in systems such as the plasma-arc in which first-burn temperatures are likely to be high. Either cerium or praseodymium may be a better choice for such systems. It should also be mentioned that cerium has been used as a surrogate for uranium with some success recently in tests of the ambient temperature magnetic separation process. In this process, micron-sized particles of paramagnetic materials are removed from a slurry pumped through a strong inhomogeneous magnetic field.[23]

3.7 VOLATILITIES

Phase stability diagrams can provide a guide to incineration chemistry provided that the elements and temperatures chosen are the dominant ones and that the database contains complete and correct information. To ensure good choices of surrogates, compound volatilities should also be compared. Figures 5 and 7 indicate that PuO_2 and CeO_2 are important contributors to plutonium and cerium volatility at low chlorine and hydrogen concentrations.

Messier[24] has investigated the effusion of $PuO_{1.82}$ from a Knudsen cell in the temperature range from 2070 to 2380 K and has fitted the data to an analytical expression of the form

$$\log p = A - B/T,$$

where p is the vapor pressure in atmospheres, T is the temperature in degrees kelvin, and A and B are constants. Similar studies have been performed on CeO_2 by Ackermann and Rauh.[25] These results are plotted on an extrapolated temperature range using the program MathCad in Fig. 26. The curve P is that for $PuO_{1.8}$, and the curves Q and R are those for CeO_2. The P and Q curves show quite good agreement over the entire extrapolated temperature range of the plots in Fig. 26. Even the R CeO_2 curve is well within an order of magnitude of the $PuO_{1.82}$ result over the temperature range of most interest (2000–5000 K). This result reinforces the choice of cerium as a surrogate for plutonium.

Figure 27 shows similar plots for UO_2. The P and Q plots in this figure were obtained from expressions listed in the *Gmelin Handbook of Inorganic Chemistry*, Supplement C5.[26] The P curve is that recommended by the International Working Group on Fast Reactors

(IWGFR). The R curve is the result of a least squares fit to earlier data quoted in *The Chemistry of Uranium* by Katz and Rabinowitch.[27] Figure 28 shows the quality of a log-linear 1/T least squares fit to the Katz and Rabinowitch data.

The P and R UO_2 curves in Fig. 27 are very similar to the P and Q curves in Fig. 26, i.e., to the $PuO_{1.82}$ and CeO_2 (over congruently evaporating Ce_2O_3) results. This again implies that, as far as the dioxide is concerned, cerium is a good choice as surrogate for uranium. Volatility data for the compounds of most interest to us here are scarce, and Figs. 26 and 27 indicate the kinds of uncertainties and temperature extrapolations involved in using the data that are available.

Recently, Waterland and Fournier have reported on the results of a series of trace metal partitioning tests performed at EPA's Incinerator Research Facility (IRF).[28] Their work concentrated on the search for potential surrogates for the Resource Conservation and Recovery Act (RCRA) metals and did not include the species of direct interest in this report. The data, however, indicated that metal partitioning among incinerator system discharges can largely be explained using only vapor pressure/temperature relationships for metal species in thermodynamic equilibrium. Specifically, they suggest that if the volatility temperatures of two metals are similar, then their partitioning within the incinerator systems should be similar and their discharges also similar. The volatility temperature is defined as the temperature at which the "effective" vapor pressure of a metal is 10^{-6} atm. The effective vapor pressure is defined as the combined equilibrium vapor pressures of all species containing the metal, reflecting the quantity of metal that would vaporize under a given set of conditions. In some cases (Sr, Mg, and Cr), the correlations with the observed incinerator run data are good for the Waterland and Fournier study, while in others (Mg and Ba; Bi and Cd; and Bi and Cu vs As, Ba, and Pb), the validity of this approach is less apparent. The volatility temperature calculations were based on the metal and oxide vapor pressures only. In these tests, feed materials were in the form of soluble nitrates with the exception of arsenic, which was added as As_2O_3. As discussed in the section that follows, nitrate feed can influence emission results under certain conditions. Chlorine content of the burn was also varied from zero to several percent. At the higher percentage values, chlorides and oxychlorides are likely to play a significant role in the incineration equilibrium and should be taken into account in calculating the volatility temperature. Figures 29a and 29b are phase stability diagrams for the Bi-O_2-Cl_2 system at 1000 and 2000 K, respectively. The oxychloride (BiOCl) phase is expected to play a major role based on these equilibrium calculations. Figures 30a and 30b are similar plots for the Cu-O_2-Cl_2 system. Here CuCl is predicted to be the dominant phase at moderate to low Cl_2 and O_2 concentrations. Figures 31a and 31b show similar results for magnesium. In this case, the chloride phase ($MgCl_2$) is less dominant, but still important at higher temperatures. Nevertheless, the data of Waterland and Fournier emphasize the general importance of volatility criteria in selecting surrogates for use in thermal treatment systems.[28]

The Gibbs program section of HSC Chemistry may be employed to estimate volatility temperatures. This program finds the phase combination and composition where the Gibbs energy of the system reaches its minimum value at an initially specified fixed mass balance. The program can also display mole fractions of the gaseous species present in equilibrium as a function of temperature under the fixed mass balance constraint. From this, vapor pressures can be obtained. Table 3 shows calculated volatility temperatures of the rad-metals of concern

Table 3. Volatility temperature of rad-metals and surrogates

	With 0% Chlorine		With 10% Chlorine	
Metal	Volatility Temperature(°C)	Principal Species	Volatility Temperature	Principal Species
Uranium	1210	UO_3	1210	UO_3
Plutonium	3560 (1880)[a]	Pu (PuO_2)	3550 (1880)[a]	Pu (PuO_2)
Ruthenium	775	RuO_4	760	RuO_4
Cesium	375	$CsOH/Cs_2(OH)_2$	500	CsCl
Strontium	1250	$Sr(OH)_2$	925	$SrCl_2$
Cerium	3030 (1734)[a]	CeO (CeO_2)	1430	$CeCl_3$
Zirconium	2700	ZrO_2	2700	ZrO_2
Molybdenum	480	$MoO_2(OH)_2$	190	MoO_2Cl_2
Manganese	1580	MnO	525	$MnCl_2$

[a]Values in parentheses are obtained from the expressions for the oxide vapor pressures in Figs. 26 and 27.

together with a number of potential surrogates. The two chlorine sets of Table 3 are calculated for 0.1 mole of metal, 10 moles of O_2, 10 moles of H_2O, 0 or 10 moles of Cl_2 (0 or 10%), and 80 or 70 moles of Ar, respectively. The results are not sensitive to the quantity of metal within the range of 0.1 to 1 mole, and for metals with higher volatility temperatures, frequently are insensitive to metal loading orders of magnitude higher. Table 4 lists the species, in both gas and condensed phases, invoked in the HSC database for these calculations. It should be noted that UO_2, PuO_2, CeO_2, and Pu chlorides gas phase data are not present in Table 4. This creates special difficulties for the U, Ce, and Pu cases. The numbers in Table 3 in the parentheses for these cases have been obtained from the vapor pressure expressions for the oxides shown in Figs. 26 and 27. It should be noted that the predicted volatility temperature of Ce is sensitive to the percentage of chlorine, changing from 1900°C to 1430°C as the chlorine percentage is increased from 5% to 10%. Table 5 shows surrogates chosen from Table 3, i.e., based on volatility temperature alone. It can be seen that the recommended choices are very similar to those arrived at earlier using phase stability diagrams and other considerations. This similarity gives us confidence that our choices are rational ones from the point of view of emissions as well as from that of the thermal treatment residuals such as the melt and ash.

3.8 EFFECTS OF PHYSICAL AND CHEMICAL NATURE OF SURROGATE FEED MATERIAL

The document *Trial Burn Manual for the Testing of Metals* is currently being prepared by a number of authors with coordination by J. Hillary of EG&G Idaho, Inc.[29] Initial chapters of this manual address issues associated with the physical and chemical form of metal feed materials. Draft copies of Chapter 1, "Mechanisms Governing the Fate of Metals During Combustion," by J. Wendt, University of Arizona, and Chapter 2, "Waste Streams," by

Table 4. Metal species considered in equilibrium calculations

	Metal Species under Consideration	
	Gas Phase	Condensed Phase
Uranium (U)	UO_3, U, UCl_3, UCl_4, UCl_5, UCl_6, $UO_2(OH)_2$	U, UCl_3, UCl_4, UCl_5, UCl_6, UH_3, UO, UO_2, UO_3, UO_3(G), U_3O_8, U_4O_9, UOCl, $UOCl_2$, $UOCl_3$, UO_2Cl_2, $UO_3 \cdot H_2O$
Plutonium (Pu)	$PuO_2(OH)_2$, PuO_3, Pu	Pu, $PuCl_3$, PuH_2, PuH_3, PuO, PuO_2, Pu_2O_3, PuOCl
Ruthenium (Ru)	Ru, $RuCl_3$, $RuCl_4$, RuO_3, RuO_4	Ru, $RuCl_3$, RuO_2, RuO_4
Cesium (Cs)	Cs, Cs_2, CsCl, Cs_2Cl_2, CsO, Cs_2O, CsOH, $Cs_2(OH)_2$	Cs, CsCl, Cs_2Cl_2, CsO_2, Cs_2O, Cs_2O_2, Cs_2O_3, CsOH
Strontium (Sr)	Sr, SrCl, $SrCl_2$, SrH, SrO, SrOH, $Sr(OH)_2$	Sr, $SrCl_2$, SrH_2, SrO, SrO_2, $Sr(OH)_2$
Cerium (Ce)	$CeCl_3$, CeO	Ce, $CeCl_3$, CeH_2, $CeO_{1.72}$, $CeO_{1.83}$, CeO_2, Ce_2O_3
Zirconium (Zr)	Zr, ZrCl, $ZrCl_2$, $ZrCl_3$, $ZrCl_4$, ZrH, ZrO, ZrO_2	Zr, $ZrCl_2$, $ZrCl_3$, $ZrCl_4$, ZrO_2
Molybdenum (Mo)	Mo, $MoCl_4$, $MoCl_5$, $MoCl_6$, MoO, MoO_2, MoO_3, $MoOCl_3$, $MoOCl_4$, MoO_2Cl_2, $MoO_2(OH)_2$	Mo, $MoCl_2$, $MoCl_3$, $MoCl_4$, $MoCl_5$, $MoCl_6$, MoO_2, $MoO_{2.75}$, $MoO_{2.875}$, $MoO_{2.889}$, MoO_3, $MoOCl_3$, $MoOCl_4$, MoO_2Cl_2
Manganese (Mn)	Mn, MnCl, $MnCl_2$, MnO	Mn, $MnCl_2$, $MnCl_3$, $MnCl_4$, MnO, MnO_2, Mn_2O_3, Mn_3O_4

Table 5. Recommended surrogates based on volatility temperature

Rad-Metal	Surrogate(s)	
	Nonchlorinated Waste	Chlorinated Waste
$^{238}U/^{235}U$	Mn	Ce
^{239}Pu	Ce	Zr (Ce)
^{103}Ru	Ru, Mo	Ru, Mn
^{137}Cs	Cs, Mo	Cs, Mn
^{90}Sr	Sr, Mn	Sr, Mn

J. Hillary, EG&G Idaho, are currently available. Though the emphasis in this document is on the toxic metals regulated by RCRA, much of the reasoning and most of the general comments and conclusions are equally applicable to our report. In particular, Chapter 1 contains a good introduction to the effects of chemical speciation and physical form of the feed on the formation of submicron particles likely to pass through the air pollution control systems and escape from the thermal treatment plant. What follows in this section are some short comments largely derived or quoted from this chapter.

In selecting a metal surrogate, the object is to mimic as closely as possible, but in a conservative way, the behavior of the actual metal as incorporated in the mixed waste. By "in a conservative way," we mean that surrogate emissions should, if anything, be greater than those of the actual metal. Certainly they should not be less. The form of the surrogate feed can influence this situation.

Frequently, the waste metal will initially be contained in contaminated soils or in mixed sludges and slurries. Upon introduction of the substances to a hot furnace, an inorganic mixture will be formed containing both the toxic metal and potential scavenging agents, such as clays and glasses commonly found in many industrial waste streams. Much of the toxic metal will normally react with the clay or glass, and only a little will be released to form a condensible vapor;[30] however, it should be noted that deviations from calculated equilibria based on selected pure condensed phases can occur.[30,31] If the surrogate is fed in a chemical form different from that of the toxic metal or is not well mixed with the bulk waste (which becomes the clay or glass scavenging agent), it is not clear that its fate will be equivalent.

The primary forms of the toxic metal—reactive metal compound, porous char, and inorganic mixture—undergo further physical transformations in the furnace environment into the following different physical forms: metal vapor, porous metal ash particle, cenospheric (hollow) ash spheroidal particle, or dense ash particle. Upon cooling, the vapor may nucleate to form tiny particles that can subsequently coagulate (homogeneous condensation), it may condense on existing particles (heterogeneous condensation), or it may chemically react on the surface of existing particles or sorbents. The first two processes require the partial pressure of the metal to exceed its vapor pressure at the ruling temperature (supersaturated vapor); the last does not require this. A key point in considering the nature of the initial feed is that chlorinated species have much higher vapor pressures than do the oxide or hydroxide. This means that the presence of chlorine has a very large influence on the volatility of toxic metal. If mixtures of metals are to be tested, but single metals will occur in practice, a large excess of chlorine should be added to yield conservative results (i.e., maximum metal vaporization).

Metal vapor may not be a prerequisite to forming a submicron fume. Mulholland and Sarofim have shown that certain metal nitrates (e.g., nickel nitrate) form hollow cenospheres, which explosively fragment into tiny submicron particles.[32] Since nickel nitrate has a low vapor pressure, one would not expect it to vaporize and subsequently condense into tiny nuclei. However, in the experiments of Mulholland and Sarofim, as many submicron particles were formed from nickel nitrate, which did not vaporize, as from lead and cadmium nitrates, which did.[32] Since nitrates are soluble in water, the nitrate form has been favored in the past as a convenient route for introducing test metals.

Mulholland and Sarofim suggest that the criterion for cenosphere formation and bursting is that the viscous relaxation time be comparable to the nitrate decomposition time.[32] During decomposition of the nitrate to the oxide, the release of nitrogen dioxide and oxygen in the core of the viscous melt results in bubble nucleation and growth. When the viscosity during decomposition is sufficiently low that the viscous relaxation time is much less than the nitrate decomposition time, the gas bubble escapes before the shell hardens. As a result, a dense particle forms from the evaporated nitrate droplet. When the viscous relaxation time is much greater than the nitrate decomposition time, a porous particle results. When the two times are comparable, cenosphere formation and bursting occurs. This implies that a critical range of viscosities occupies the region between 10^2 and 10^3 $N \cdot s/m^2$ (see Fig. 32). If surrogates are to be fed in nitrate form, it seems advisable to take this criterion into account.

3.9 COST, PURITY, AND SUPPLIERS OF SURROGATE COMPOUNDS

The cost of a surrogate material will depend upon the quantity needed. Other important considerations are its cost relative to that of the testing procedures, and the capital investments involved in the thermal treatment plant. Table 2 contains some comments on cost and suggests, for instance, the use of potassium as a substitute for cesium and the use of iron as a substitute for ruthenium. More exact chemical and physical analogues to radionuclides may be well worth paying for if surrogates are to be used to help qualify emerging technologies for potential use in thermal treatment of mixed wastes. The regulatory and legal issues involved in using surrogates and the relevance of these issues to the "permitting process" have not been fully examined. The issues of surrogate standardization and distribution within the thermal treatment industry also remain open. As an aid to dealing with the issue of surrogate cost, we include Table 6, which lists costs, chemical forms, and suppliers of various potential surrogate materials.

3.10 SURROGATE RECOMMENDATIONS

It is clear that the process of surrogate selection is a complex one from both the scientific and the "real world" points of view. Any proposed list of surrogates necessarily contains compromises. It must draw on previous practical experience and on intuitions and suggestions obtained through modeling. Our knowledge of the complex processes occurring in thermal treatment systems and our ability to model them are both limited. The chemical databases involved are incomplete, and information on relevant kinetics is only slowly accumulating. Nevertheless, from the information and arguments presented in the preceding sections, it seems reasonable to suggest the following surrogates for the radioactive elements listed in Table 1:

Radioisotope	Surrogate
^{238}U, ^{235}U	Ce (natural cerium)
^{99}Tc	Ru (natural ruthenium)
^{137}Cs	Cs (natural cesium)
^{90}Sr	Sr (natural strontium)
^{239}Pu	Ce (natural cerium)
^{103}Ru	Ru (natural ruthenium)

Table 6. Cost and related information for potential radioactive surrogates

Radioactive surrogates	Cost	Assay	Impurities	Supplier/comments
$CaCO_3$	$7.45/lb @ 100 lb	>99.0%	Na - 0.1% Sr - 0.1% Cl - 0.001%	Spectrum Chemicals (800) 772-8786; (908) 214-1300 powder, hygroscopic
CaO	$1.25/lb @ 100 lb	>95% CaO	N/A	Spectrum/powder, moisture sensitive
$Ca(NO_3)_2$	$4.25/lb @ 100 lb	99.0–103.0% as $Ca(NO_3)_2 \cdot 4H_2O$	Cl - 0.005% Ba - 0.005% Heavy metals (as PB) - 0.005%	Spectrum/crystal
MoO_3	$17.80/lb @ 55 lb	>99.5%	0.002% Cl Heavy metals (as Pb) - 0.005 %	Spectrum/powder
$Mo(CO_3)_3$	None in Alfa, Sigma, Cerac, Chemical Buyers Directory			
$Mo(NO_3)_6$				
K_2CO_3	$1.65/lb @ 100 lb	>99.0%	N/A	Spectrum
KNO_3	$3.75/lb @ 110 lb	>99.0%	Cl - 0.002% Heavy metals (as Pb) - 0.005%	Spectrum
CH_3COOK	$3.55/lb @ 100 lb	>99%		Spectrum/crystal or granular
$SrCO_3$	$1.40/lb @ 100 lb	98.0%	$BaCO_3$ - 0.5% $CaCO_3$ - 0.5%	Barium & Chemicals (614) 282-9776 powder—10μm
$Sr(NO_3)_2$	$1.60/lb @ 100 lb	>99.0%		Barium chemicals powder - 200 mesh
$Sr(OH)_2$	$4.75/1000 lb order			Barium chemicals

Table 6 (continued)

Radioactive surrogates	Cost	Assay	Impurities	Supplier/comments
CeO_2	$55/500g	>99.9%		Aldrich Chemicals (800) 231-8327
Ce_2O_3	$949/500g	99.9%		Cerac Inc. (414) 289-9800
$Ce(CO_3)_3$	$60/kg @ 100 kg			Alchemie USA Inc. (203) 621-2470
$Ce(NO_3)_3$	$214/2 kg	99.5% (metals basis), crystals		Alfa (800) 343-0660
	$2.90/lb @ 300 lb	39% aqueous solution		Molycorp (914) 997-8880
Cs_2CO_3	$185/kg @ 100 kg	>99.5%	N/A	Alchemie -40 mesh powder
Cs_2O	$171/50 g	99% (metals basis)		Alfa/<2.5 cm yellow brown pieces
$CsOOCCH_3$ acetate	$78.00/250 g	Technical		Alfa/lump
Pr_6O_{11}	$16.80/lb @ 300 lb	96%	<3% Nd <1% Ce	Molycorp
$Pr(NO_3)_3 \cdot 6H_2O$	$87.00/ 250 g	99.9% (metals basis)		Alfa/green crystalline
$Pr_2(CO_3)_3 \cdot 8H_2O$	$47.00/100 g	99.9% (metals basis)		Alfa/crystalline
ReO_2	$181/10 g	99.9% (metals basis)		Alfa/black powder
$RuO_2 \cdot XH_2O$	$182/25 g	58% Ru		Alchemie/black powder

We suggest that the surrogate "spike" package for the radioactive species be composed of the stable oxides of the various elements discussed where these exist, i.e., CeO_2, Pr_2O_3, and RuO_2. For cesium and strontium, the pure metals are flammable under normal atmospheric conditions and the oxides readily hydrolyze. The nitrates or carbonates may be suitable choices (but see Sect. 3.8, "Effects of Physical and Chemical Nature of Surrogate Feed Material"). The issue of chlorine addition to the thermal treatment system is a very important one, which must be dealt with on a case-by-case basis. It is possible that in certain cases, use of the surrogate in chloride form may be more desirable and/or economical than other choices. Another important point is that of possible burn temperature changes caused by surrogate feed. Indirect evidence from the K-25 Site TSCA incinerator indicates that uranium metal within the feed results in high effective uranium burn temperatures and formation of submicron particulates contaminated with uranium.[33] Sulfides or organometallics will tend to raise burn temperatures (they can be combustible), while most other forms will tend to lower the burn temperature if enough surrogate is fed. Again, these factors must be considered on a case-by-case basis.

4. REFERENCES

1. "Mixed Waste Characterization Code Descriptions," memo from Wayne Ross, Pacific Northwest Laboratory, to John Mayberry, SAIC, Idaho Falls, Idaho, 83401, February 5, 1993.

2. R. L. Gillins, L. M. DeWitt, and A. L. Wollerman, *Mixed Waste Integrated Program Interim Evaluation Report on Thermal Treatment Technologies*, DOE/MWIP-2, SAIC, Idaho Falls, Idaho, 83401, 1993.

3. W. Hoffelner et al., "Plasma Technology for Rapid Oxidation, Melting, and Vitrification of Low/Medium Radioactive Waste," *Nucl. Eng. Internat.* 14 (October 1992). Also see *Applications Analysis Report*, EPA/540/A5-91/007, Retech, Inc., Plasma Centrifugal Furnace, USEPA, Office of Research and Development, Washington, D.C., June 1992.

4. *An Investigation of the Need for the Hold, Test and Release Option for the Rocky Flats Fluidized Bed Unit*, L-14805, Lawrence Livermore National Laboratory, June 1992.

5. W. D. Bostick et al., "Effluent Testing at the Oak Ridge Mixed Waste Incinerator," *Proceedings of the 85th Annual Meeting and Exposition of the Air and Waste Management Association*, Kansas City, Mo., June 1992.

6. L. J. Meile et al., *Rocky Flats Plant Fluidized Bed Incinerator*, RFP-3249, Rockwell International, Rocky Flats Plant, Golden, Colo., March 8, 1982.

7. R. Geimer, J. Batdorf, and P. Wolfe, "Test Results from the Demonstration of the Plasma Hearth Process," p. 301, *Proceedings of the Incineration Conference*, Knoxville, Tenn., May 1993.

8. M. R. Funfschilling and R.C. Eschenbach, "A Plasma Centrifugal Furnace for Treating Hazardous Waste, Muttenz, Switzerland," presented at Electrotech 92, Montreal, Canada, June 1992.

9. W. J. Bjorklund, *Development and Use of Sintered Metal Filters with Fluidized Bed and Spray Calcination of Simulated High-Level Waste*, BNWL-2074, Batelle Pacific Northwest Laboratories, Richland, Wash., July 1976.

10. Antti Roine, *HSC Chemistry for Windows—Chemical Reaction and Equilibrium Software with Extensive Thermochemical Database*, Version 1.10, Outokumpu Research Oy, Information Service, P.O. Box 60, SF-28101 Pori, Finland, 1993.

11. F*A*C*T is operated by the McGill University Computing Center on a time-sharing system known as MUSIC-F. Inquiries should be directed to W.T. Thompson, Director, On-line F*A*C*T System, Dept. of Chemistry and Chemical Engineering, Royal Military College of Canada, Kingston, Ontario K7K5LO. Tel: 613-544-6159, Fax: 613-544-7900.

12. O. H. Krikorian et al., *Evaluation of Actinide Volatilities in Mixed Waste Processors: Interim Report*, UCRL-ID-111352, Lawrence Livermore National Laboratory, Livermore, Calif., August 24, 1992.

13. S. O. Bates, *Definition and Compositions of Standard Waste Streams for Evaluation of Buried Waste Integrated Demonstration Treatment Technologies*, EGG-WTD-10660, Idaho National Engineering Laboratory, January 1993.

14. C. Shapiro, K. Garcia, and J. Bella, "Treatment of a Simulated Mixed Waste with Supercritical Water Oxidation," p. 10.3.1 in *Proceedings of the 2nd International Symposium on Mixed Waste*, Baltimore, Md., 1993.

15. *Electro-Refining of Cerium, Part II, Cerium as a Surrogate for Plutonium in Electro-Refining Studies*, MT/EXT/092/010, Colorado School of Mines, 1992.

16. A. Raraz, B. Mishra, and W. A. Averill, *Application of Surrogate Materials in Process Study of Actinides*, RFP-4628, Rockwell International, Rocky Flats Plant, Golden, Colo., 1993.

17. Private communication from W. D. Bond, Oak Ridge National Laboratory, Martin Marietta Energy Systems, Inc., to J. Stockdale, 1993.

18. G. D. Del Cul, *Luminescence, Raman and Absorption Spectrophotometric Studies of Selected Lanthanide and Actinide Compounds in the Solid State*, Ph.D. Thesis, Department of Chemistry, University of Tennessee, Knoxville, Tenn., December 1990. Also issued as U.S. Department of Energy Report DOE/ER/13865-029, 1990.

19. O. H. Krikorian et al., *Experimental Studies and Thermodynamic Modeling of Volatilities of Uranium, Plutonium, and Americium from Their Oxides and from Their Oxides Interacted with Ash*, UCRL-ID-114774, Lawrence Livermore National Laboratory, September 1993.

20. Private communication from G. D. Del Cul, K-25 Site, Martin Marietta Energy Systems, Inc., Oak Ridge, Tenn., to J. Stockdale, 1993.

21. *A Systematic Analysis of the Spectra of the Lanthanides Doped into Single Crystal LaF3*, ANL-88-8, U.S. Department of Energy, 1988.

22. Private communication from B. Ebbinghaus, Lawrence Livermore National Laboratory, Livermore, Calif., to J. Stockdale, 1993.

23. L. A. Worl et al., "Remediation of Hanford Tank Waste Using Magnetic Separation," *Proceedings of Waste Management Symposium*, Tucson, Ariz., 1993.

24. D. R. Messier, *J. Am. Ceram. Soc.* 51, 710 (1968).

25. R. J. Ackermann and E.G. Rauh, "A High Temperature Study of the Stoichiometry, Phase Behavior, Vaporization Characteristics, and Thermodynamic Properties of the Cerium + Oxygen System," *J. Chem. Thermodynam.* 3, 609 (1971).

26. *Gmelin Handbook of Inorganic Chemistry*, Suppl. 5, 8th edition, Springer-Verlag, Berlin, 1986.

27. J. J. Katz and E. Rabinowitch, *The Chemistry of Uranium*, McGraw-Hill, New York, 1951.

28. L. R. Waterland and D. J. Fournier, "Potential Surrogate Metals for Incinerator Trial Burns," p. 433, *Proceedings of the 1993 Incineration Conference*, Knoxville, Tenn., May 5, 1993.

29. J. Hillary, ed., *Trial Burn Manual for the Testing of Metals*, EG&G Idaho, Inc. (Draft copy courtesy of T.C. Ho, July 1993.)

30. J. S. Eddings and J. C. Lighty, "A Study of Metal Contaminant Behavior in a Pilot Scale Rotary Kiln," poster presented at the 24th International Symposium on Combustion, Sydney, Australia, July 1992.

31. P. B. Queneau, C. D. May, and D. E. Cregar, "Application of Slag Technology to Recycling of Solid Wastes," p. 69, *Proceedings of the 1991 Incineration Conference*, Knoxville, Tenn., May 1991.

32. J. A. Mulholland and A. F. Sarofim, "Mechanisms of Inorganic Particle Formation during Suspension Heating of Simulated Aqueous Wastes," *Environ. Sci. Technol.* 25, 268 (1991).

33. Private communication from J. Shor, Oak Ridge National Laboratory, Martin Marietta Energy Systems, Inc., to J. Stockdale, 1993.

Appendix A

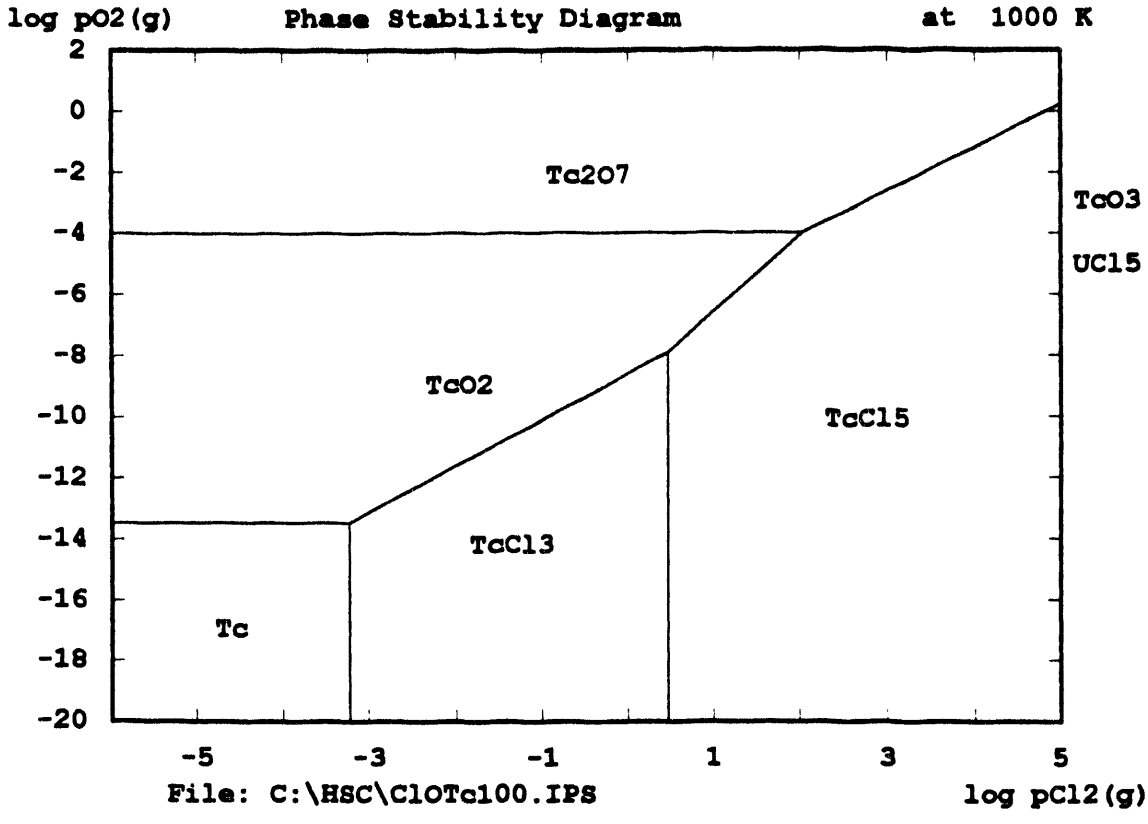

Fig. 1a. Phase stability diagram for technetium-oxygen-chlorine at 1000 K.

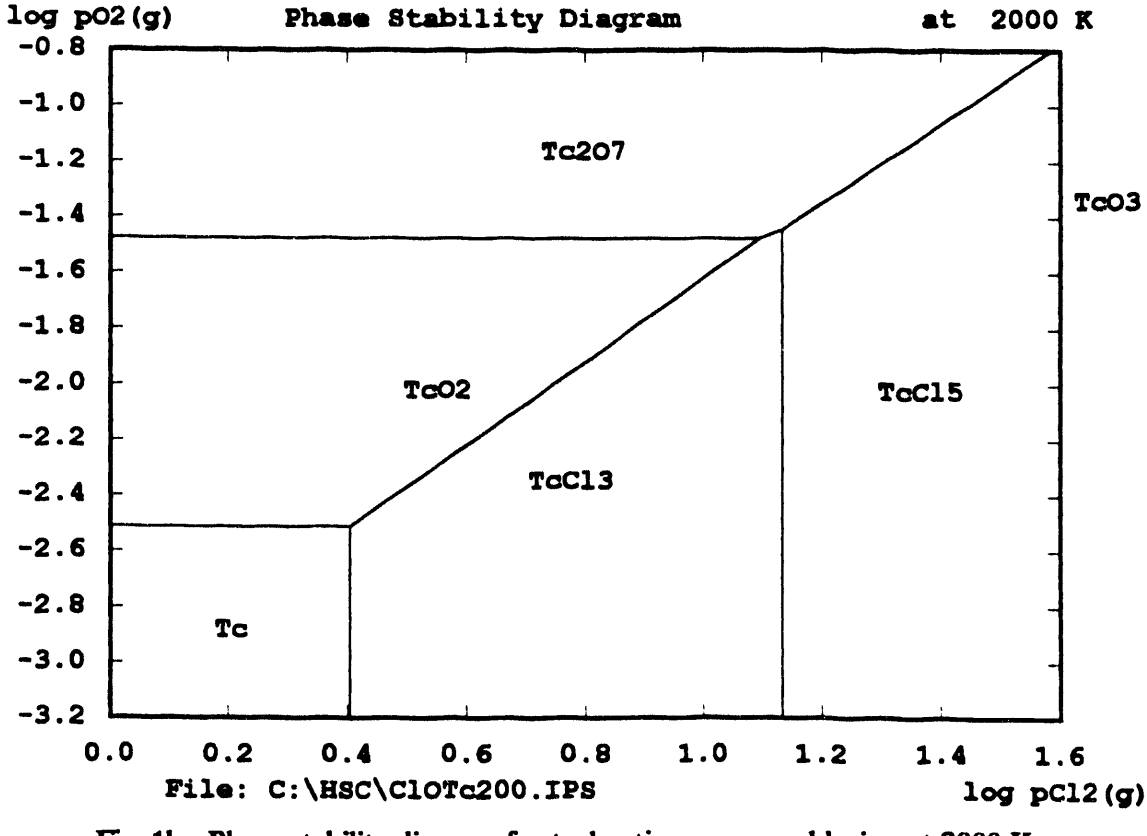

Fig. 1b. Phase stability diagram for technetium-oxygen-chlorine at 2000 K.

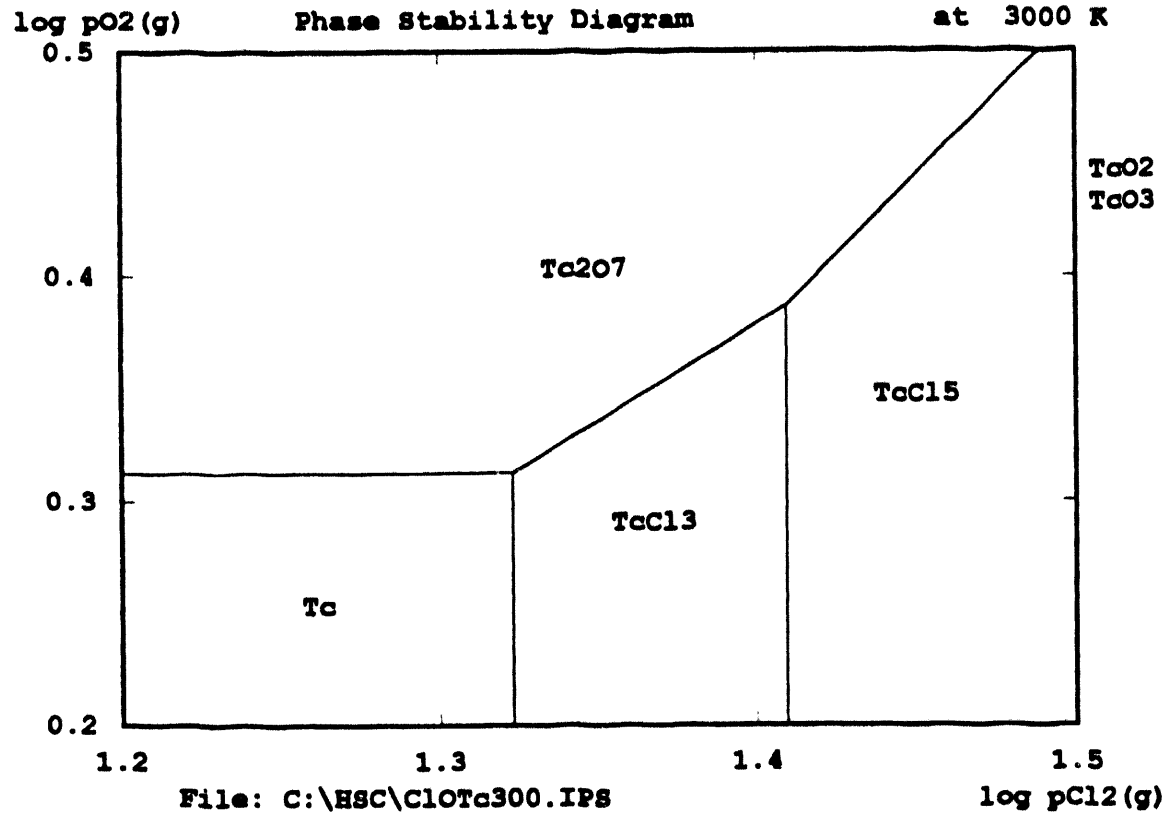

Fig. 1c. Phase stability diagram for technetium-oxygen-chlorine at 3000 K.

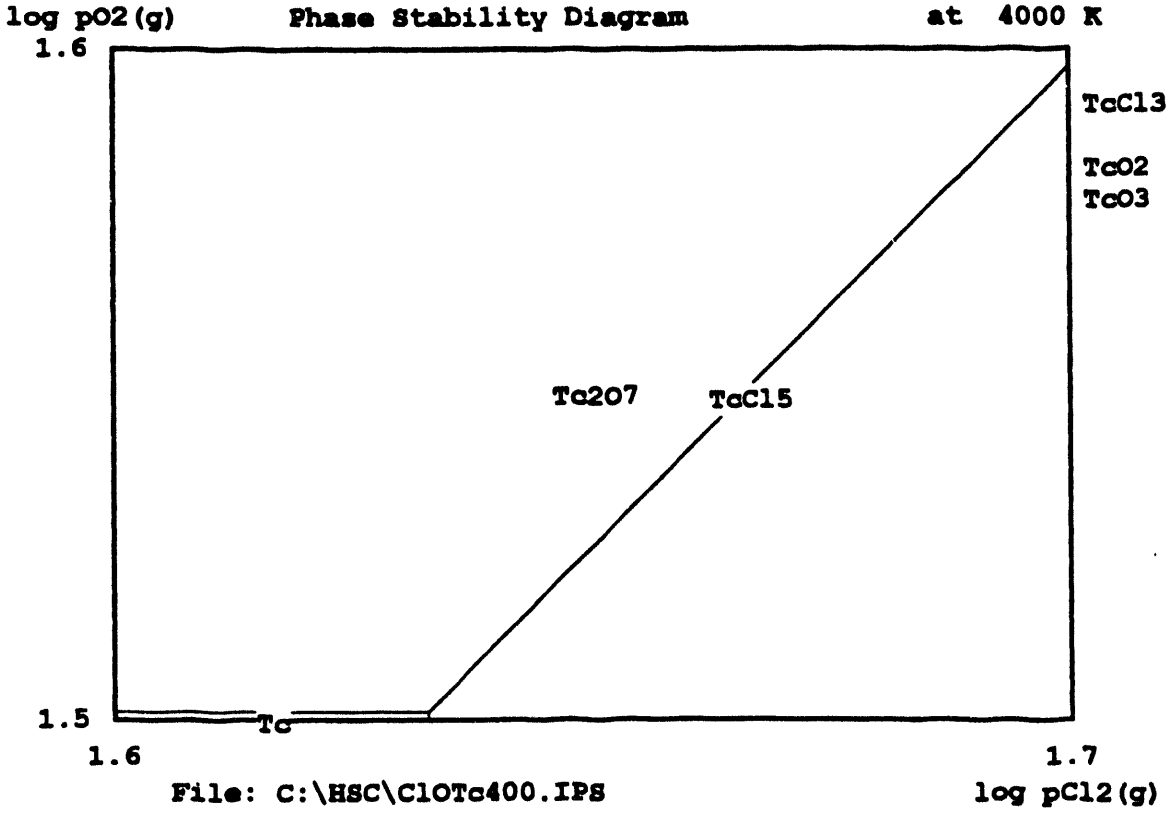

Fig. 1d. Phase stability diagram for technetium-oxygen-chlorine at 4000 K.

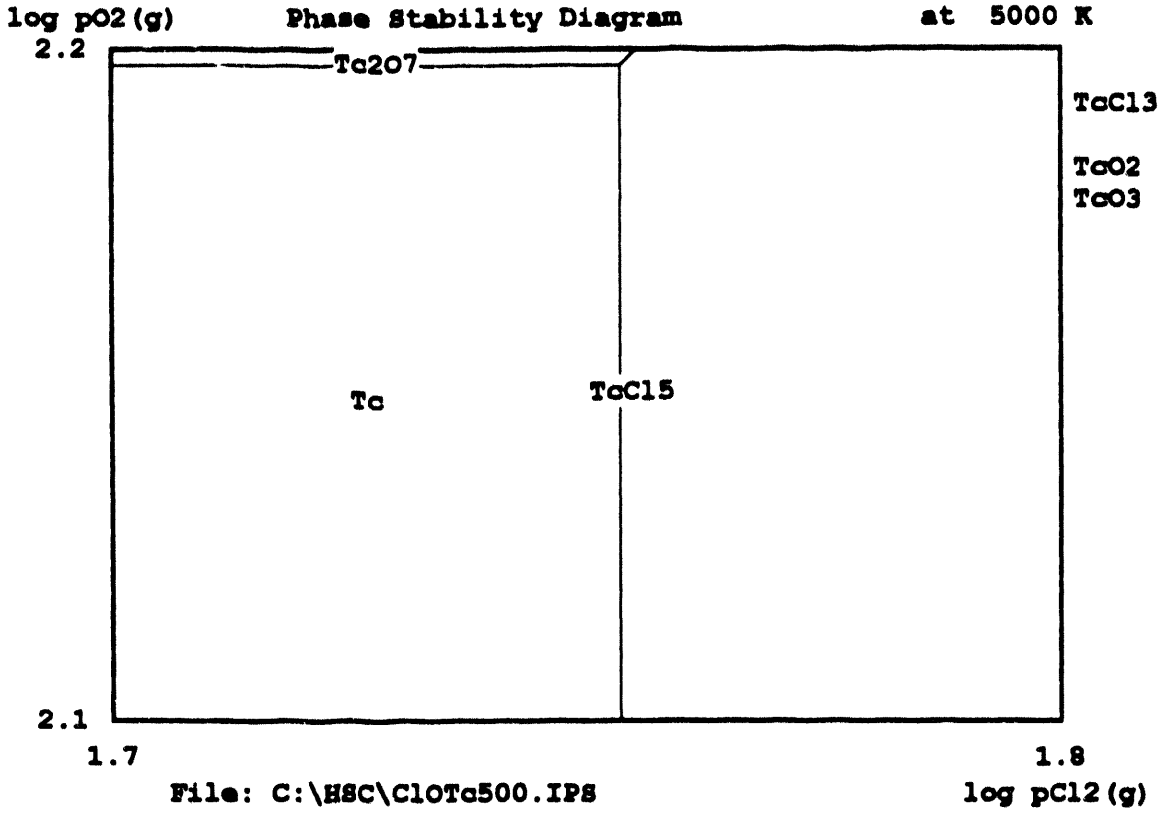

Fig. 1e. Phase stability diagram for technetium-oxygen-chlorine at 5000 K.

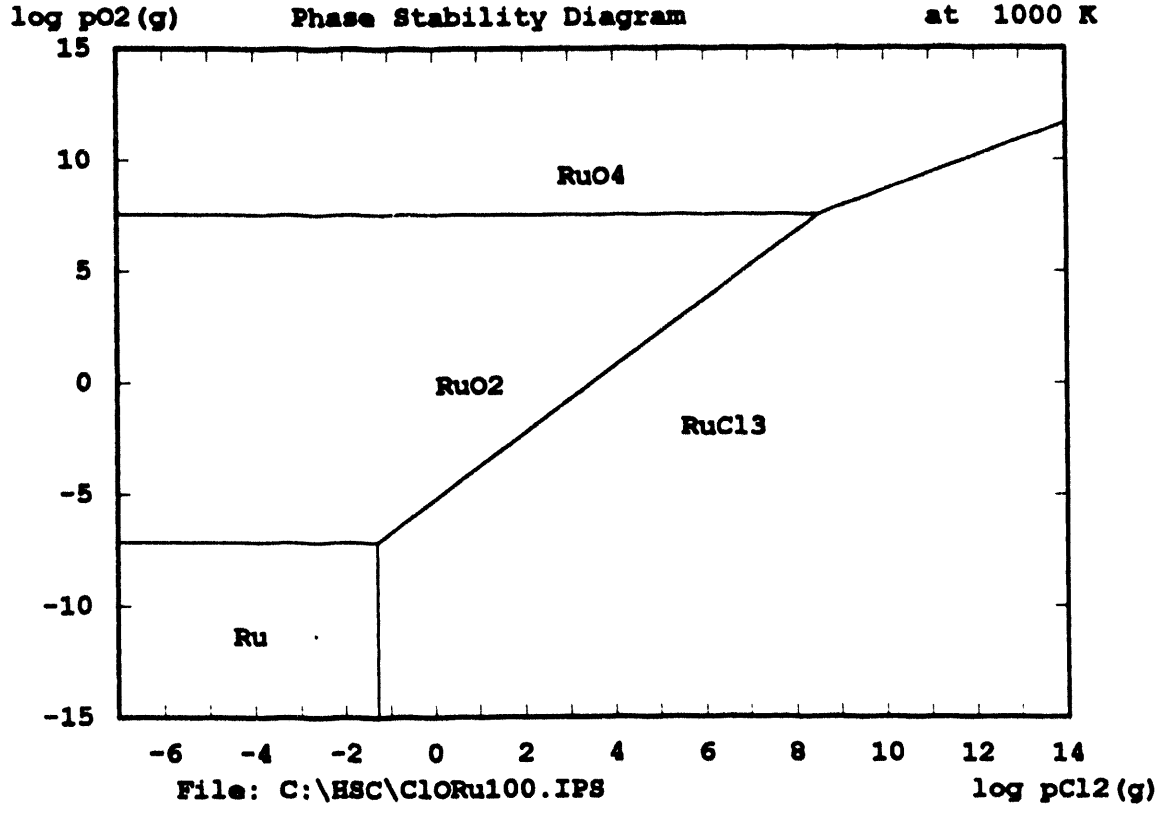

Fig. 2a. Phase stability diagram for ruthenium-oxygen-chlorine at 1000 K.

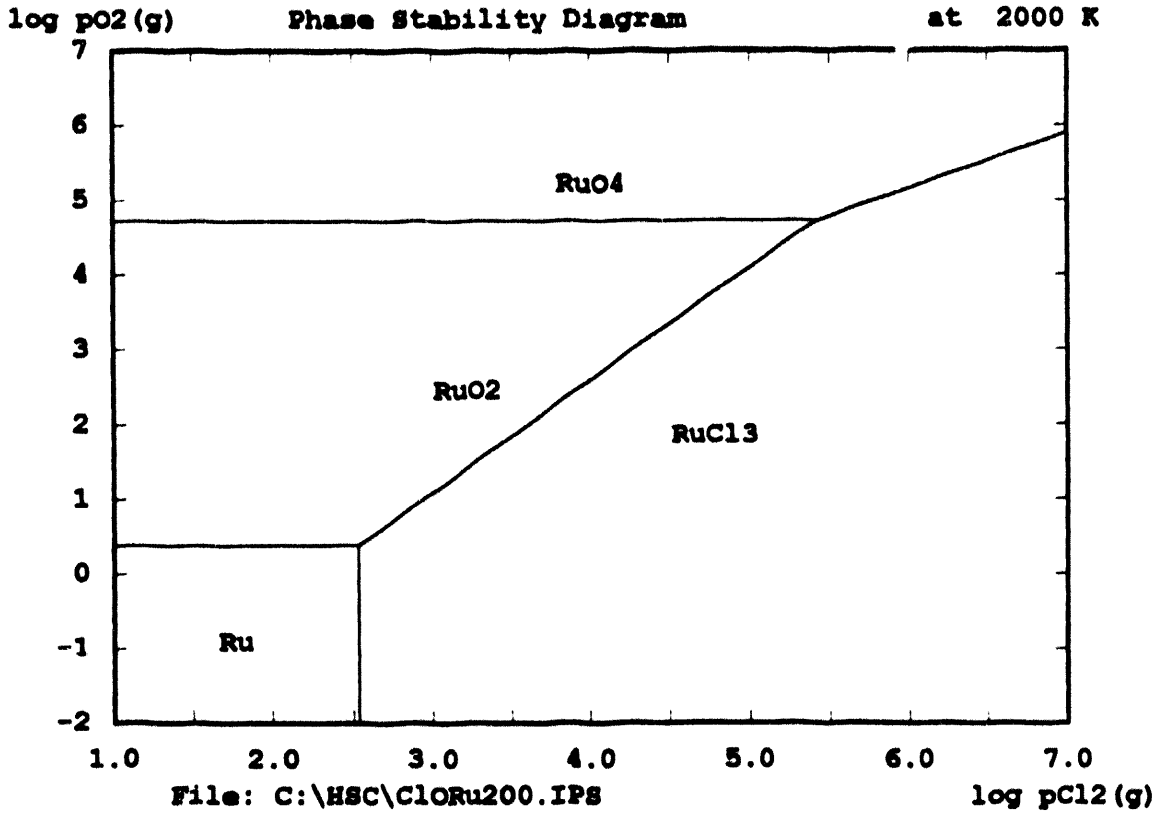

Fig. 2b. Phase stability diagram for ruthenium-oxygen-chlorine at 2000 K.

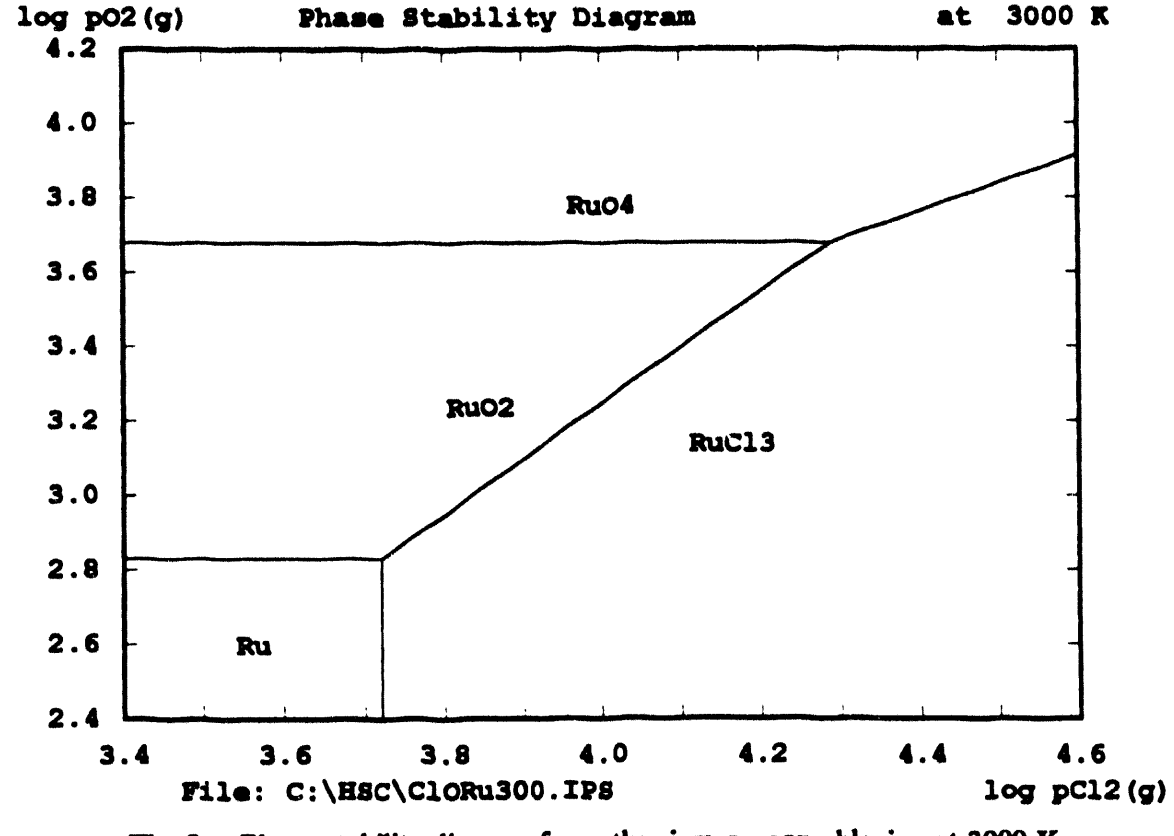

Fig. 2c. Phase stability diagram for ruthenium-oxygen-chlorine at 3000 K.

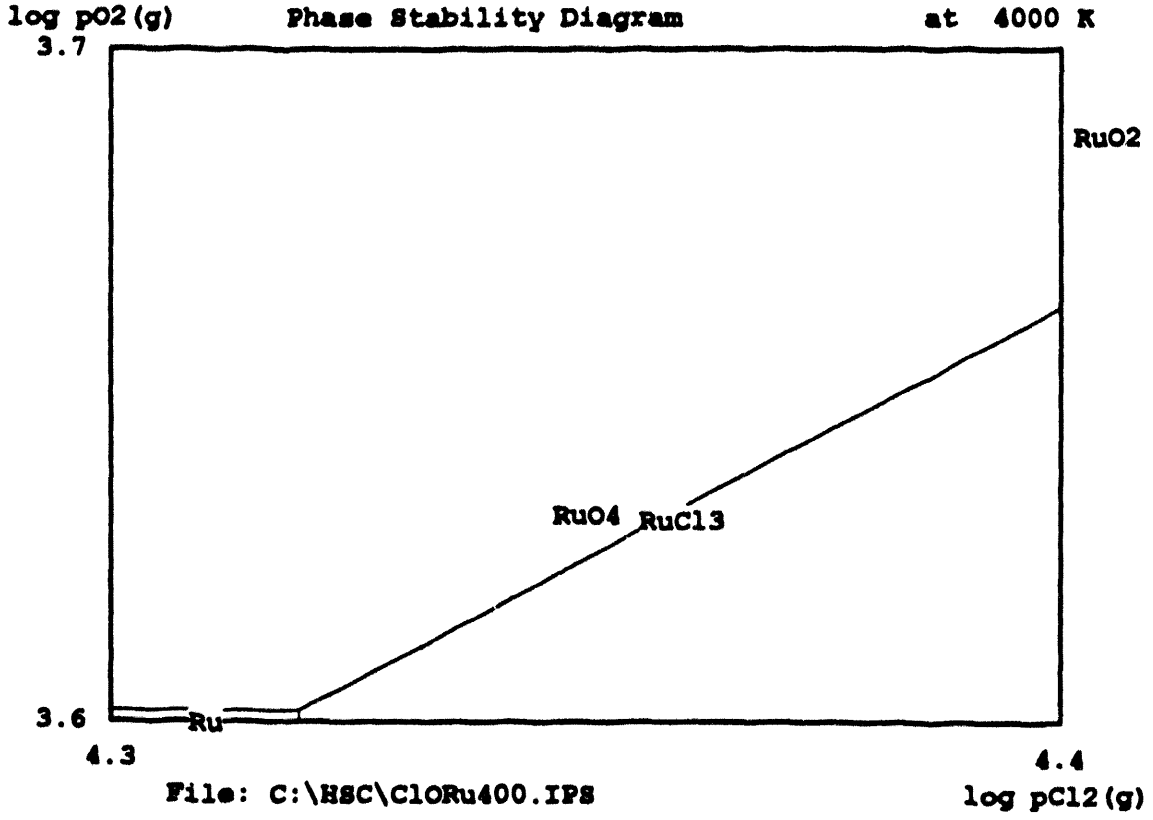

Fig. 2d. Phase stability diagram for ruthenium-oxygen-chlorine at 4000 K.

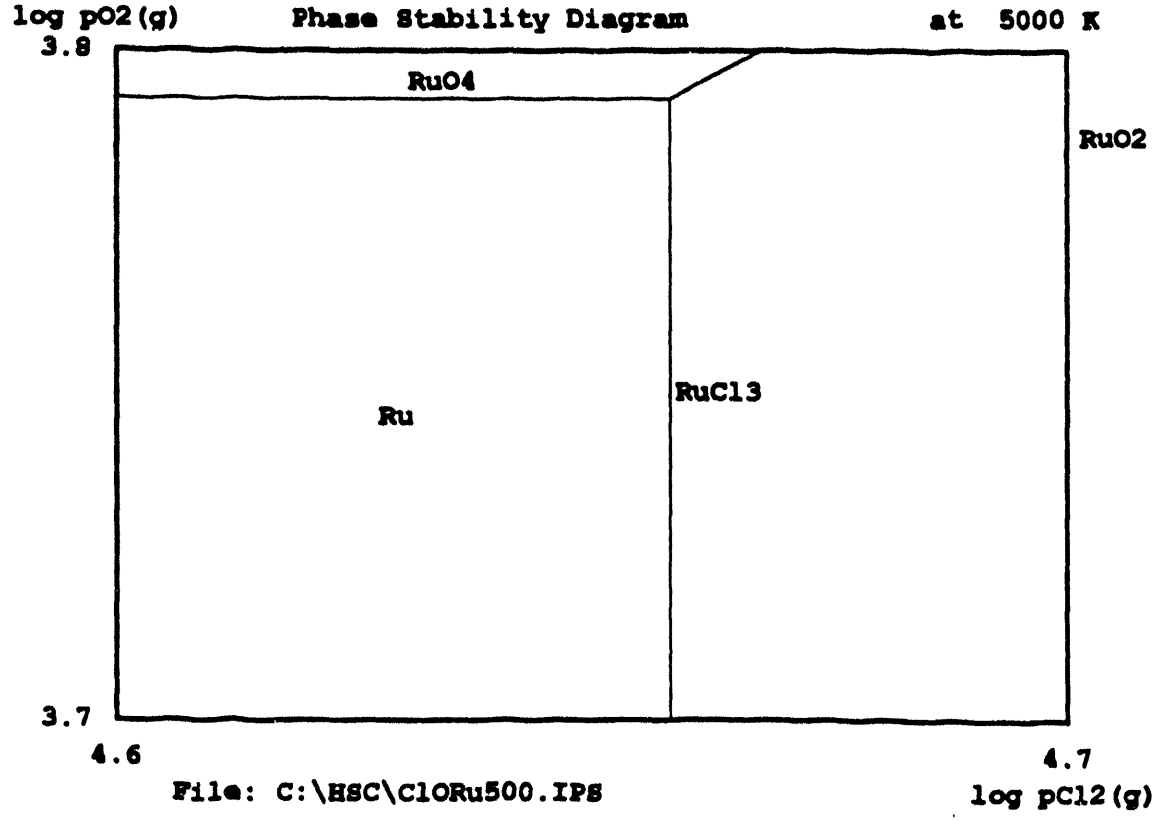

Fig. 2e. Phase stability diagram for ruthenium-oxygen-chlorine at 5000 K.

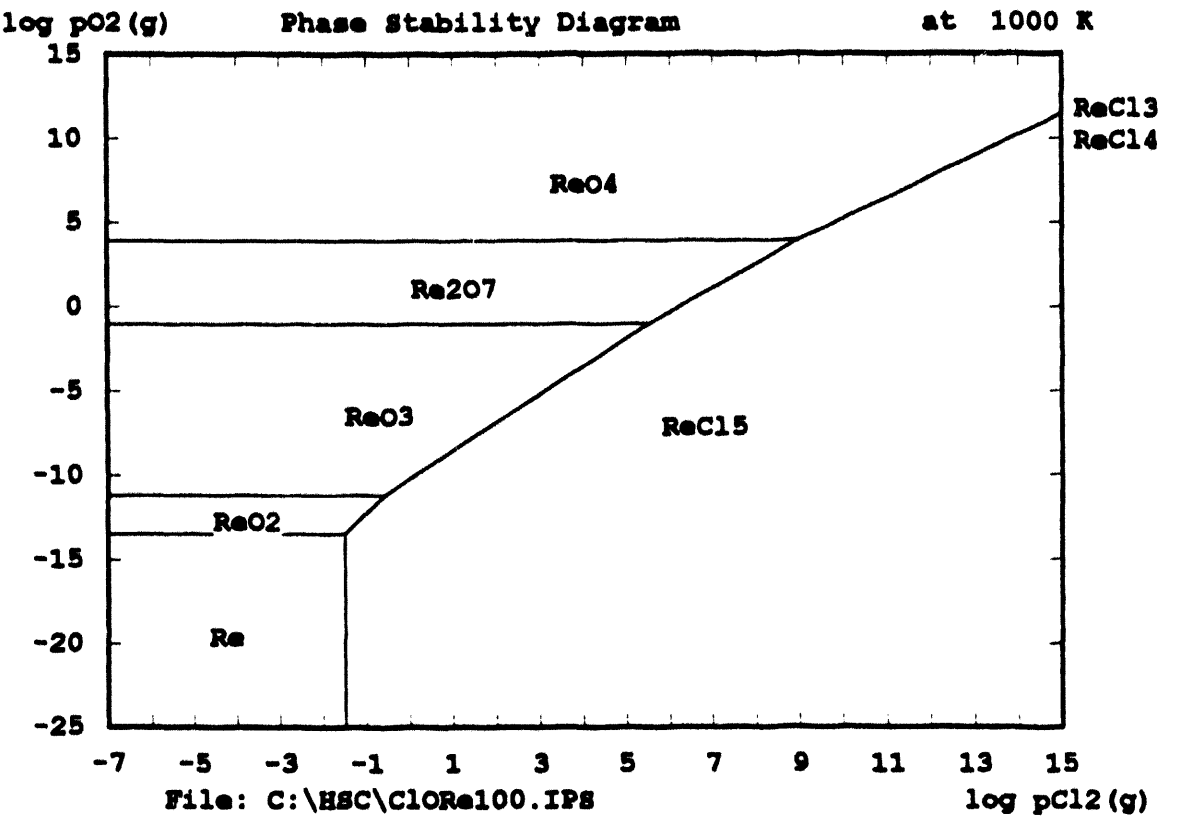

Fig. 3a. Phase stability diagram for rhenium-oxygen-chlorine at 1000 K.

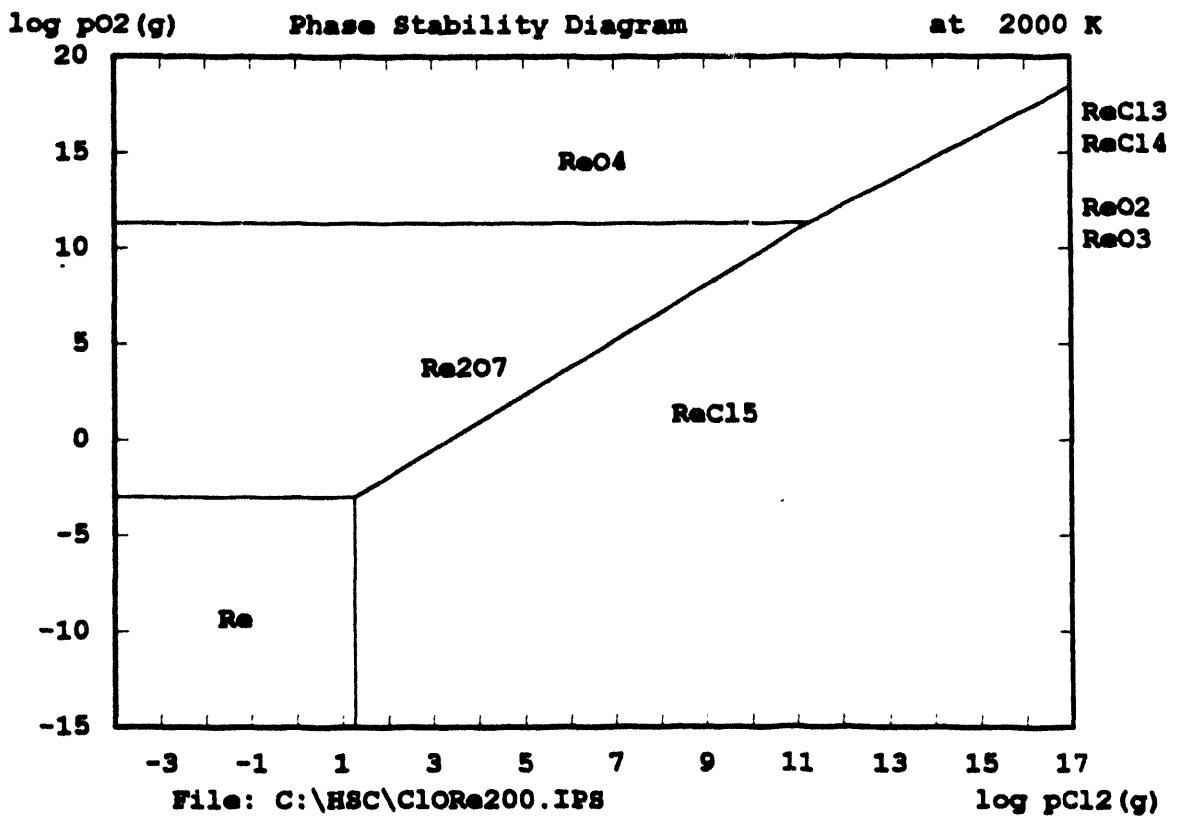

Fig. 3b. Phase stability diagram for rhenium-oxygen-chlorine at 2000 K.

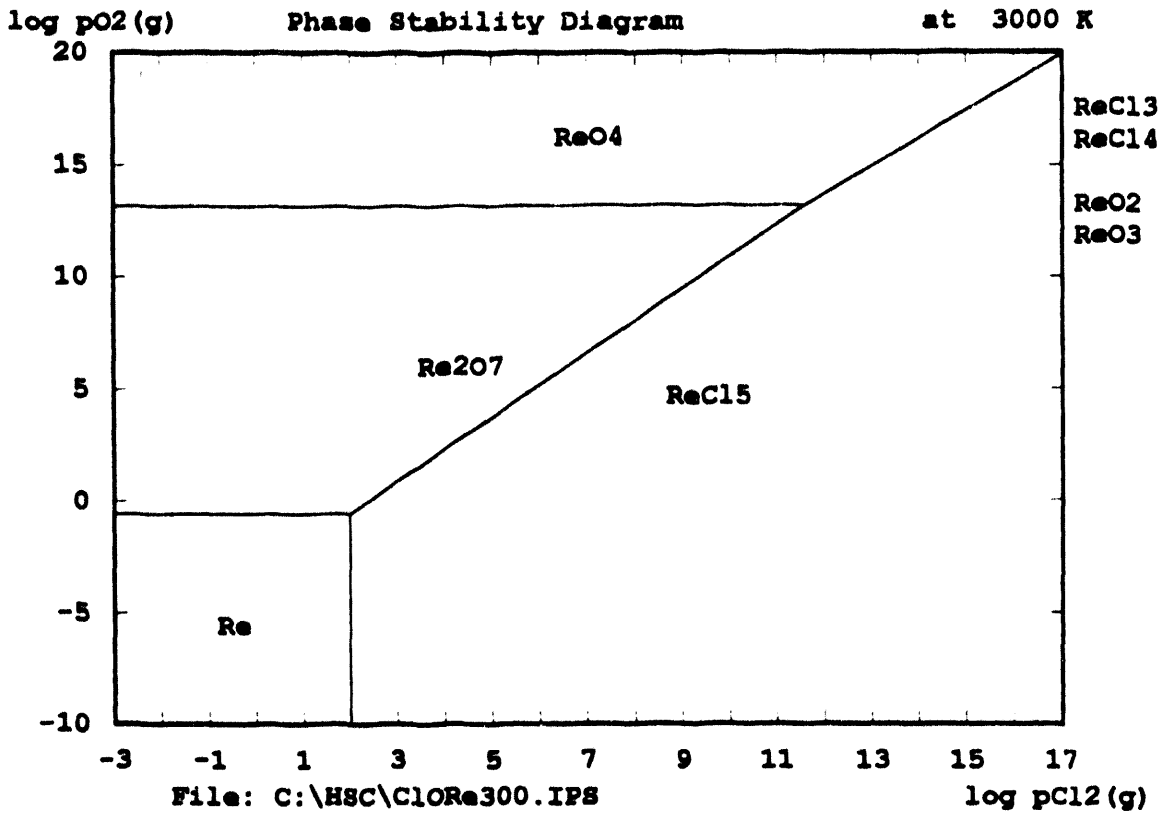

Fig. 3c. Phase stability diagram for rhenium-oxygen-chlorine at 3000 K.

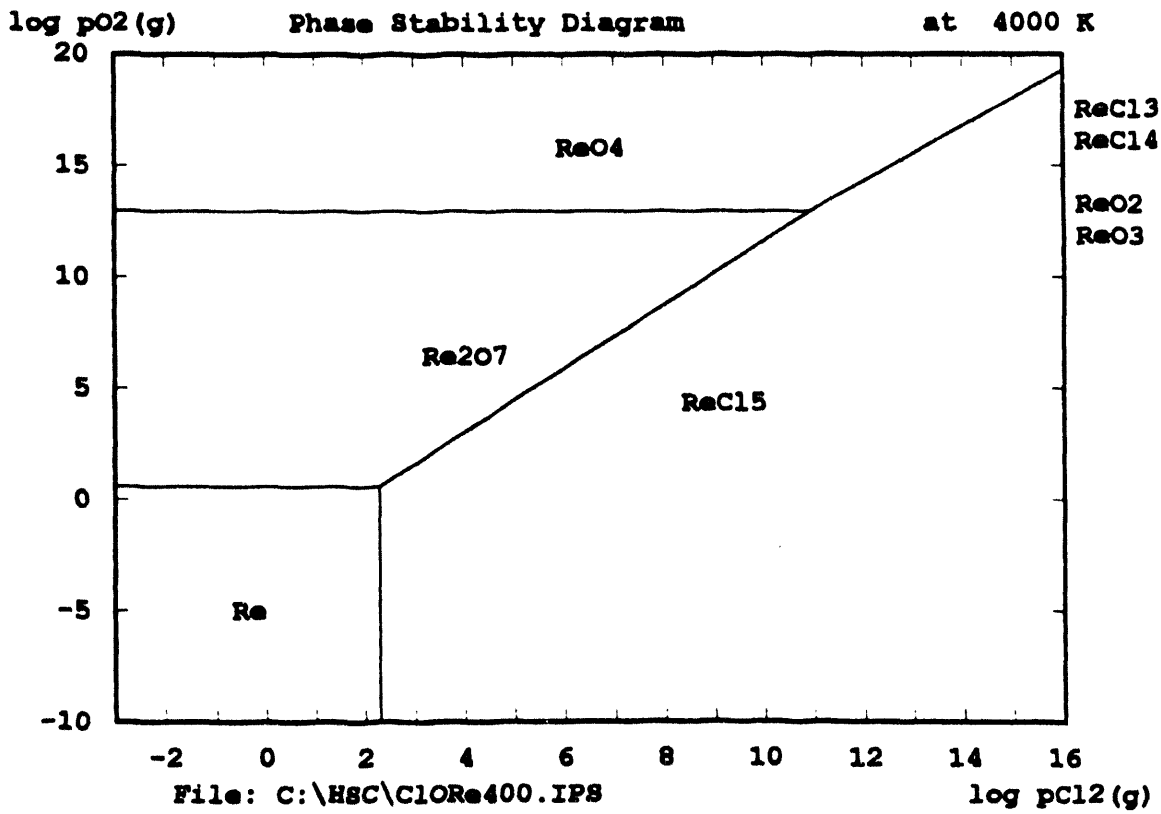

Fig. 3d. Phase stability diagram for rhenium-oxygen-chlorine at 4000 K.

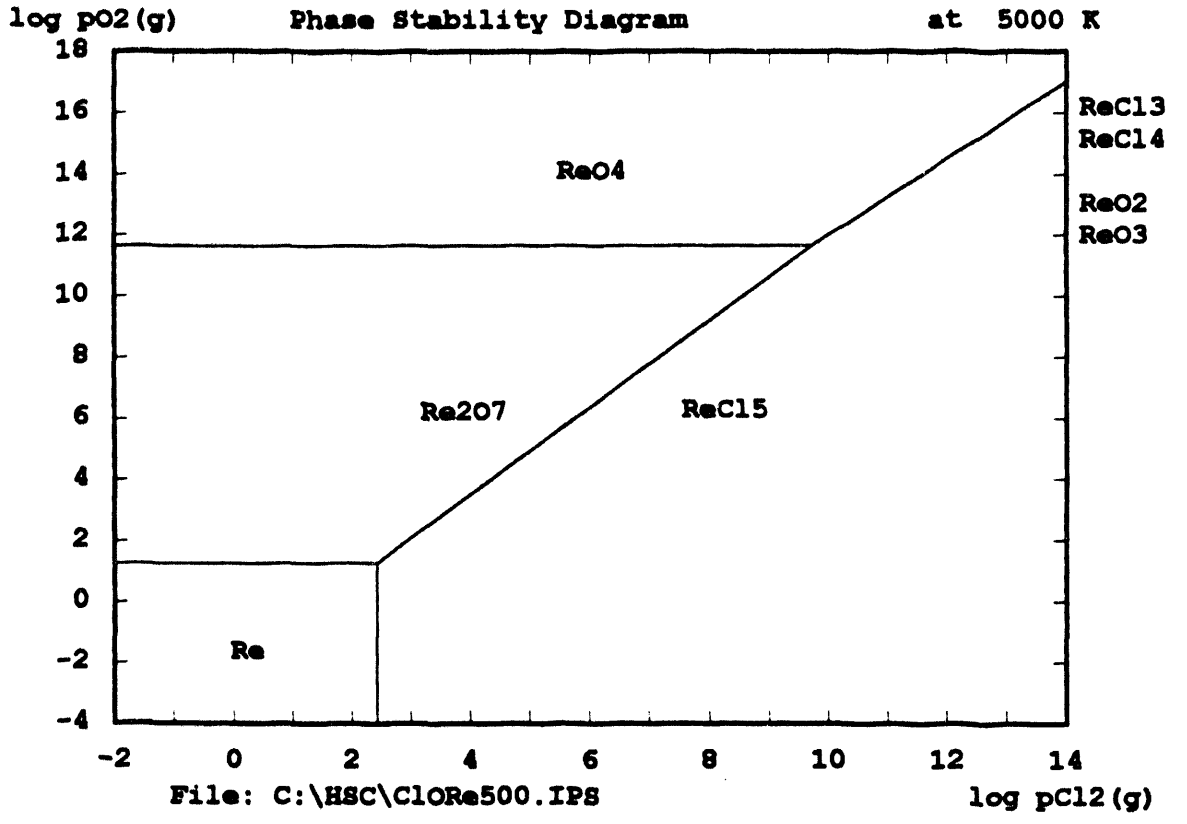

Fig. 3e. Phase stability diagram for rhenium-oxygen-chlorine at 5000 K.

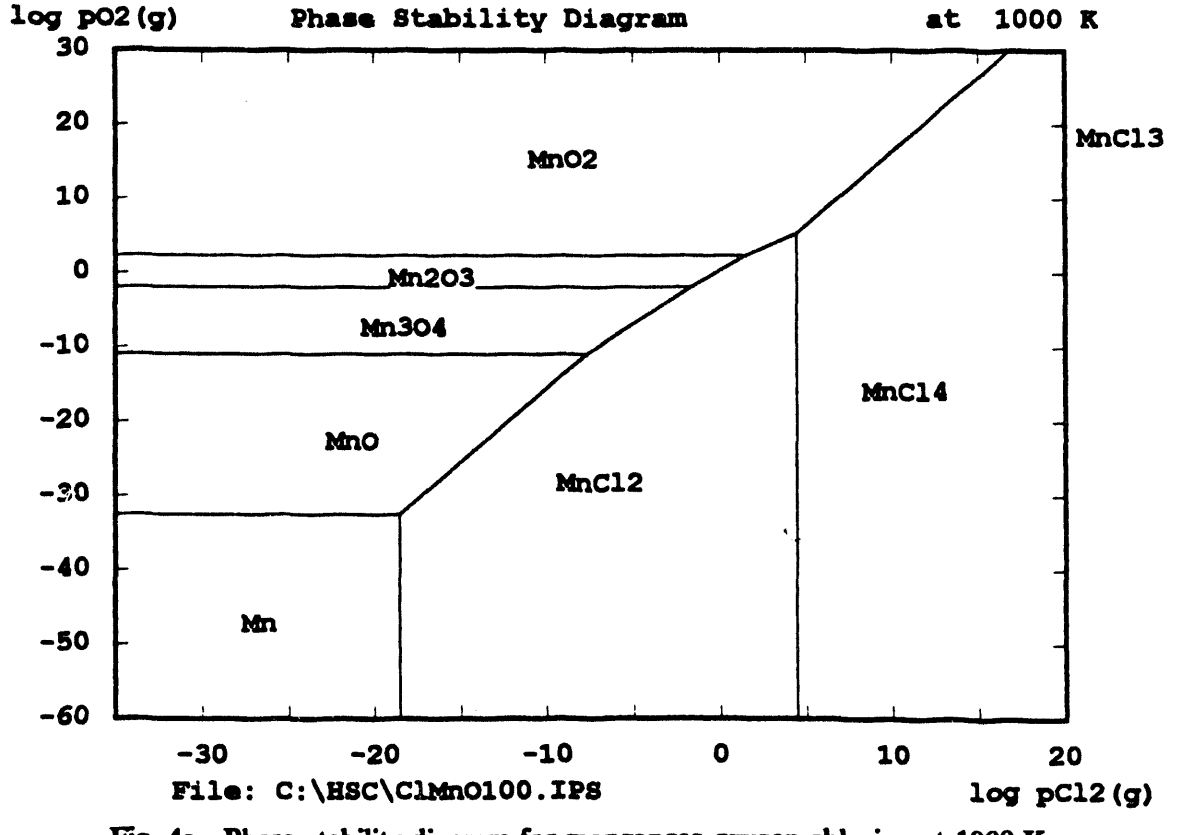

Fig. 4a. Phase stability diagram for manganese-oxygen-chlorine at 1000 K.

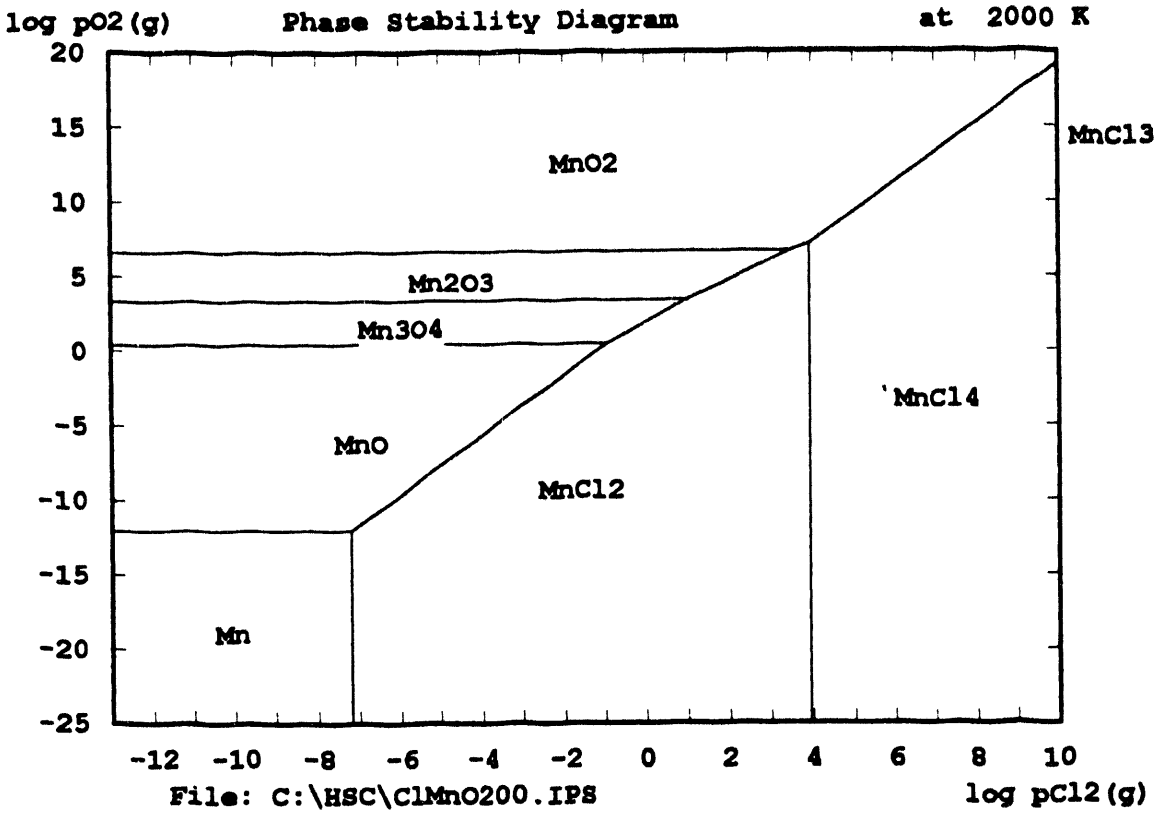

Fig. 4b. Phase stability diagram for manganese-oxygen-chlorine at 2000 K.

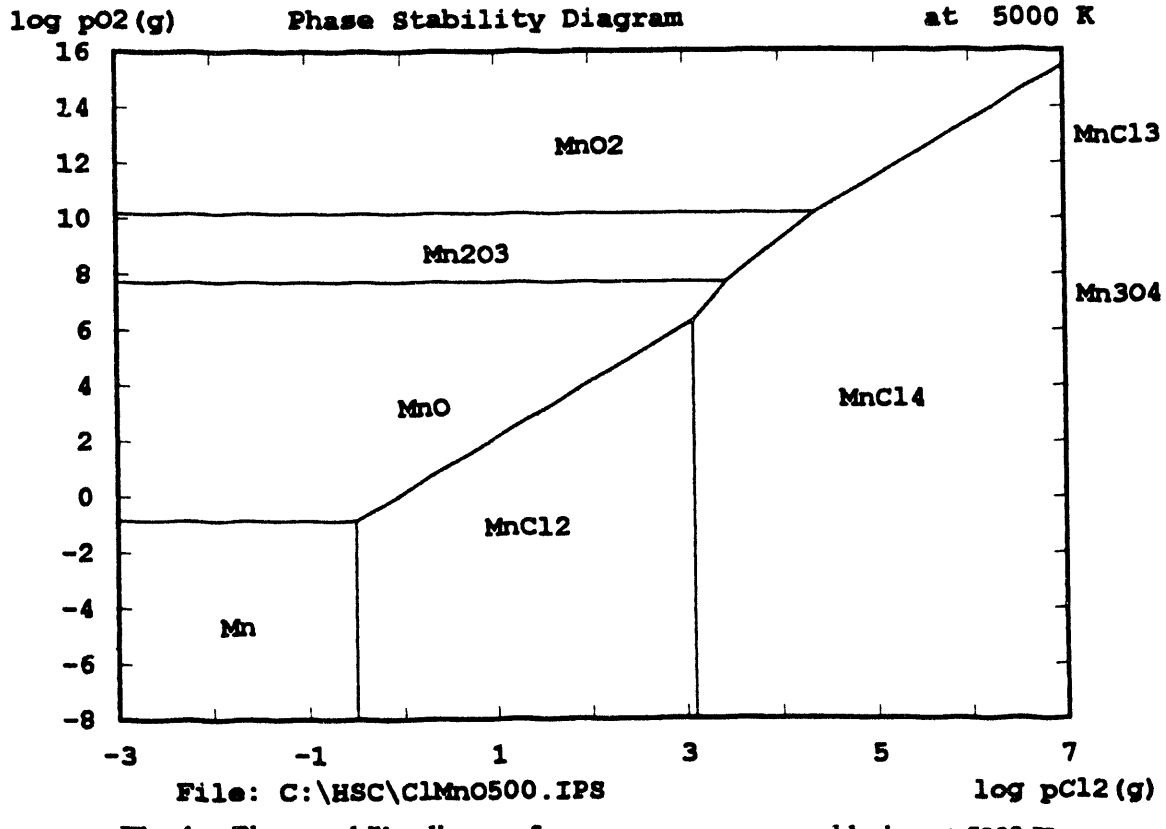

Fig. 4c. Phase stability diagram for manganese-oxygen-chlorine at 5000 K.

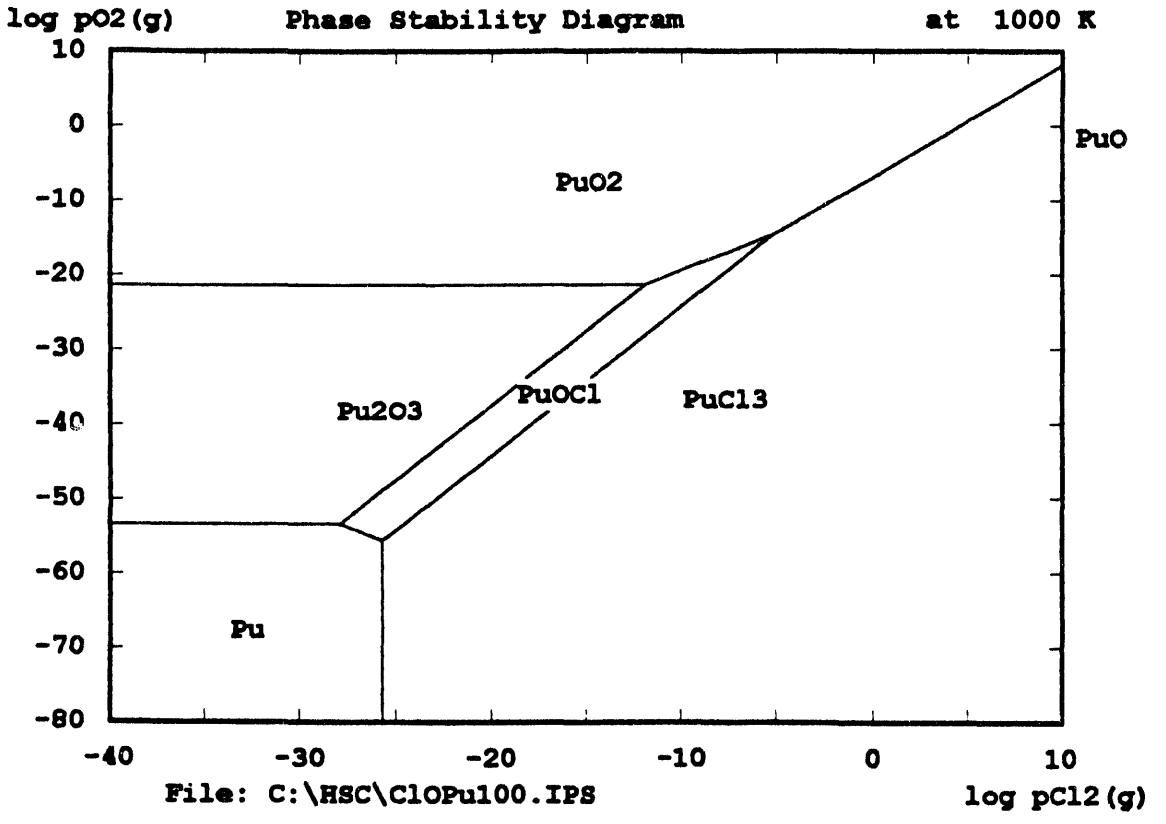

Fig. 5a. Phase stability diagram for plutonium-oxygen-chlorine at 1000 K.

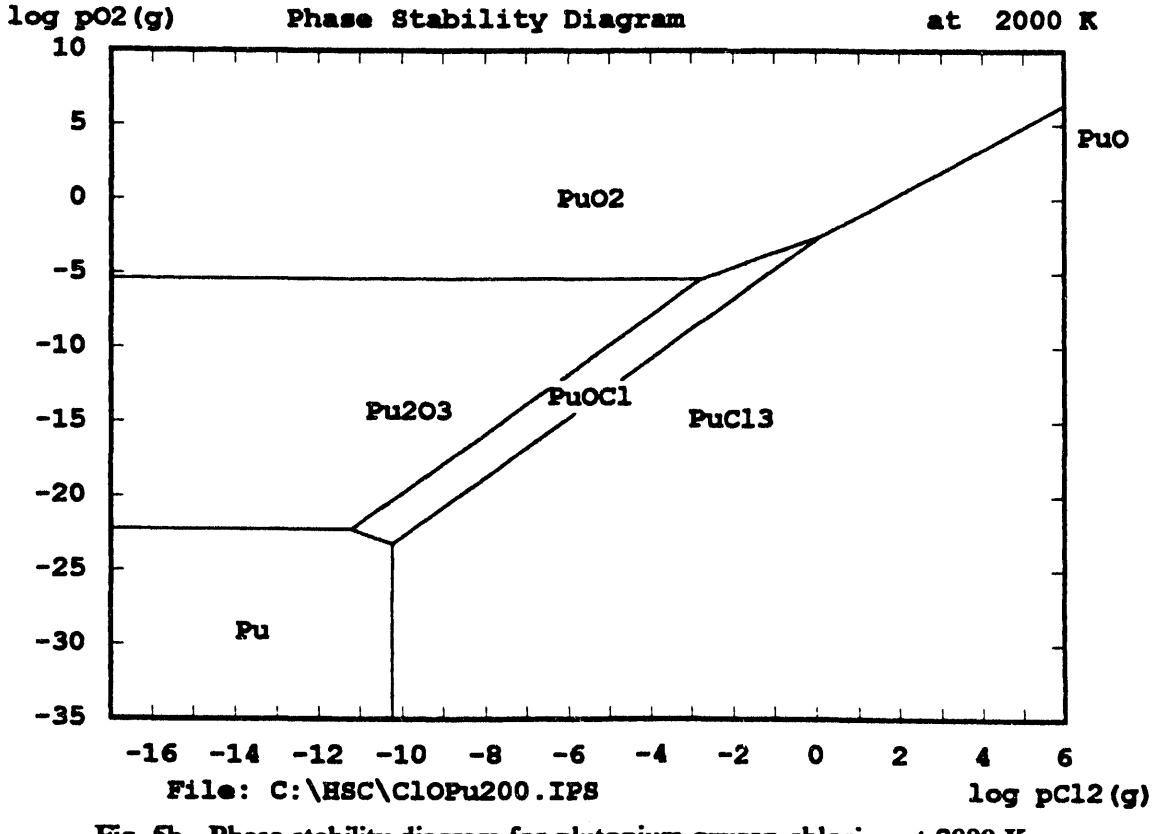

Fig. 5b. Phase stability diagram for plutonium-oxygen-chlorine at 2000 K.

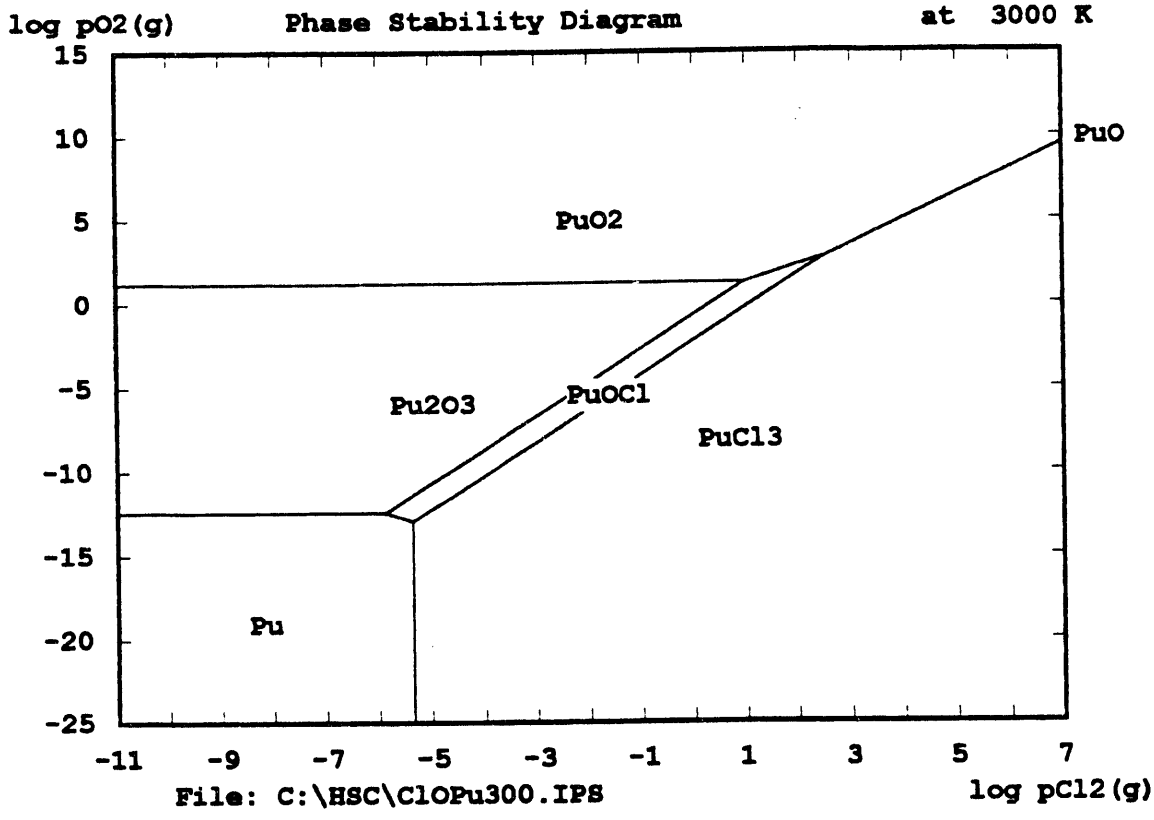

Fig. 5c. Phase stability diagram for plutonium-oxygen-chlorine at 3000 K.

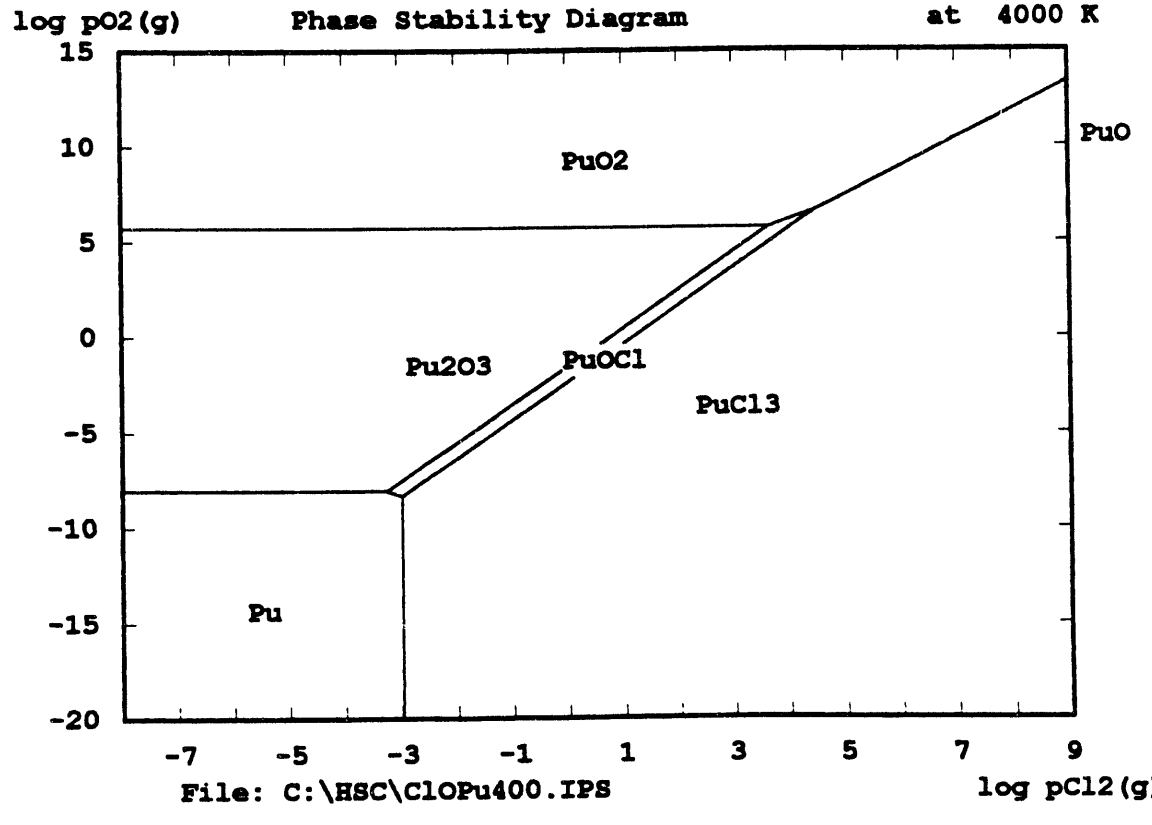

Fig. 5d. Phase stability diagram for plutonium-oxygen-chlorine at 4000 K.

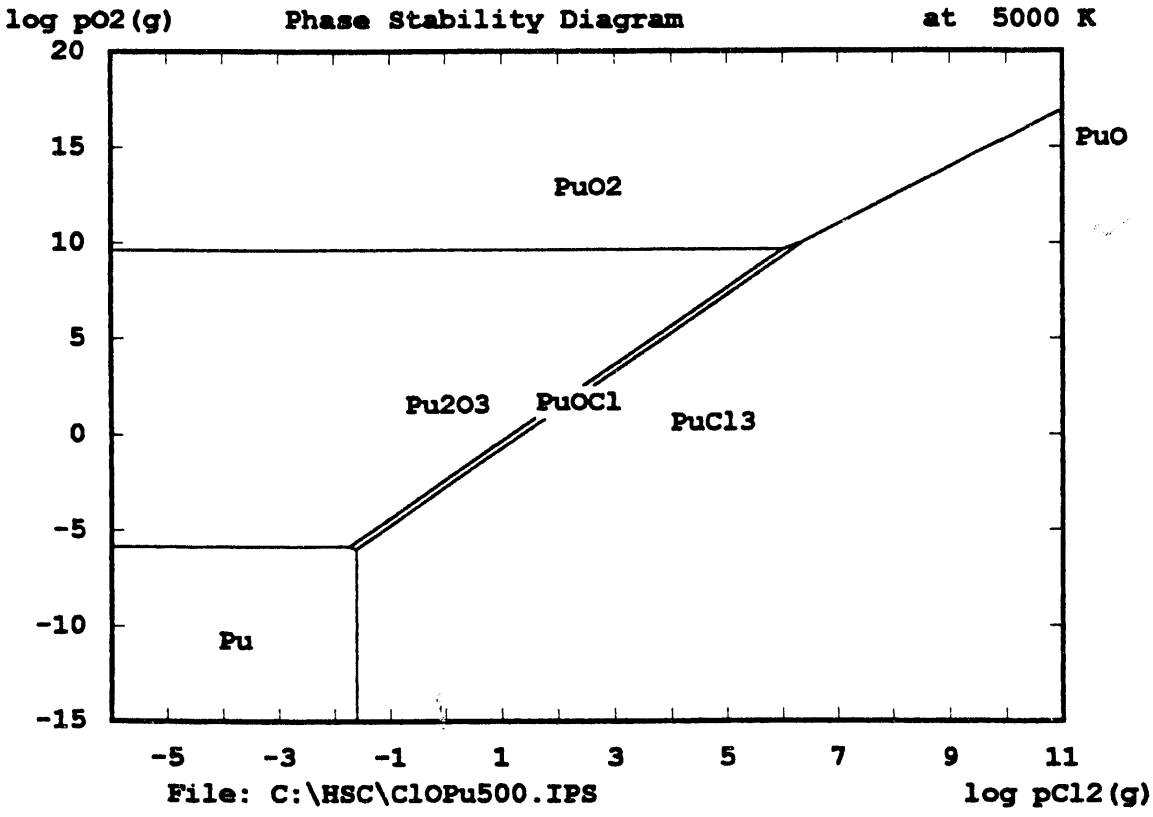

Fig. 5e. Phase stability diagram for plutonium-oxygen-chlorine at 5000 K.

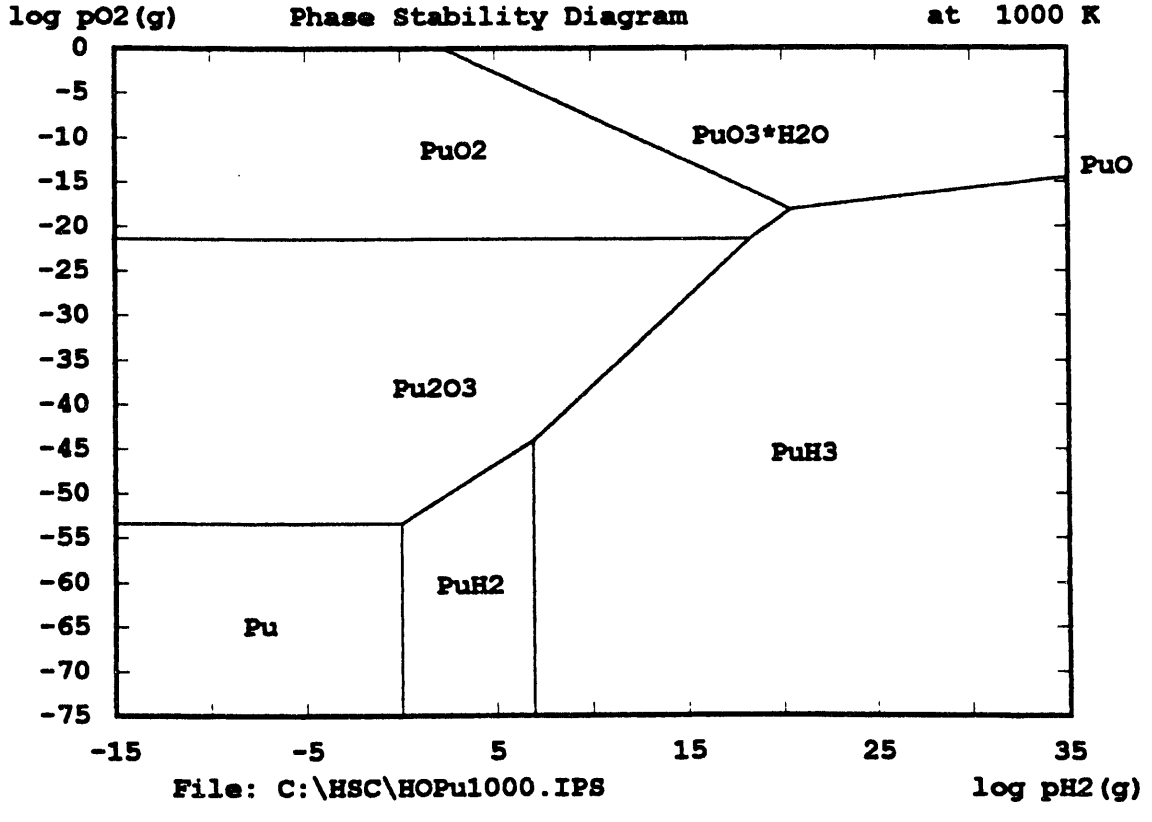

Fig. 6a. Phase stability diagram for plutonium-oxygen-hydrogen at 1000 K.

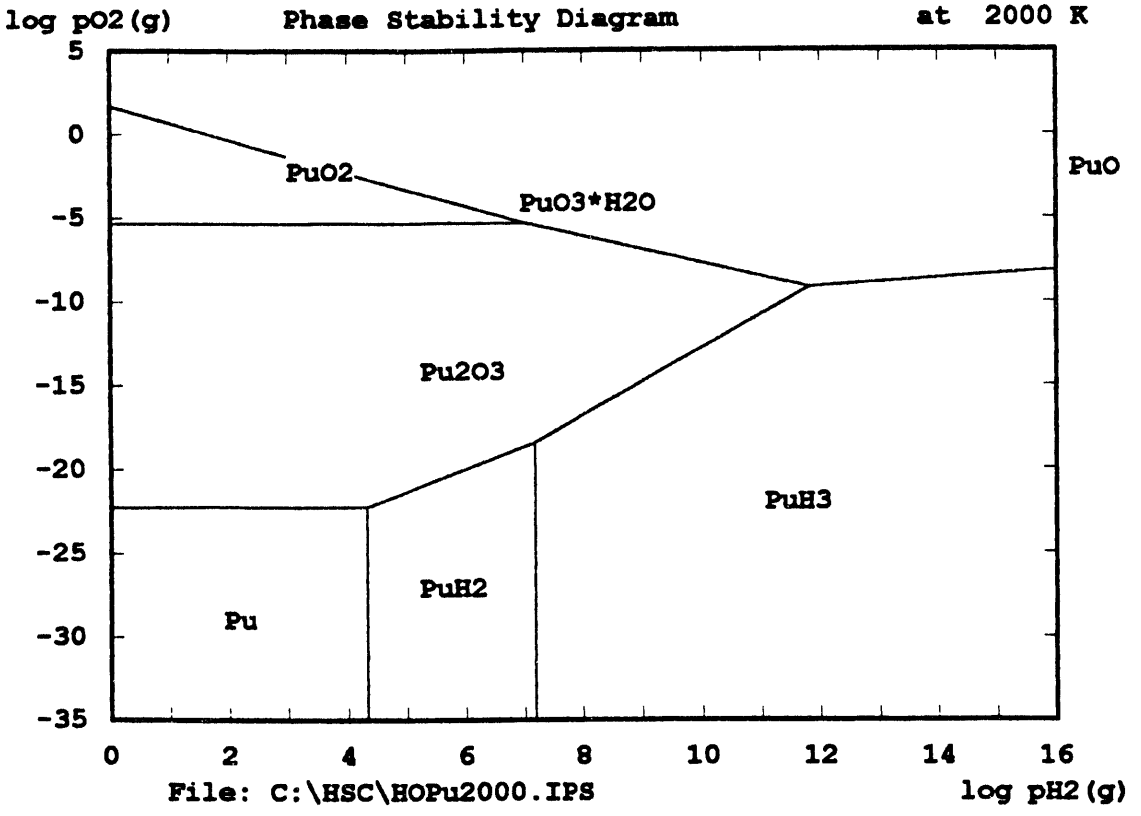

Fig. 6b. Phase stability diagram for plutonium-oxygen-hydrogen at 2000 K.

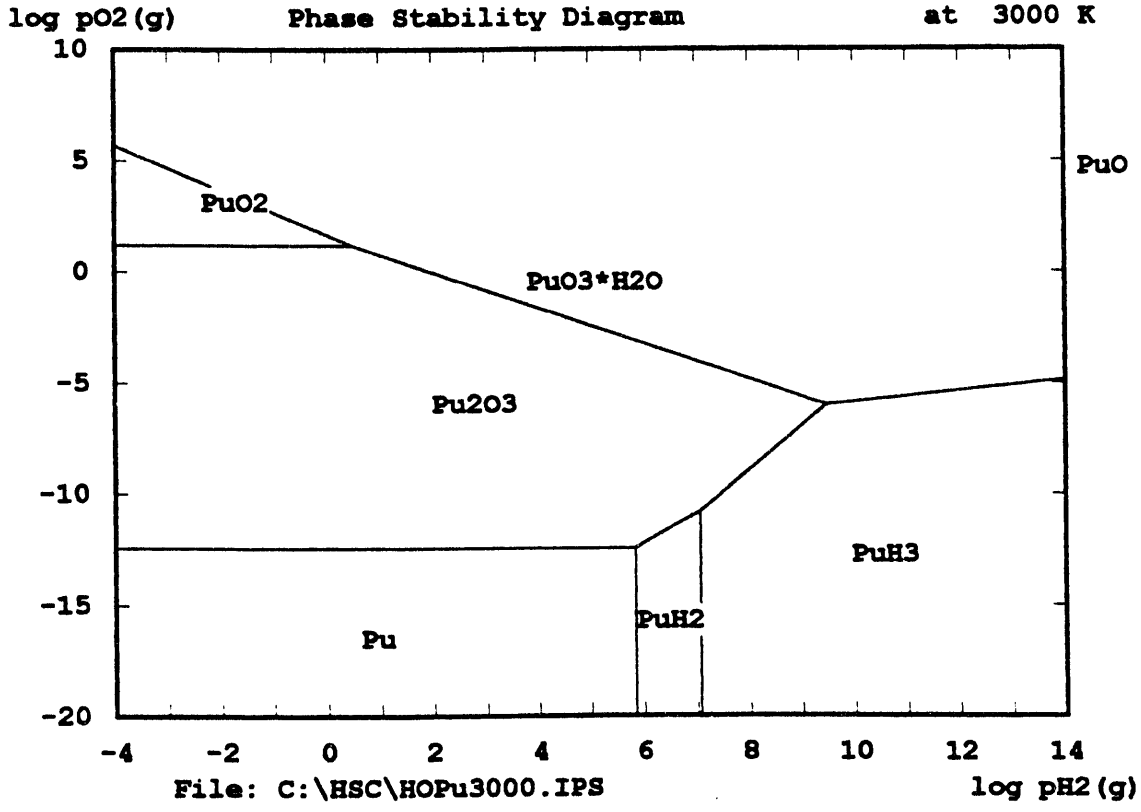

Fig. 6c. Phase stability diagram for plutonium-oxygen-hydrogen at 3000 K.

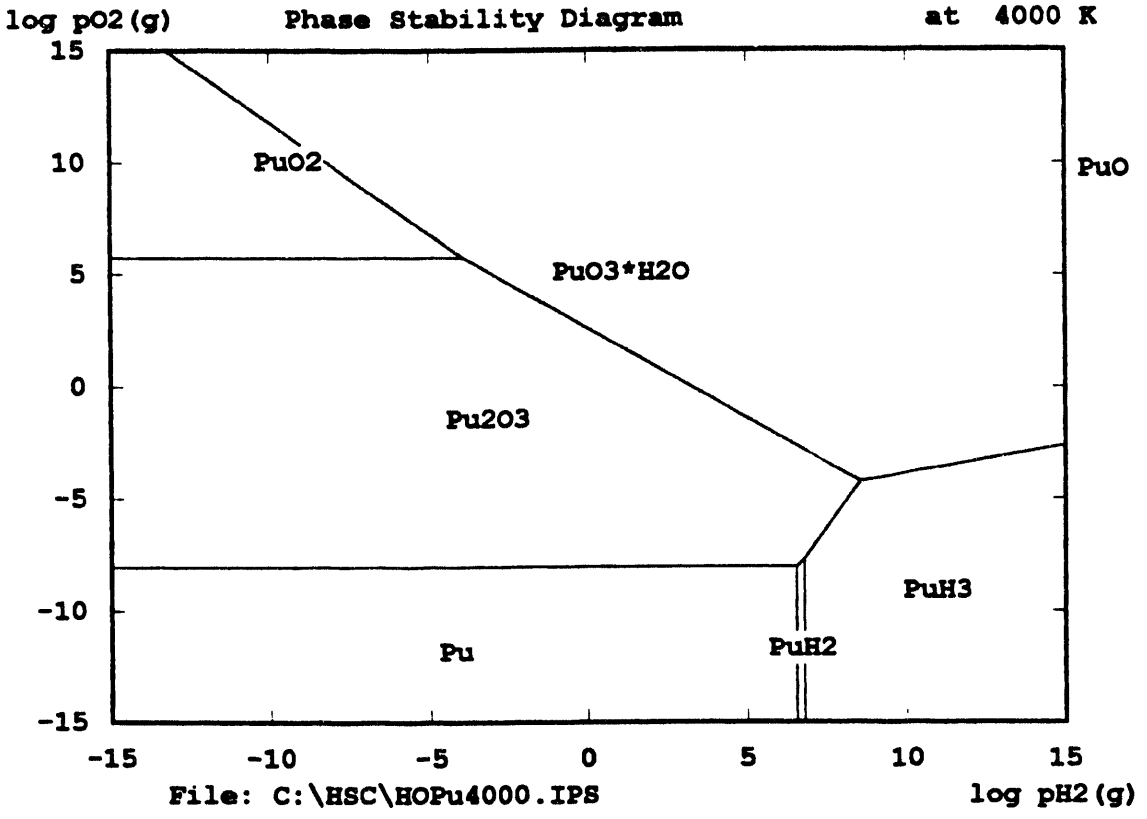

Fig. 6d. Phase stability diagram for plutonium-oxygen-hydrogen at 4000 K.

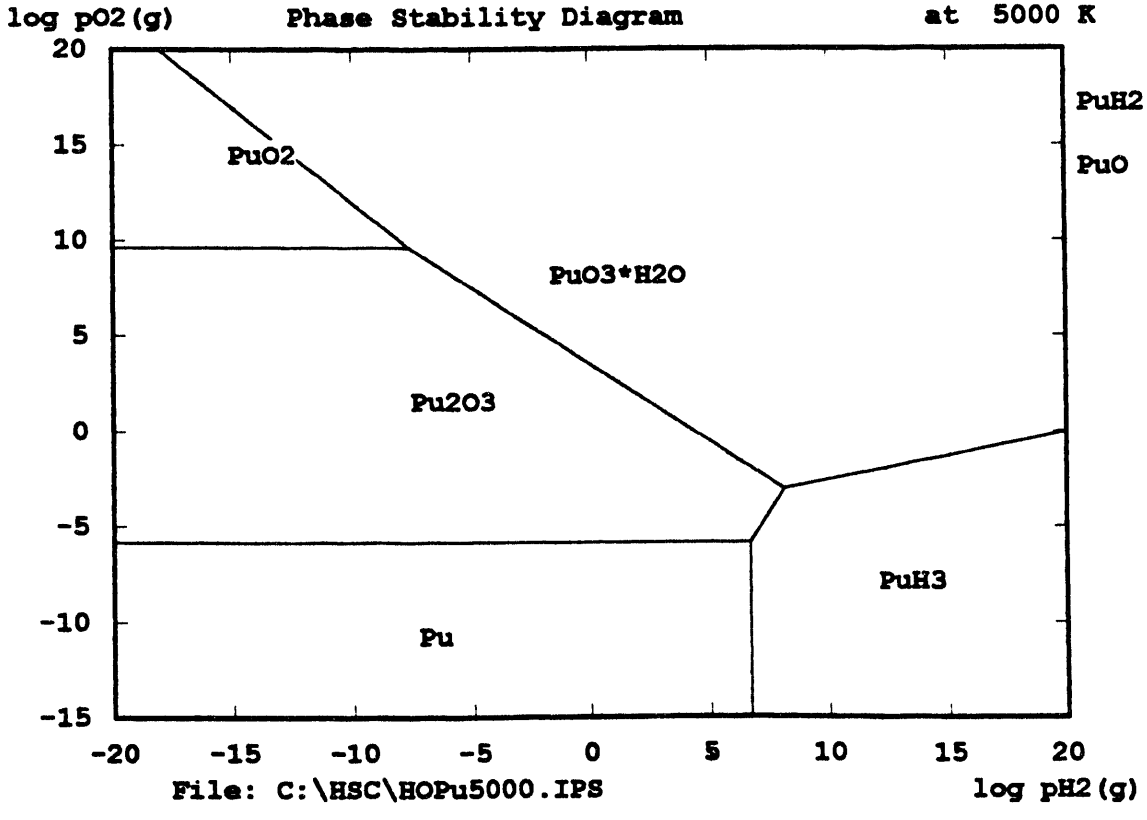

Fig. 6e. Phase stability diagram for plutonium-oxygen-hydrogen at 5000 K.

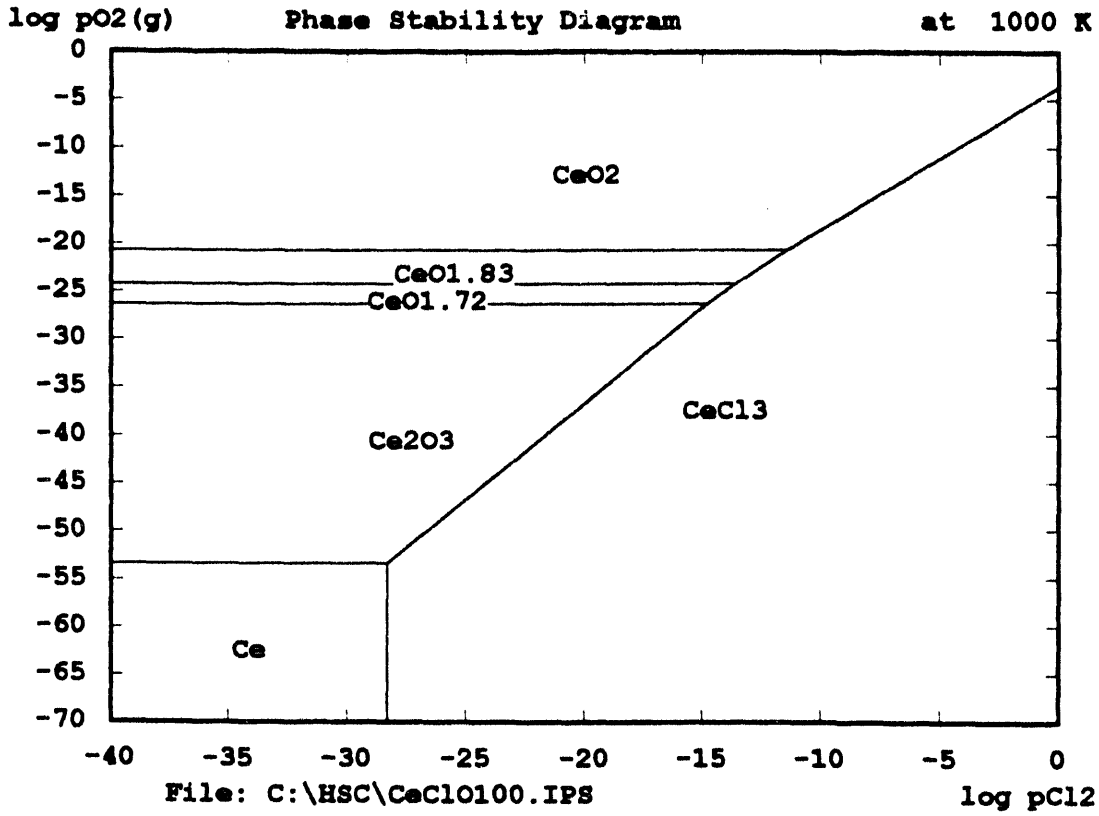

Fig. 7a. Phase stability diagram for cerium-oxygen-chlorine at 1000 K.

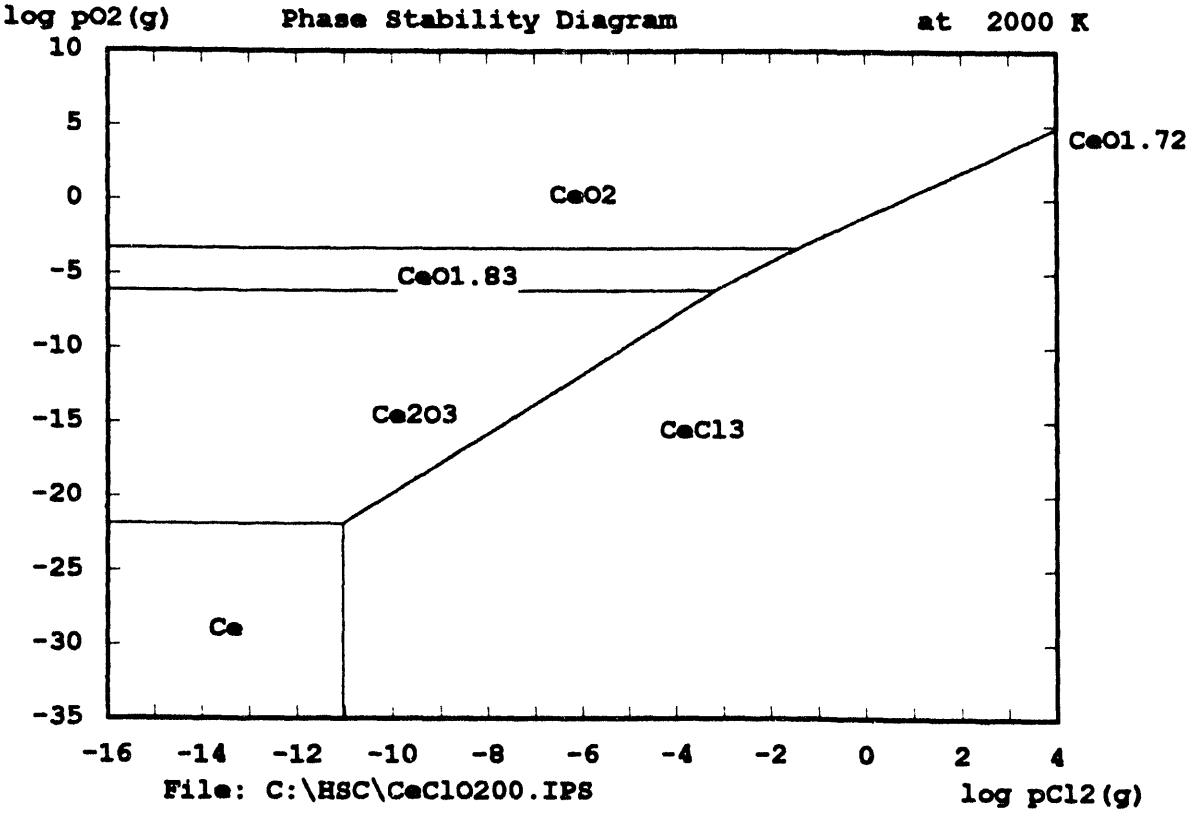

Fig. 7b. Phase stability diagram for cerium-oxygen-chlorine at 2000 K.

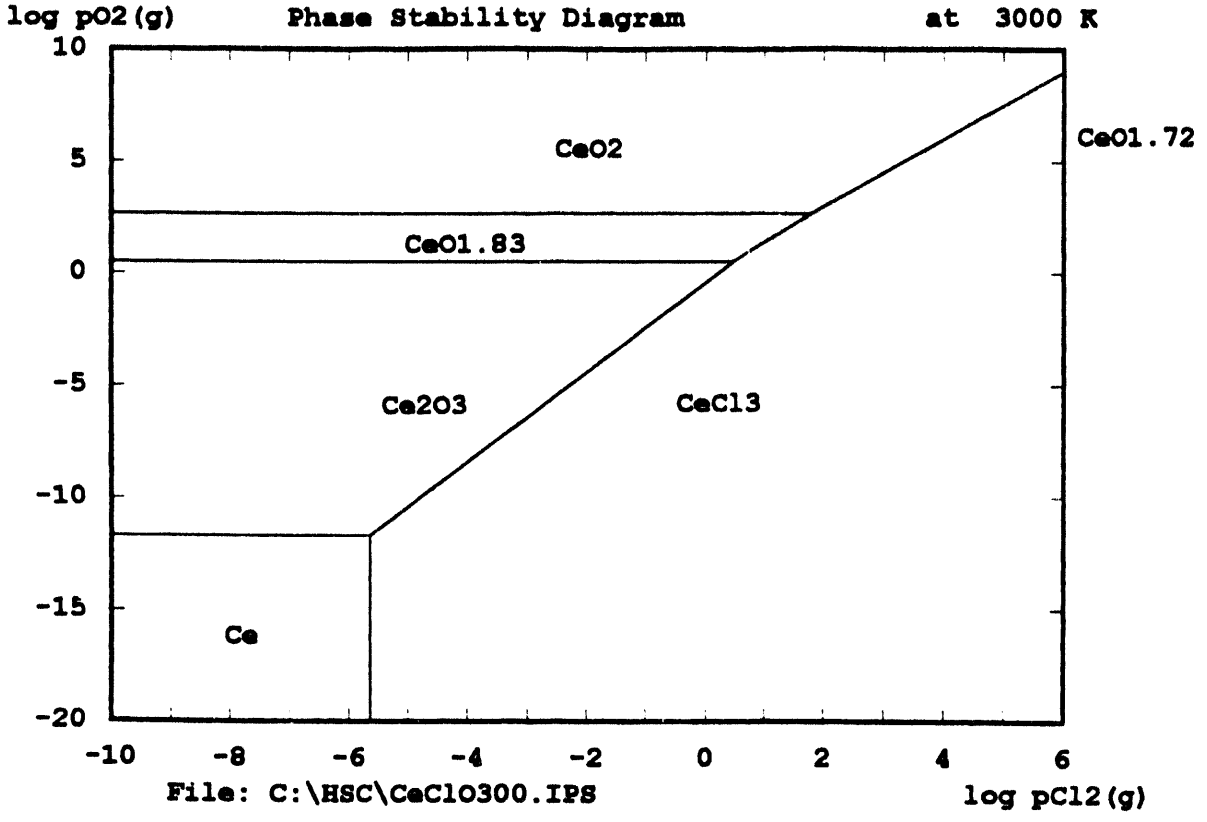

Fig. 7c. Phase stability diagram for cerium-oxygen-chlorine at 3000 K.

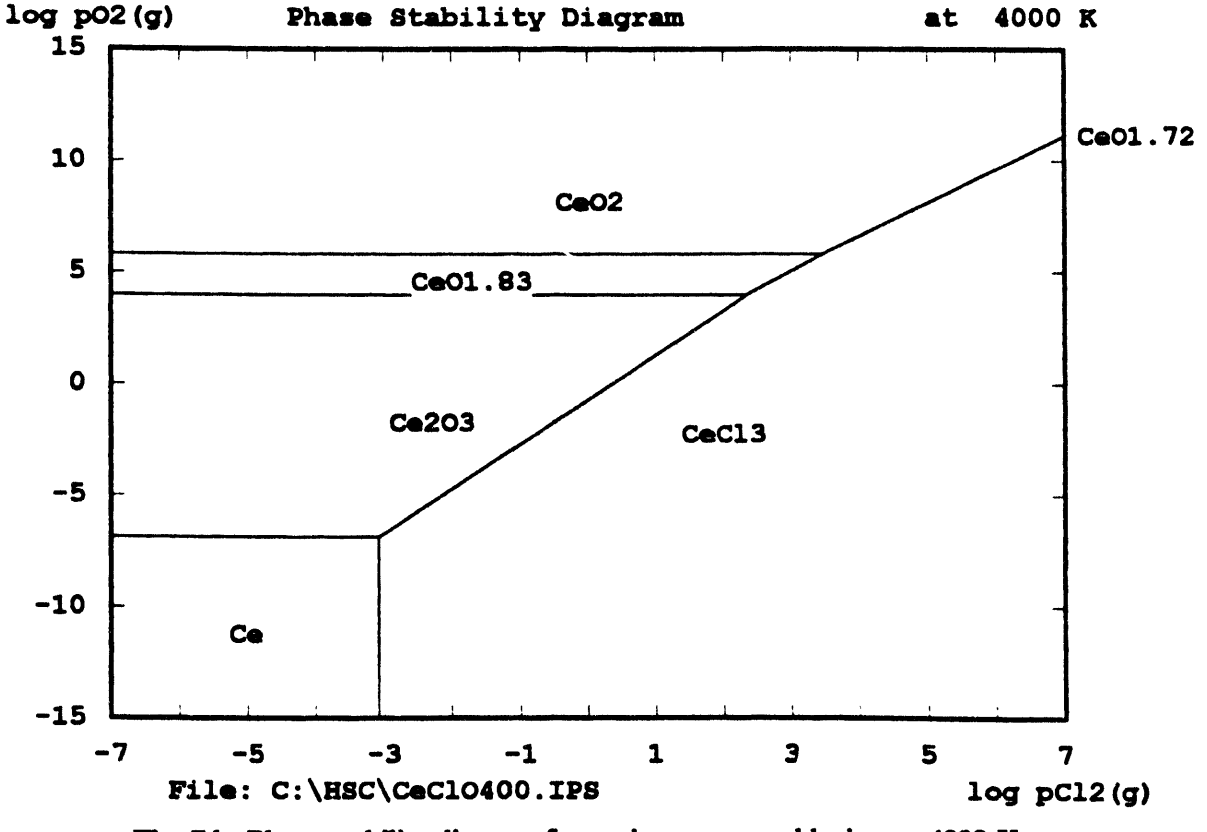

Fig. 7d. Phase stability diagram for cerium-oxygen-chlorine at 4000 K.

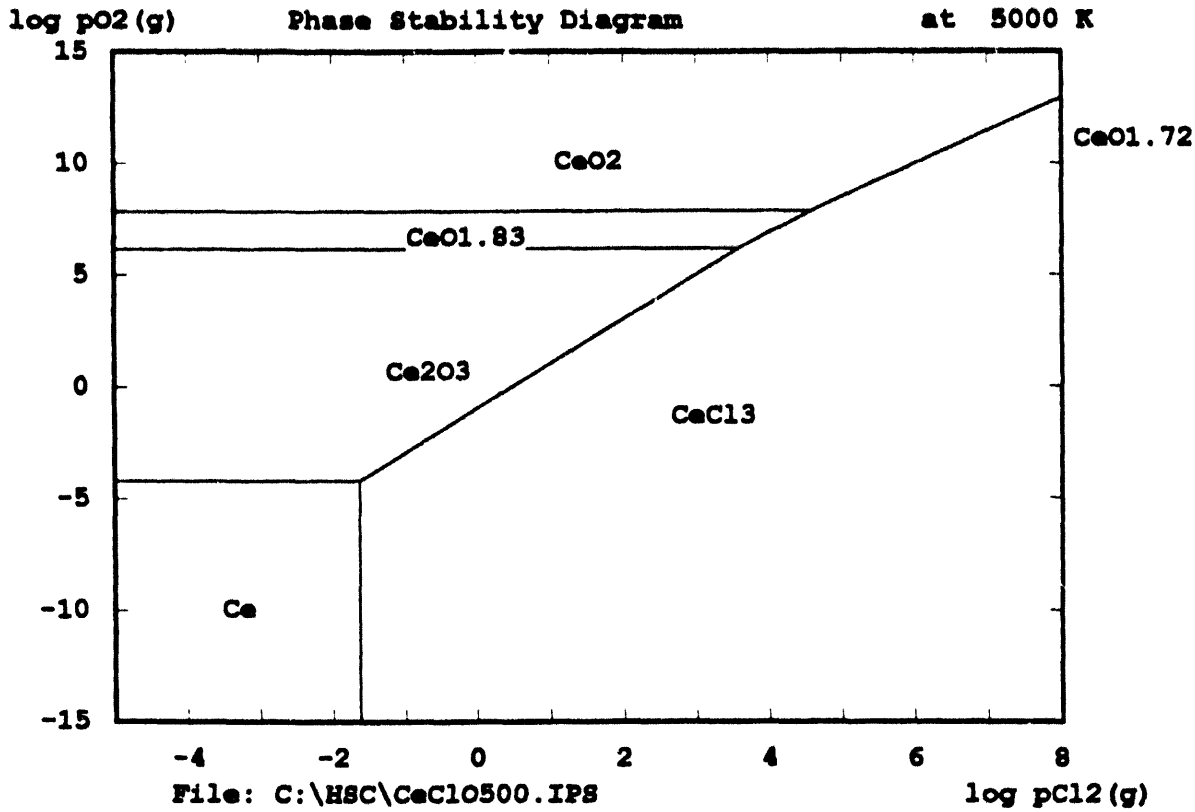

Fig. 7e. Phase stability diagram for cerium-oxygen-chlorine at 5000 K.

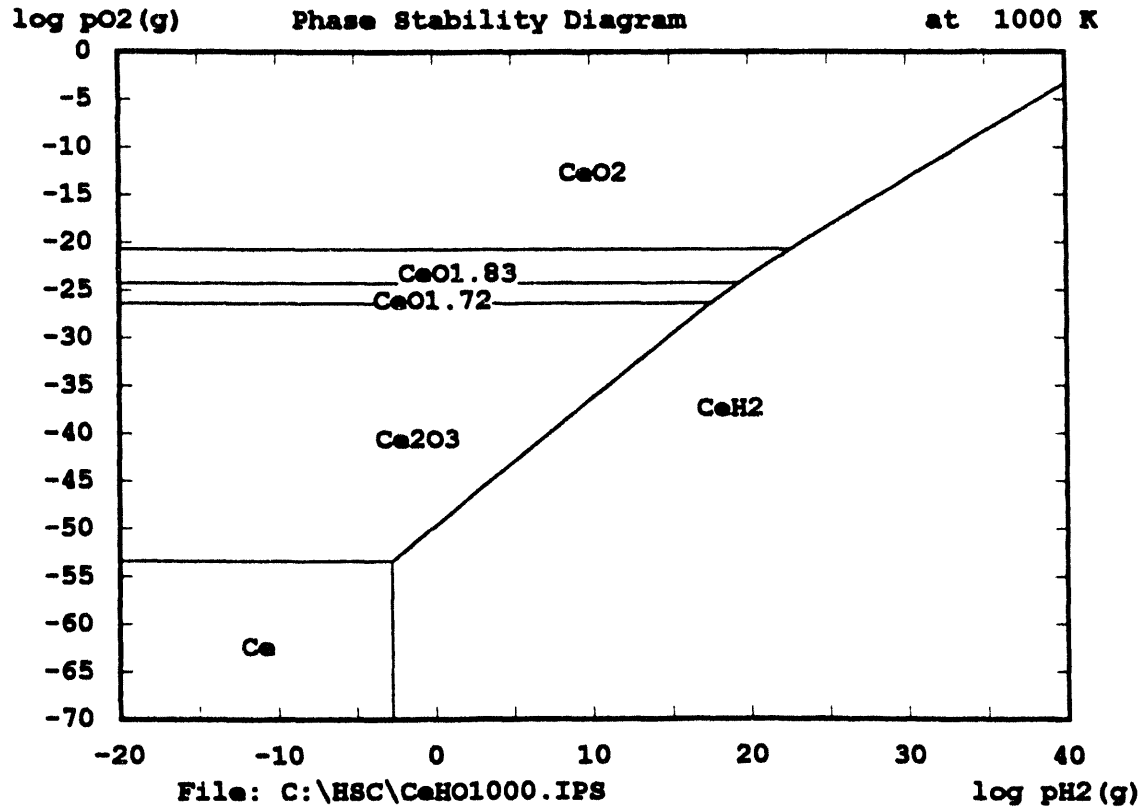

Fig. 8a. Phase stability diagram for cerium-oxygen-hydrogen at 1000 K.

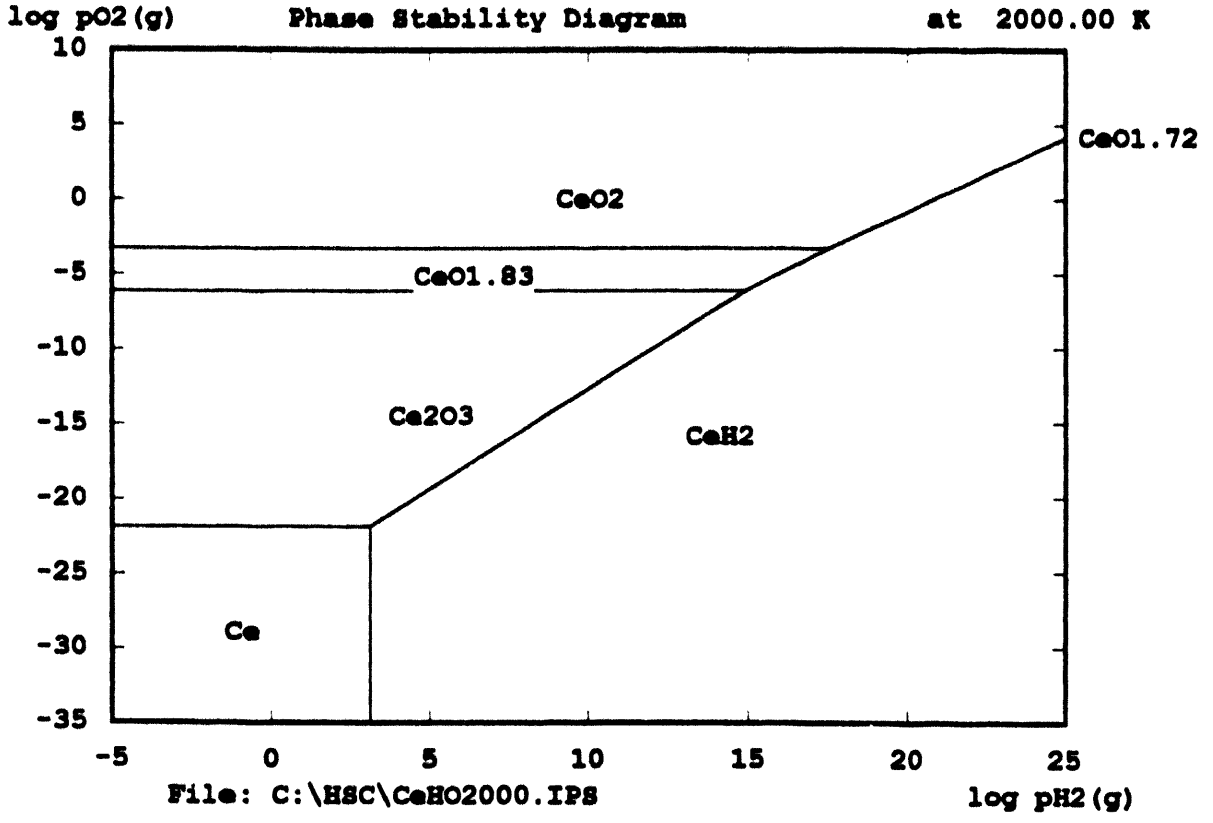

Fig. 8b. Phase stability diagram for cerium-oxygen-hydrogen at 2000 K.

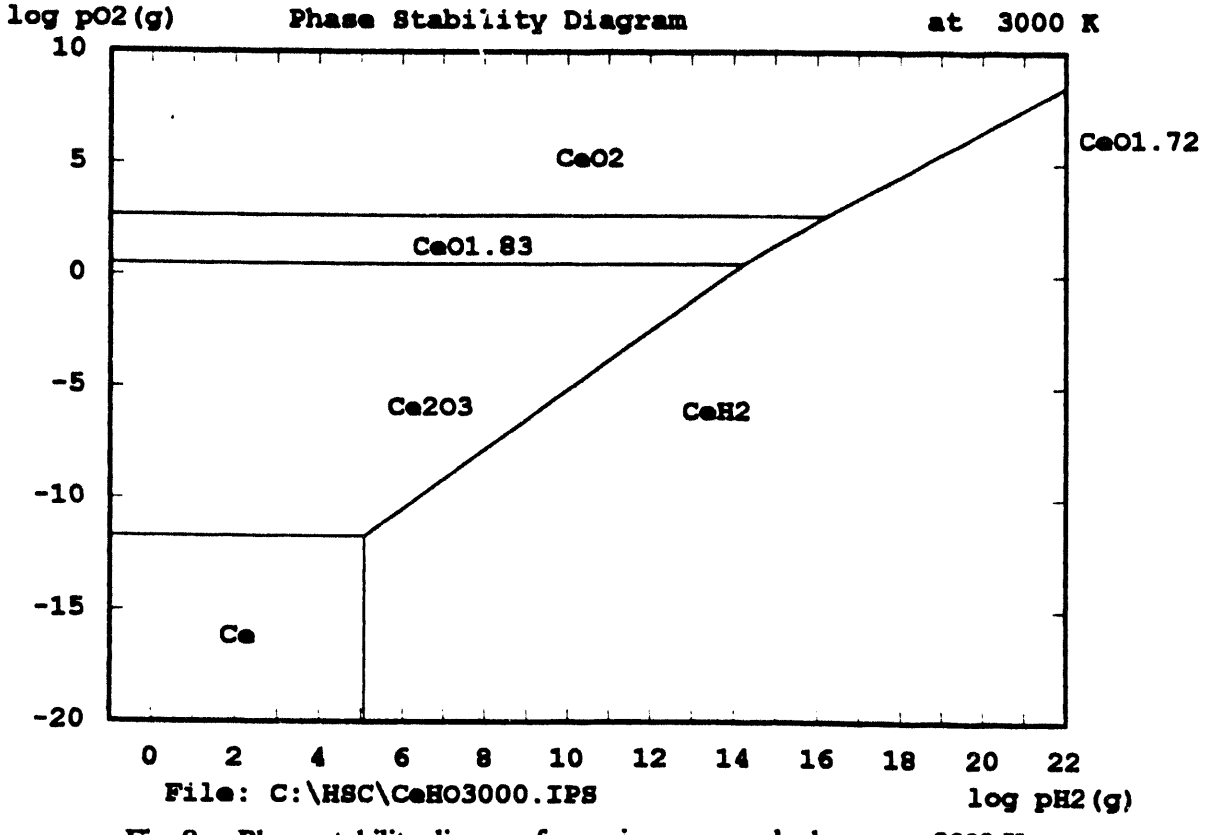

Fig. 8c. Phase stability diagram for cerium-oxygen-hydrogen at 3000 K.

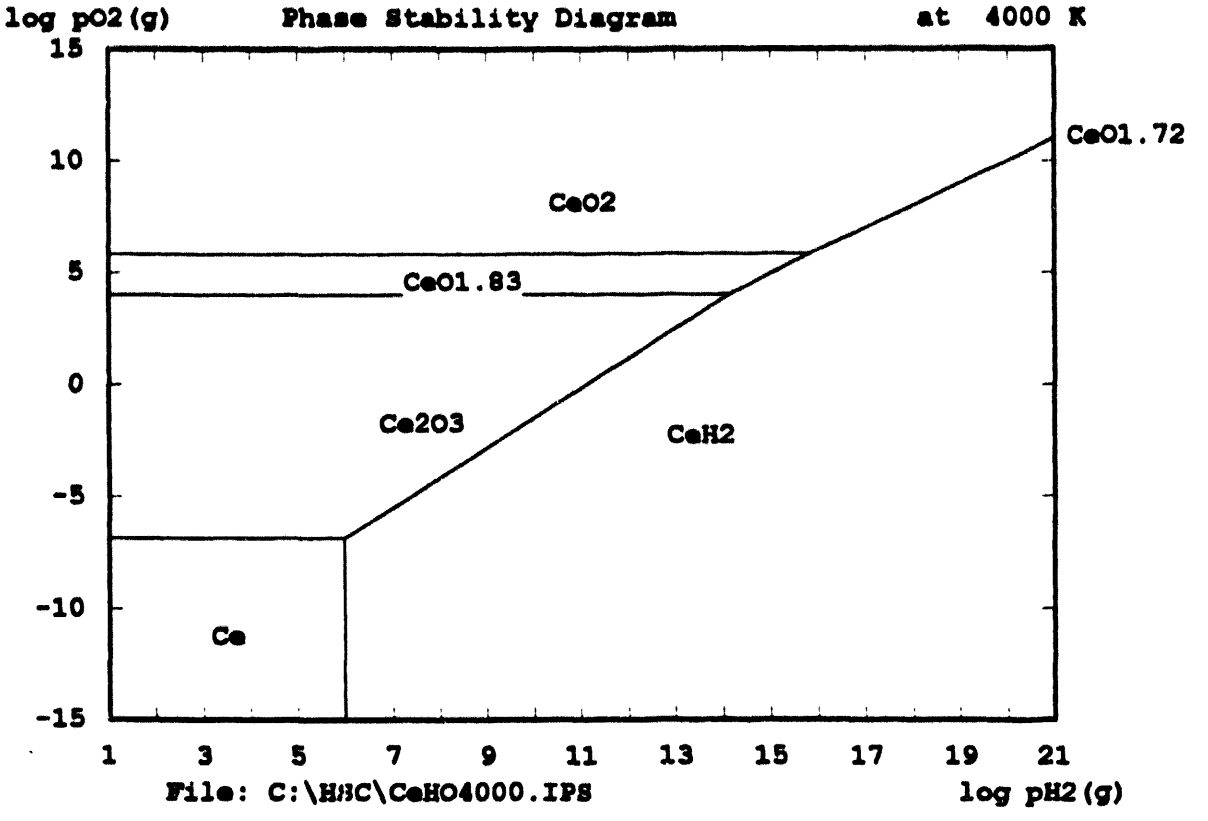

Fig. 8d. Phase stability diagram for cerium-oxygen-hydrogen at 4000 K.

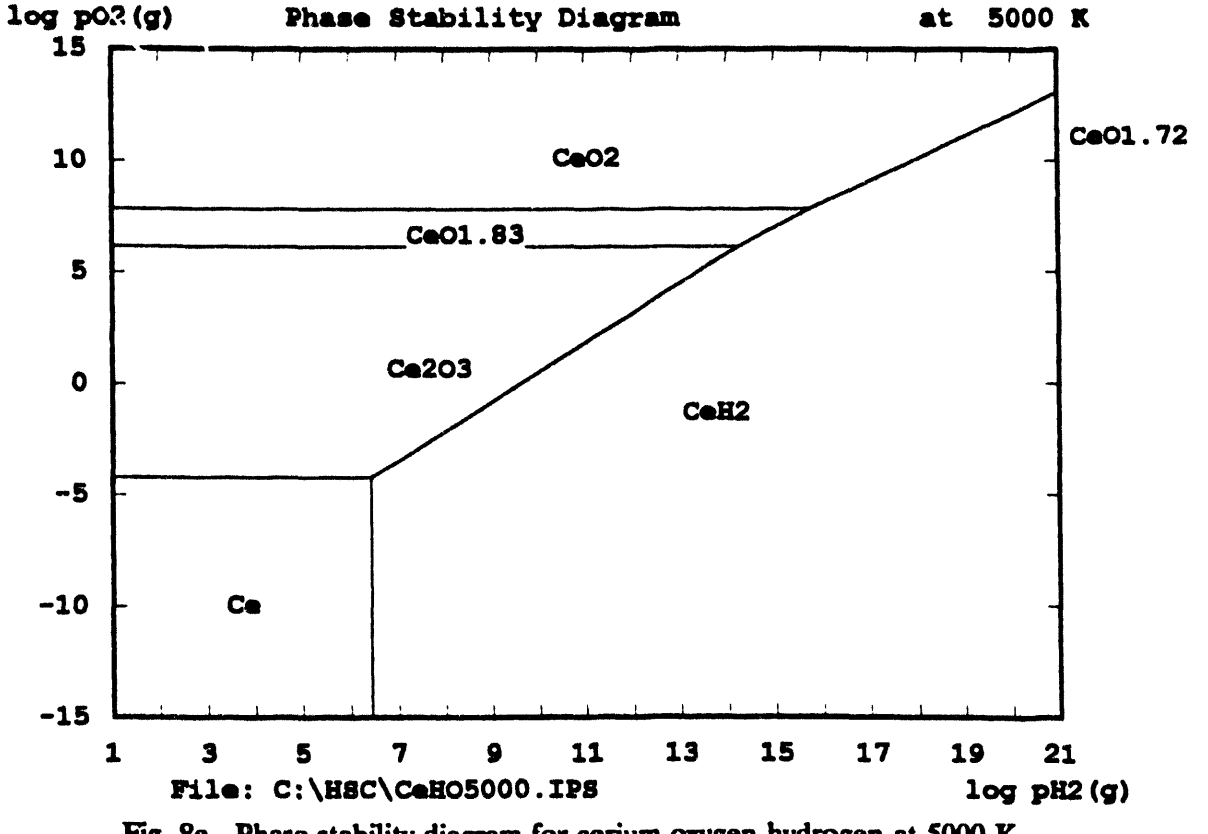

Fig. 8e. Phase stability diagram for cerium-oxygen-hydrogen at 5000 K.

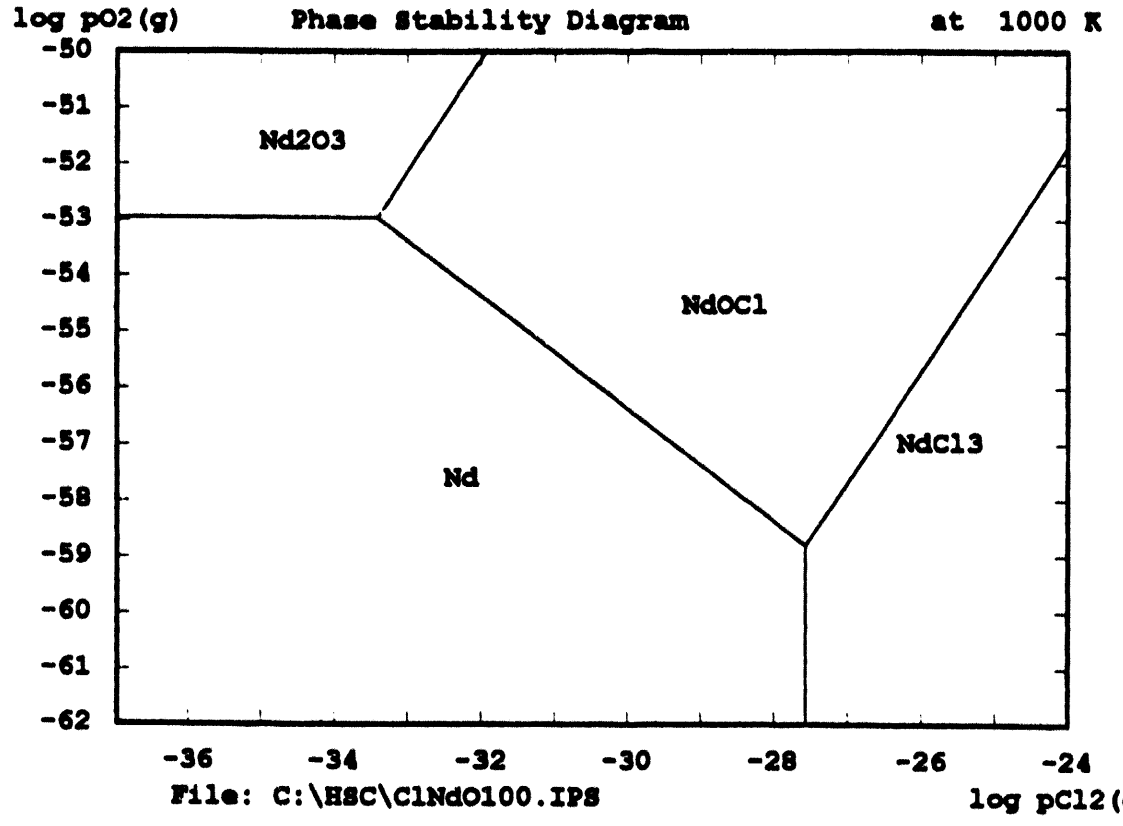

Fig. 9a. Phase stability diagram for neodymium-oxygen-chlorine at 1000 K.

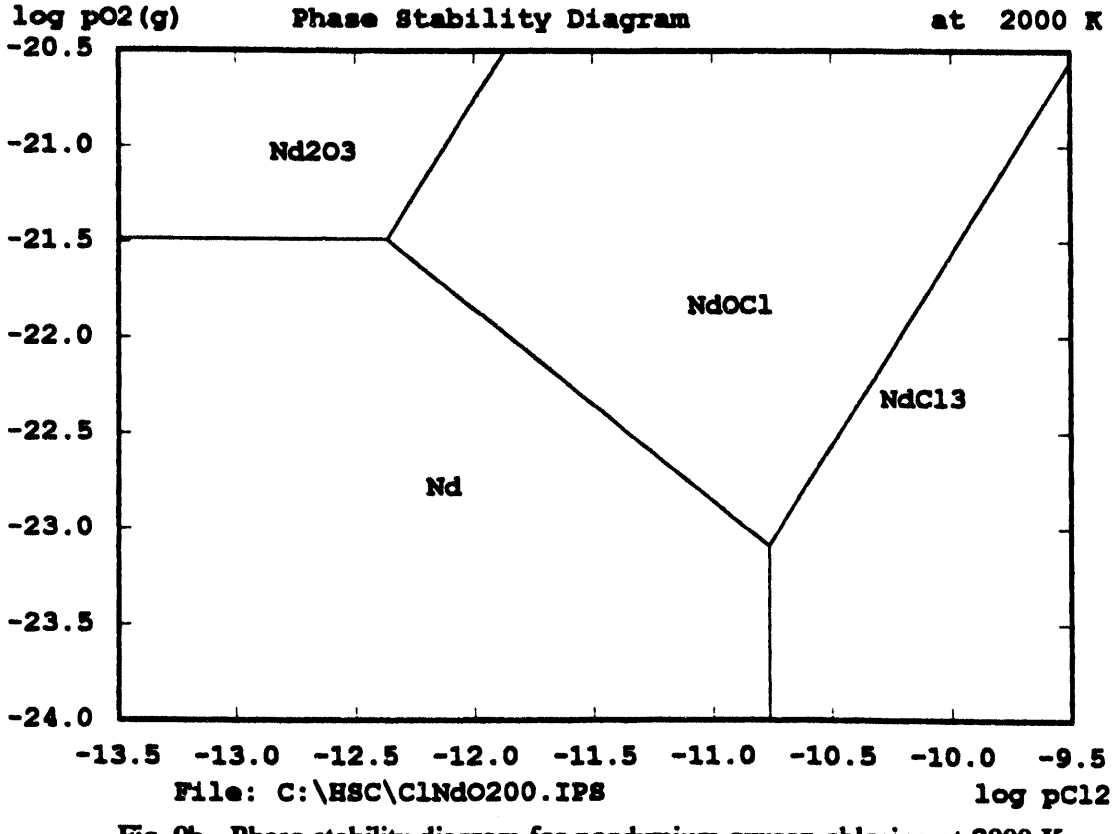

Fig. 9b. Phase stability diagram for neodymium-oxygen-chlorine at 2000 K.

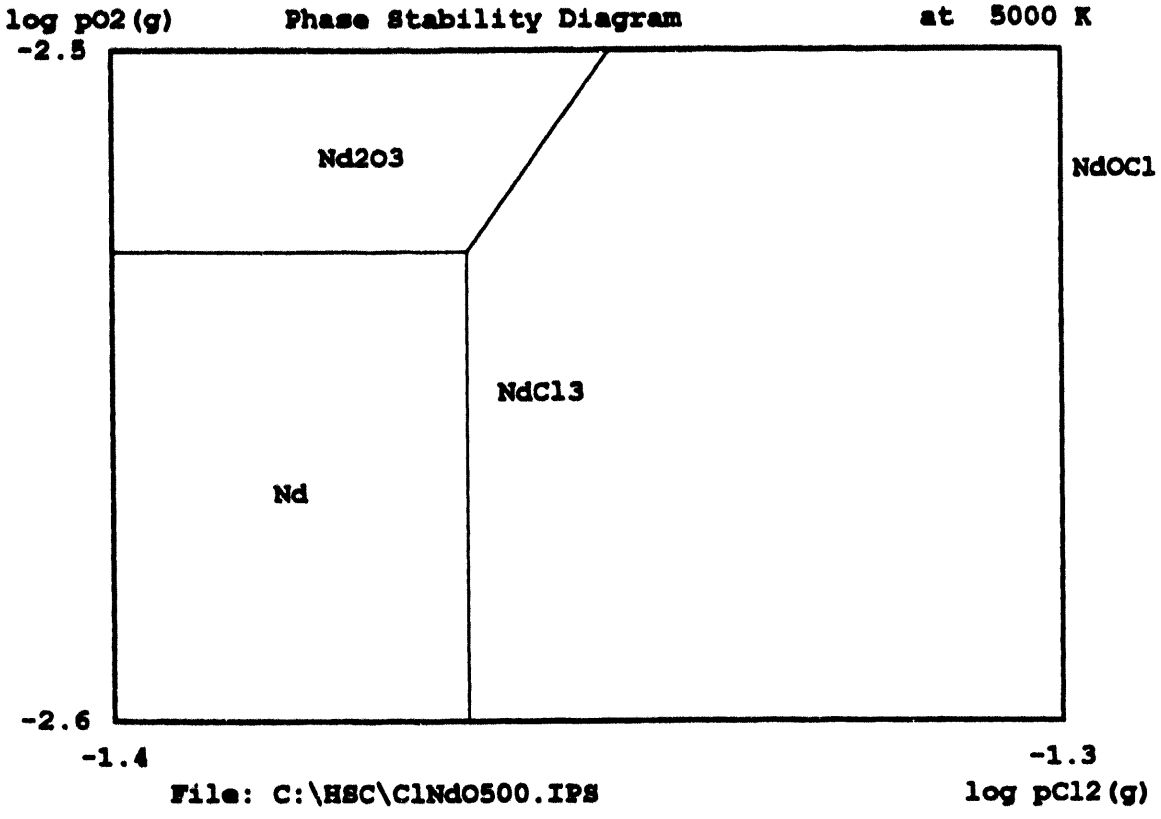

Fig. 9c. Phase stability diagram for neodymium-oxygen-chlorine at 5000 K.

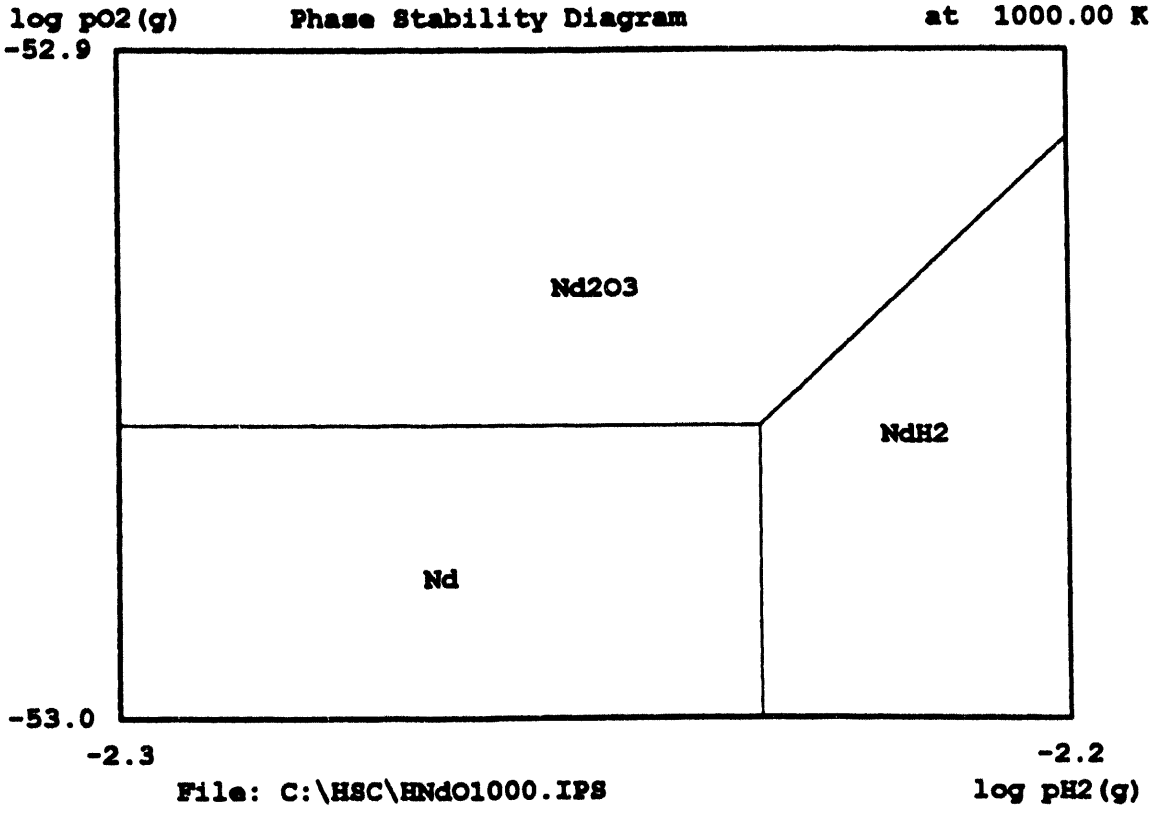

Fig. 10a. Phase stability diagram for neodymium-oxygen-hydrogen at 1000 K.

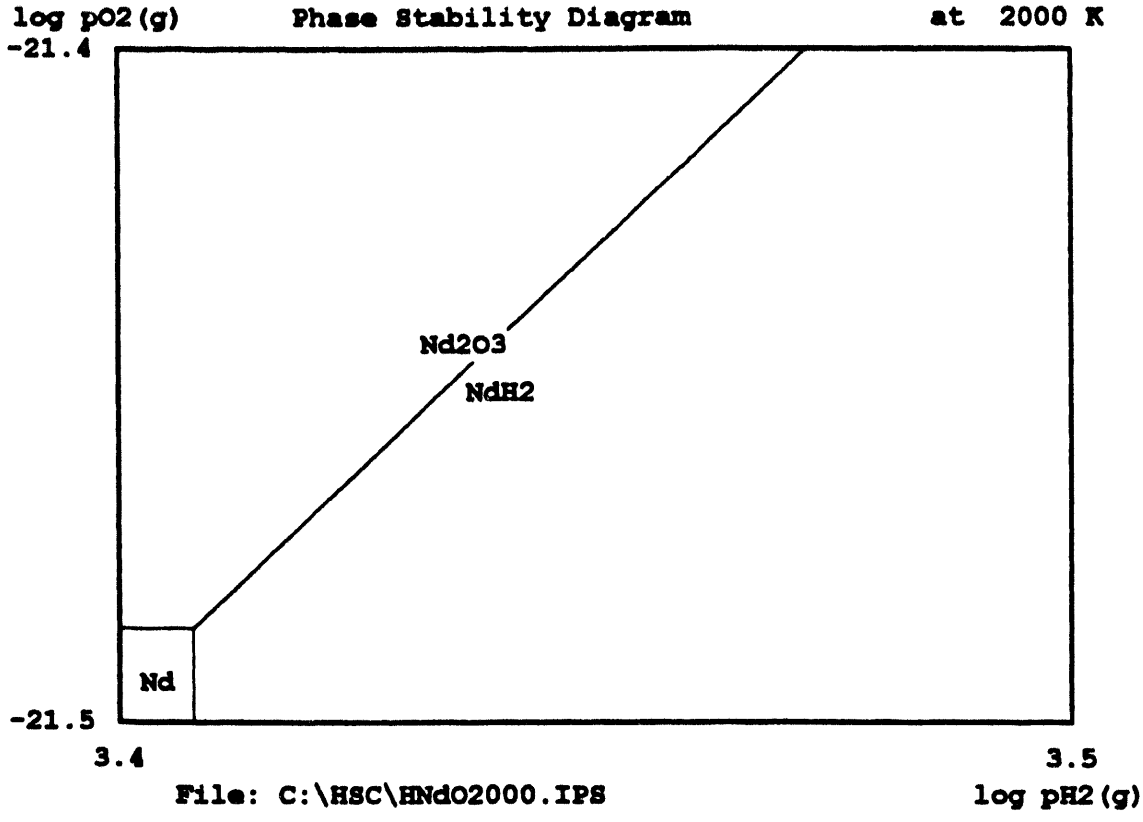

Fig. 10b. Phase stability diagram for neodymium-oxygen-hydrogen at 2000 K.

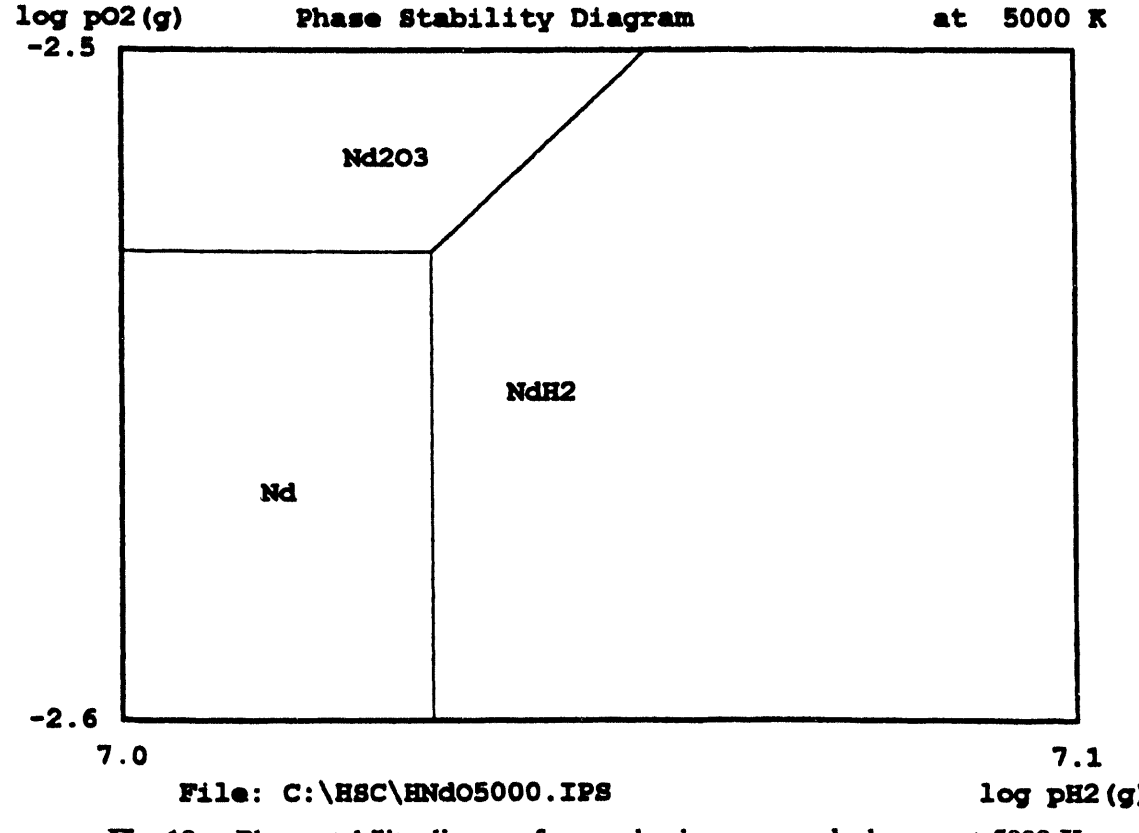

Fig. 10c. Phase stability diagram for neodymium-oxygen-hydrogen at 5000 K.

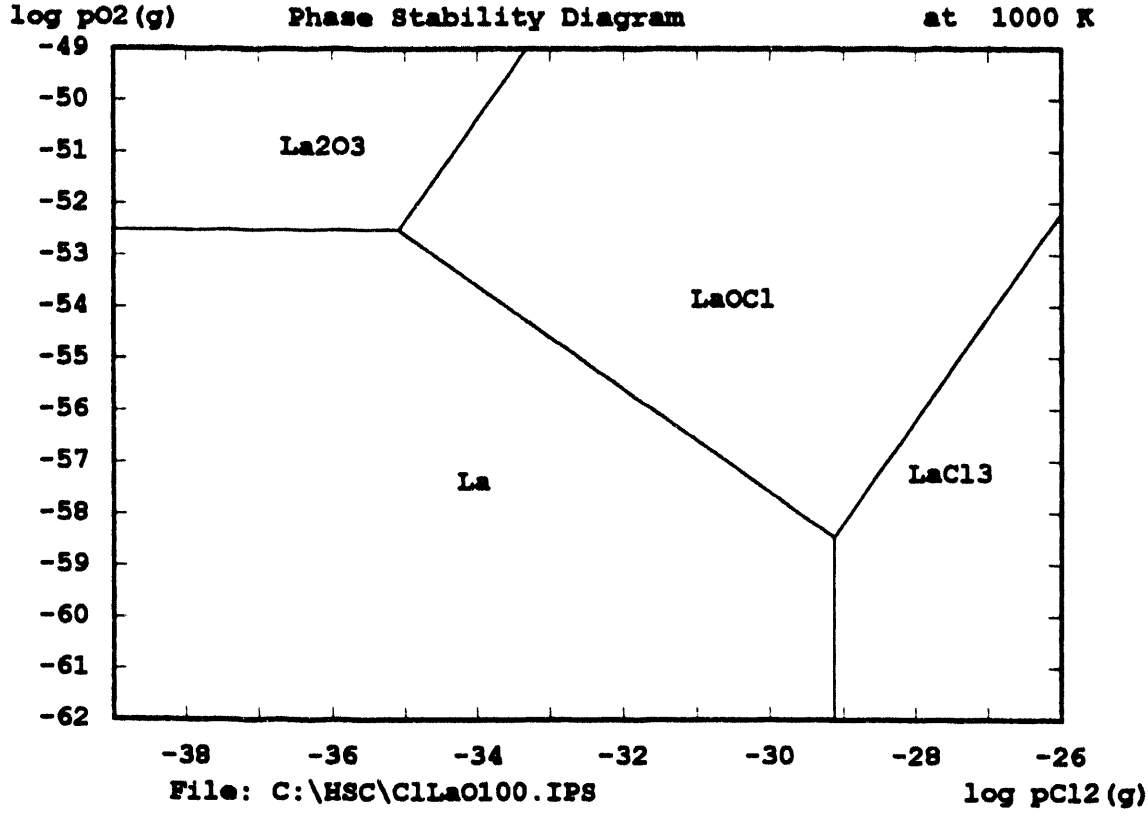

Fig. 11a. Phase stability diagram for lanthanum-oxygen-chlorine at 1000 K.

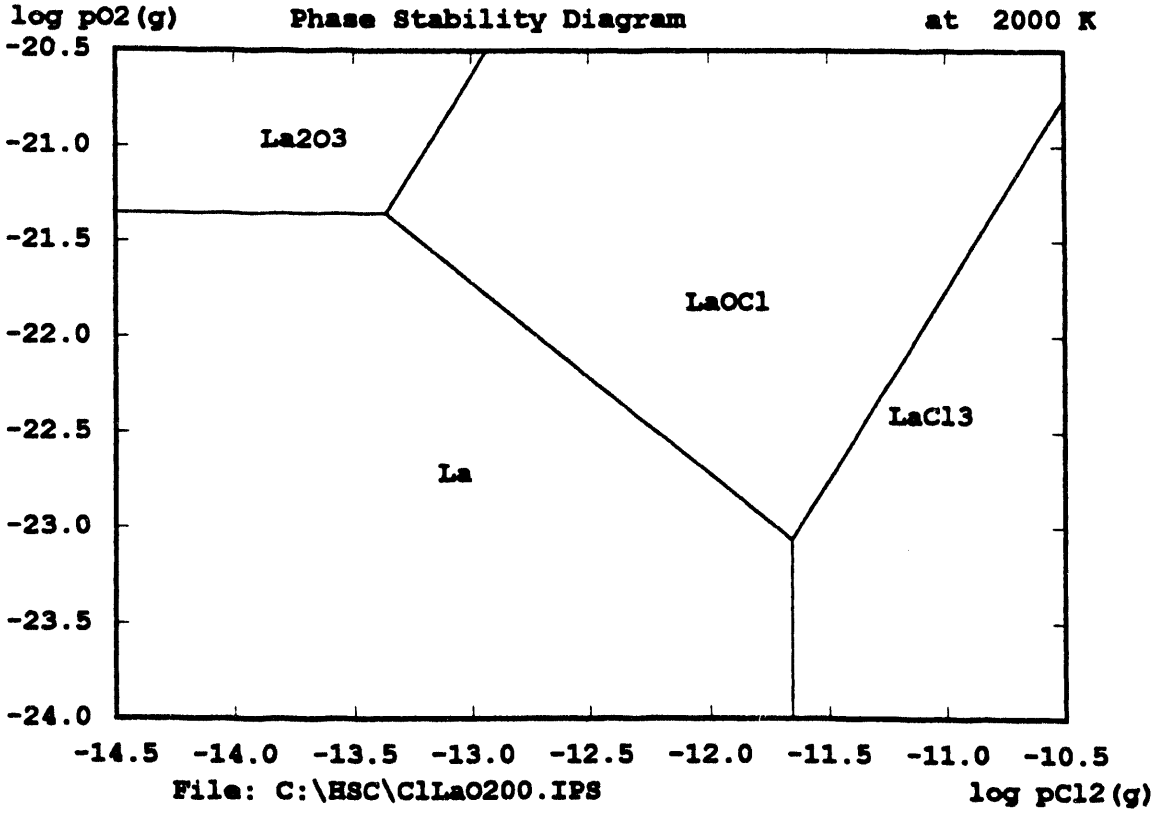

Fig. 11b. Phase stability diagram for lanthanum-oxygen-chlorine at 2000 K.

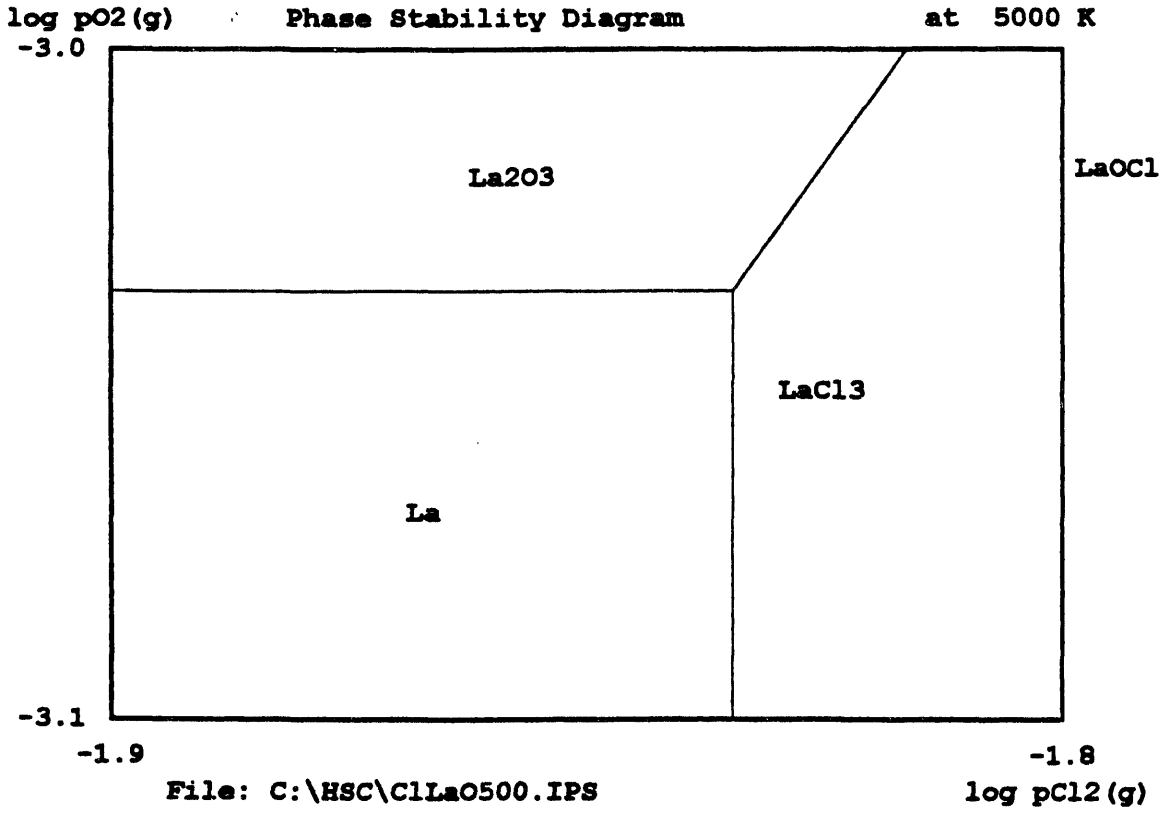

Fig. 11c. Phase stability diagram for lanthanum-oxygen-chlorine at 5000 K.

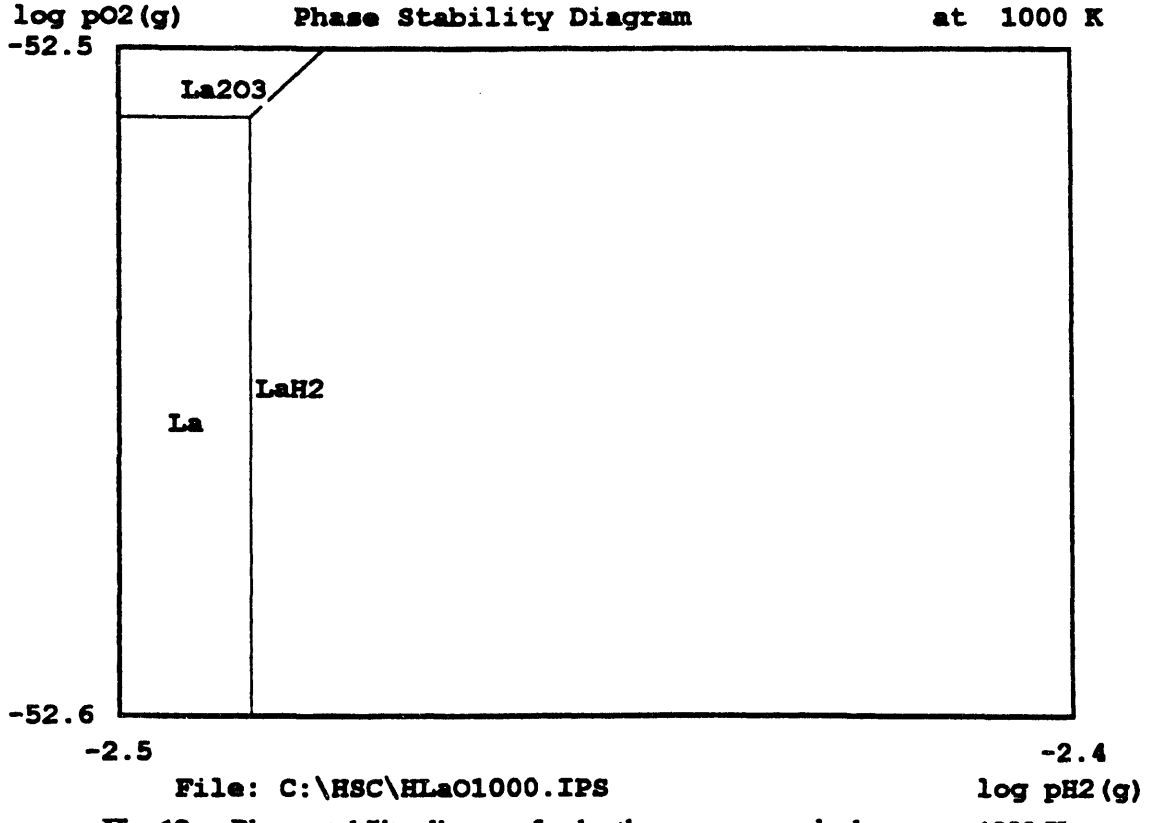

Fig. 12a. Phase stability diagram for lanthanum-oxygen-hydrogen at 1000 K.

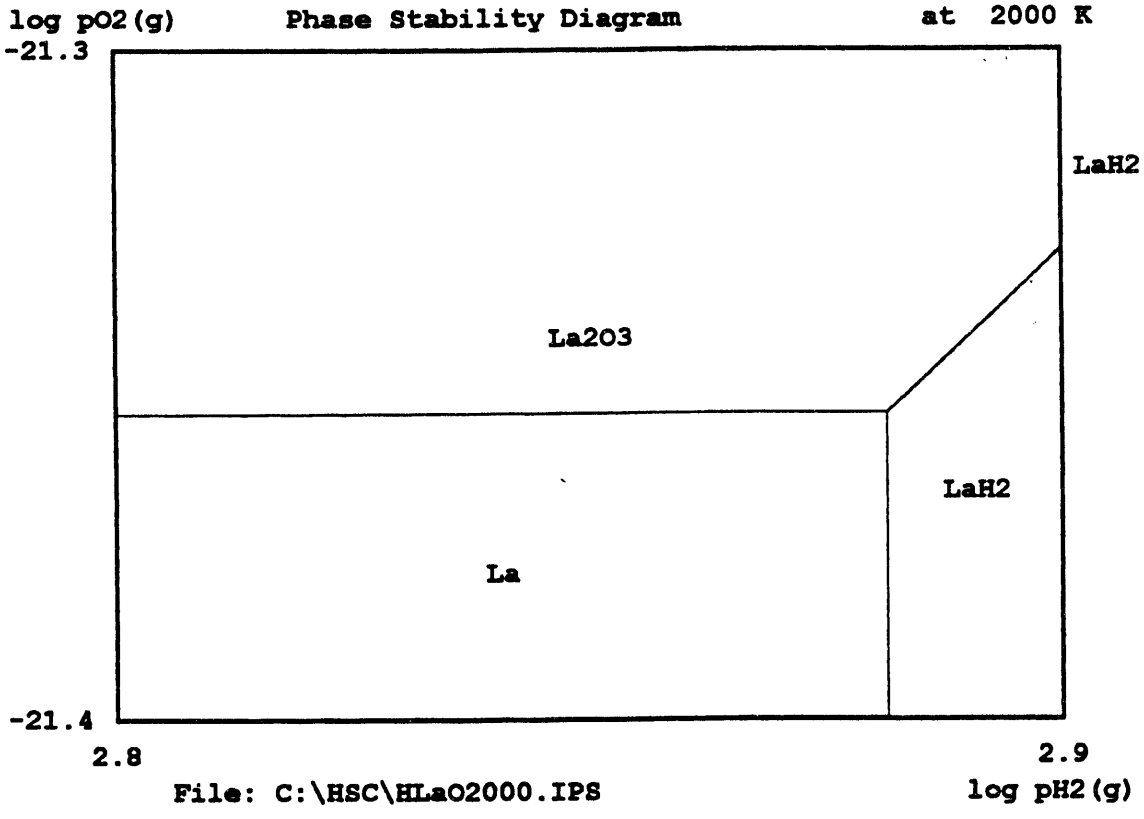

Fig. 12b. Phase stability diagram for lanthanum-oxygen-hydrogen at 2000 K.

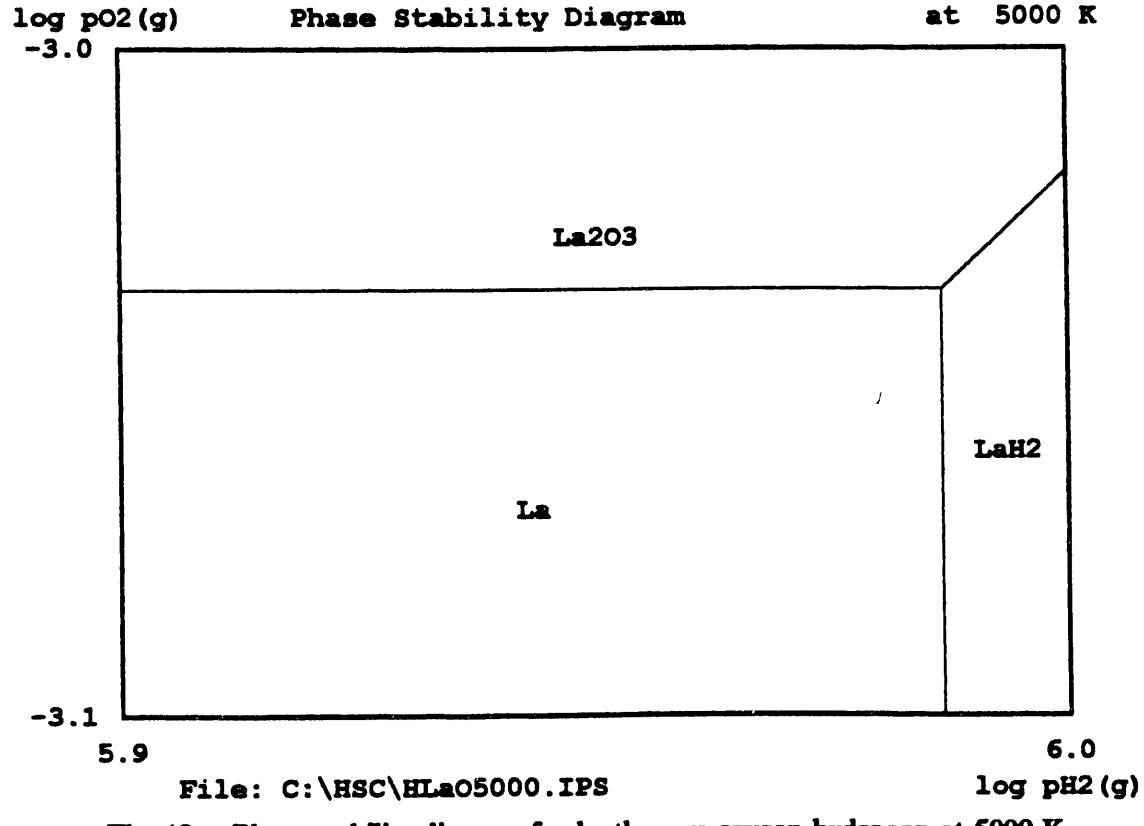

Fig. 12c. Phase stability diagram for lanthanum-oxygen-hydrogen at 5000 K.

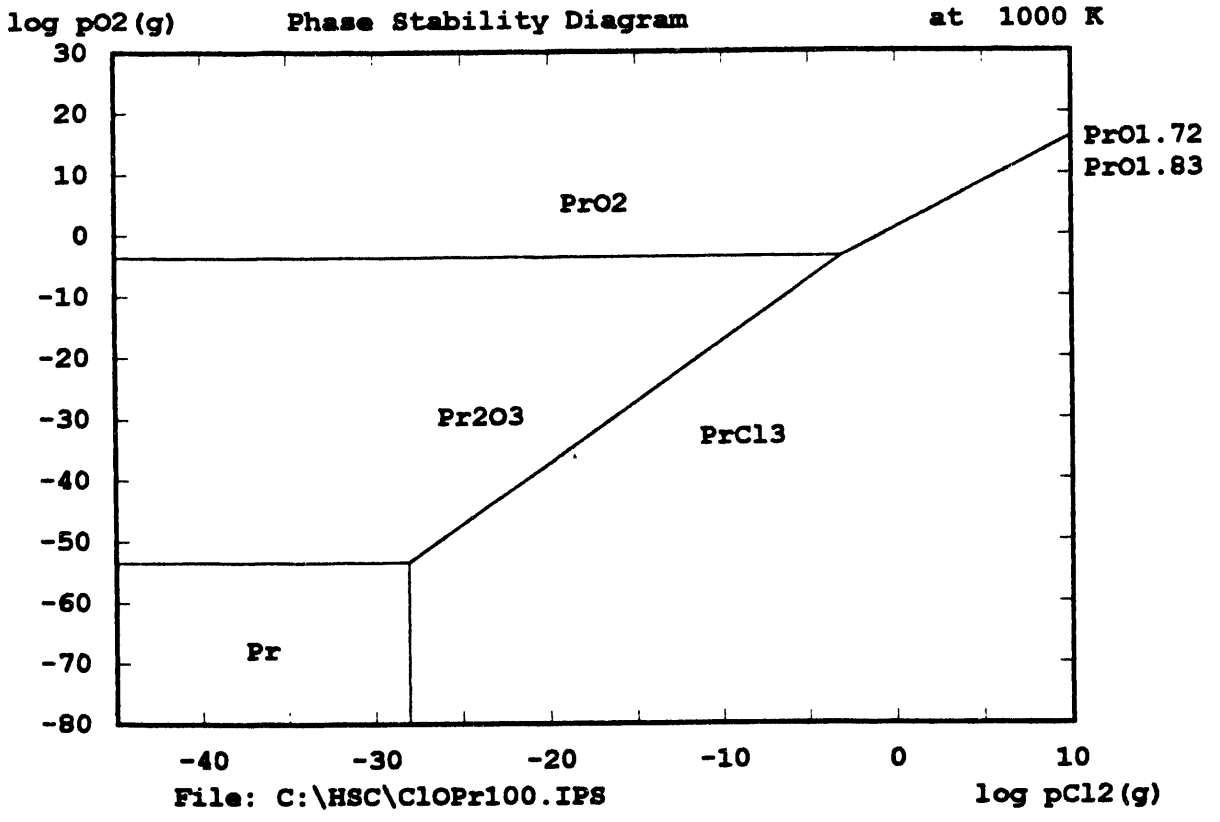

Fig. 13a. Phase stability diagram for praseodymium-oxygen-chlorine at 1000 K.

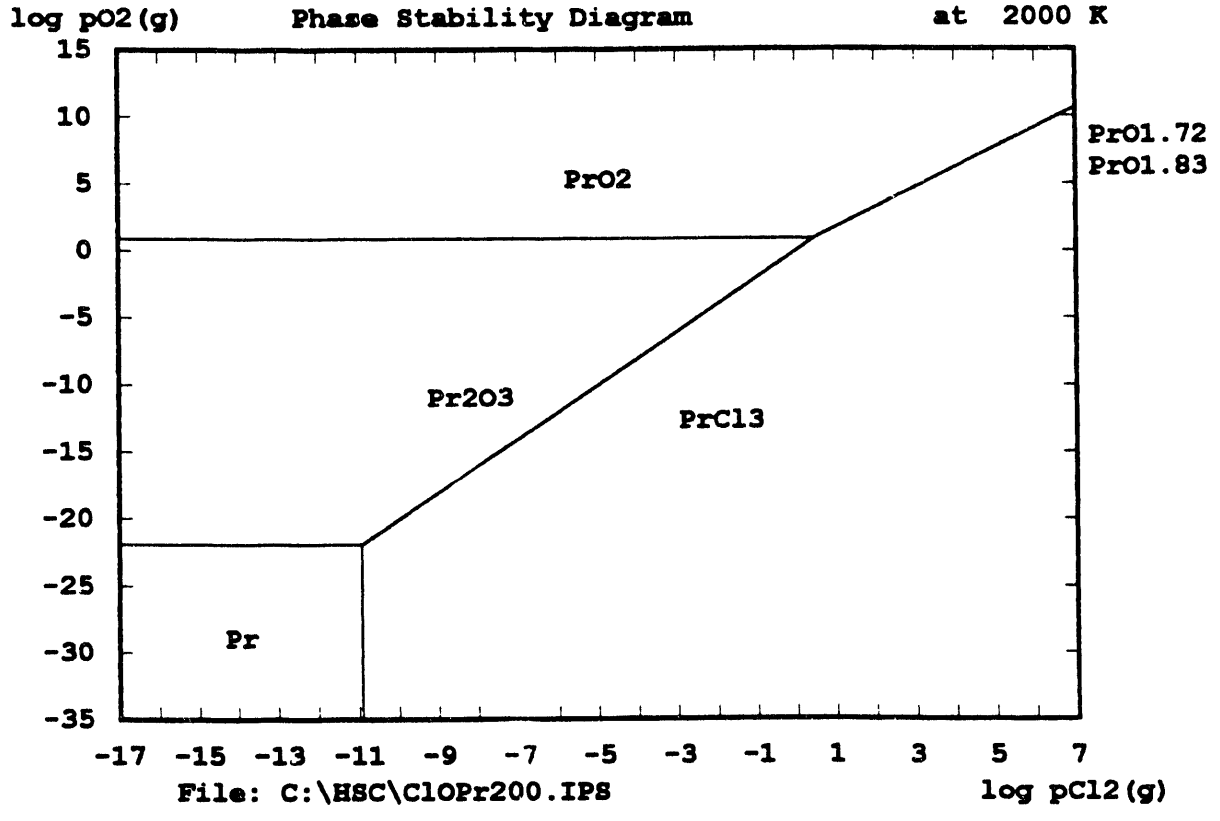

Fig. 13b. Phase stability diagram for praseodymium-oxygen-chlorine at 2000 K.

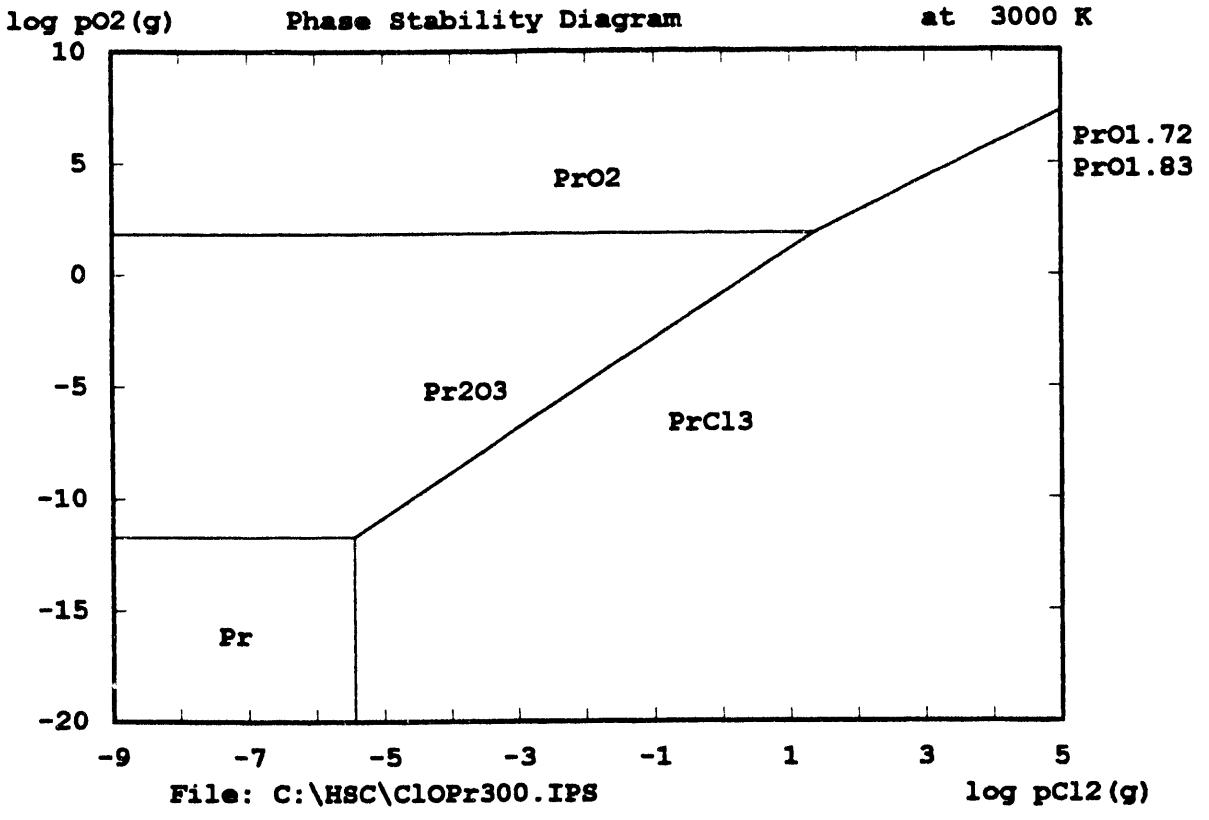

Fig. 13c. Phase stability diagram for praseodymium-oxygen-chlorine at 3000 K.

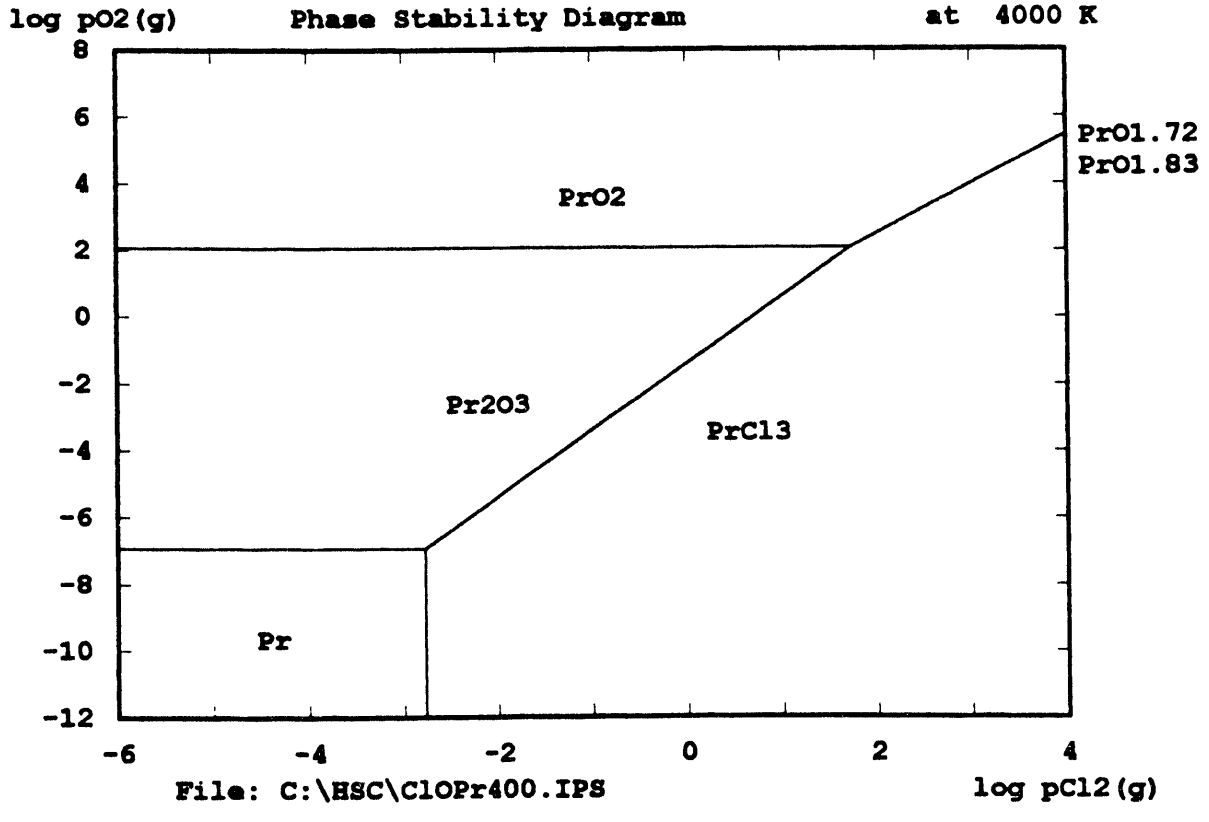

Fig. 13d. Phase stability diagram for praseodymium-oxygen-chlorine at 4000 K.

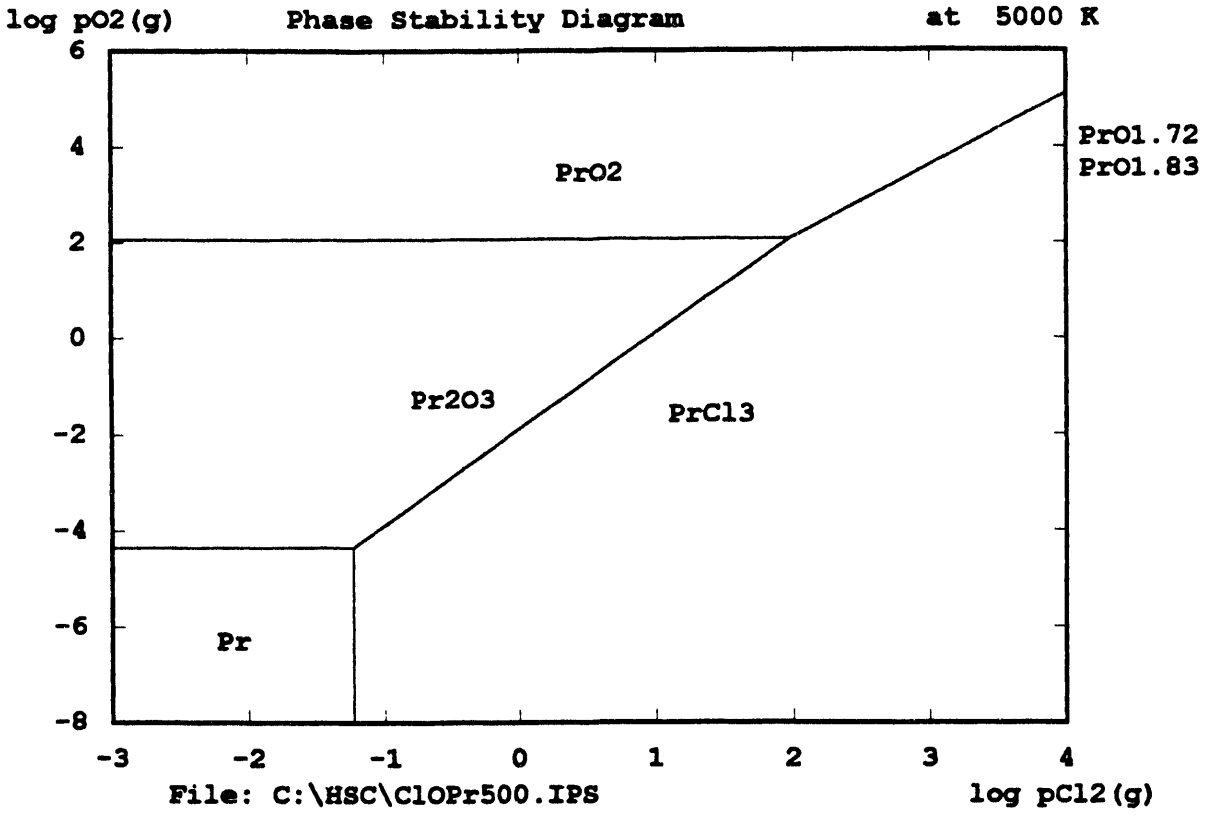

Fig. 13e. Phase stability diagram for praseodymium-oxygen-chlorine at 5000 K.

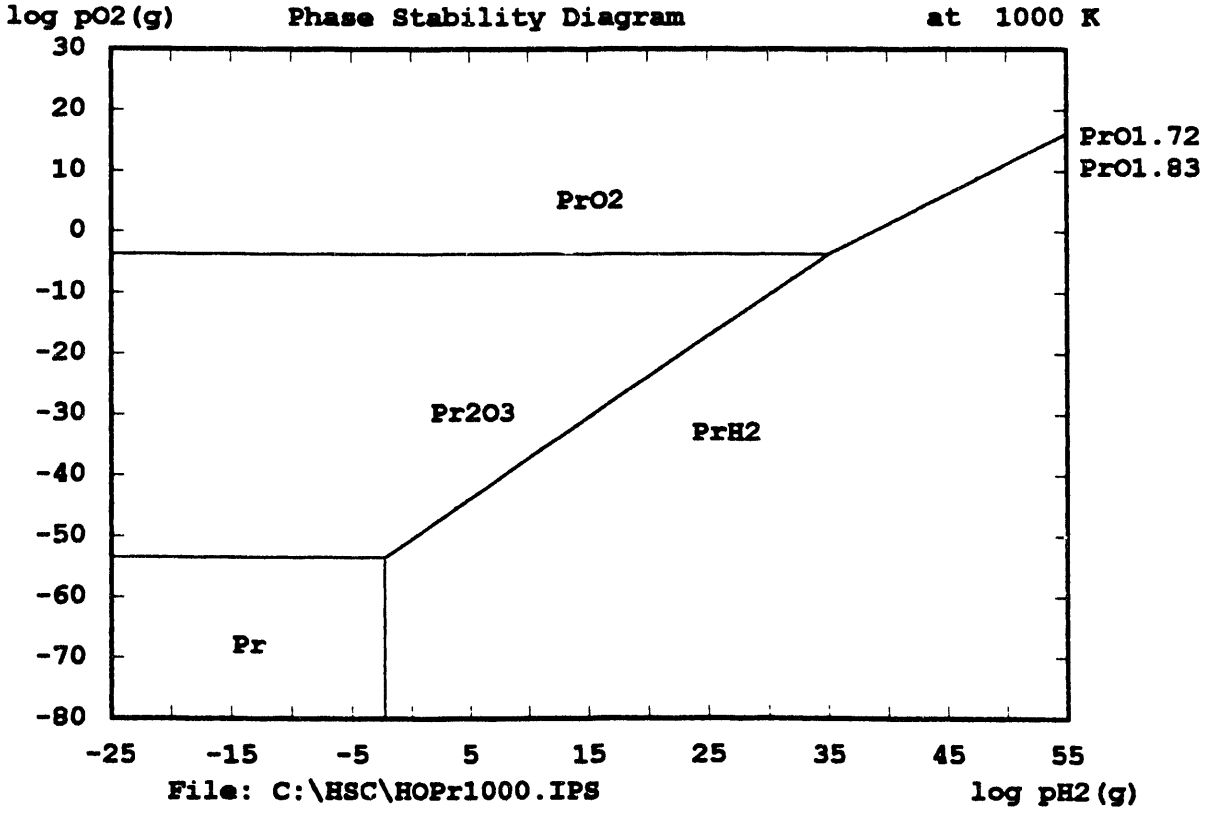

Fig. 14a. Phase stability diagram for praseodymium-oxygen-hydrogen at 1000 K.

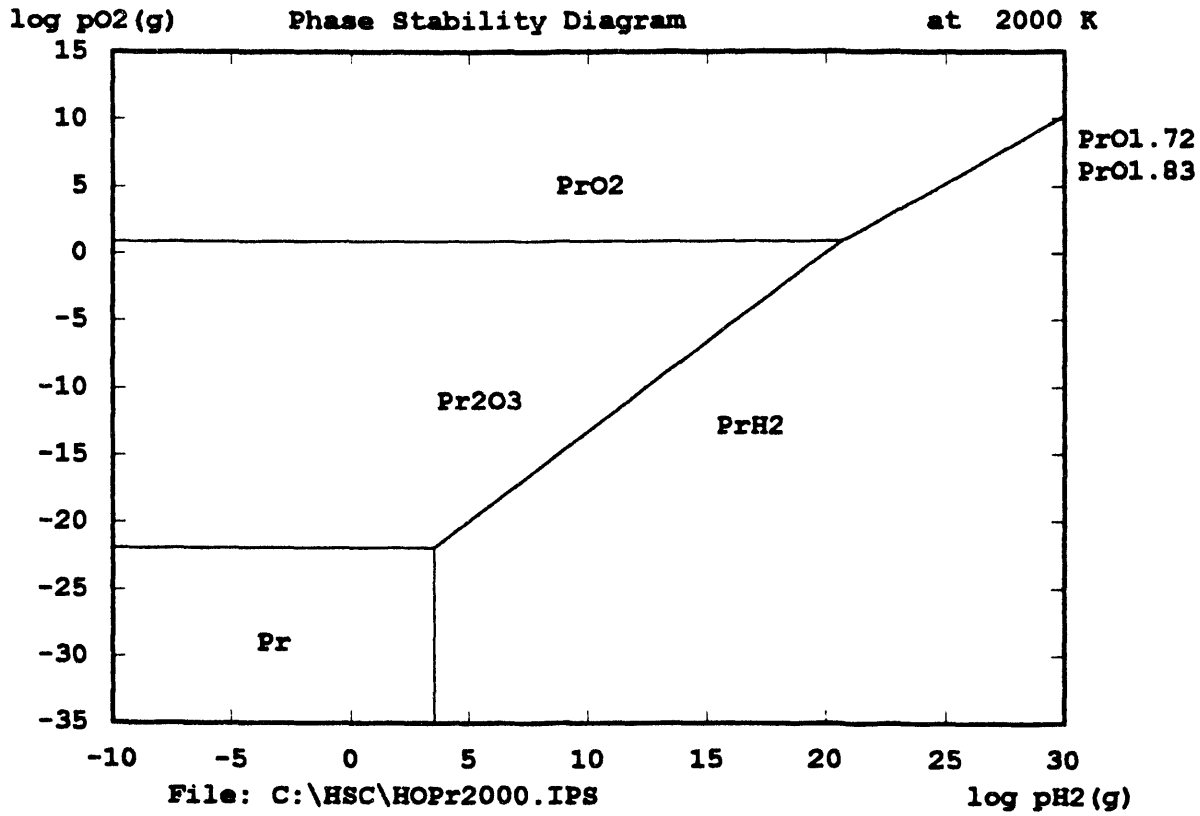

Fig. 14b. Phase stability diagram for praseodymium-oxygen-hydrogen at 2000 K.

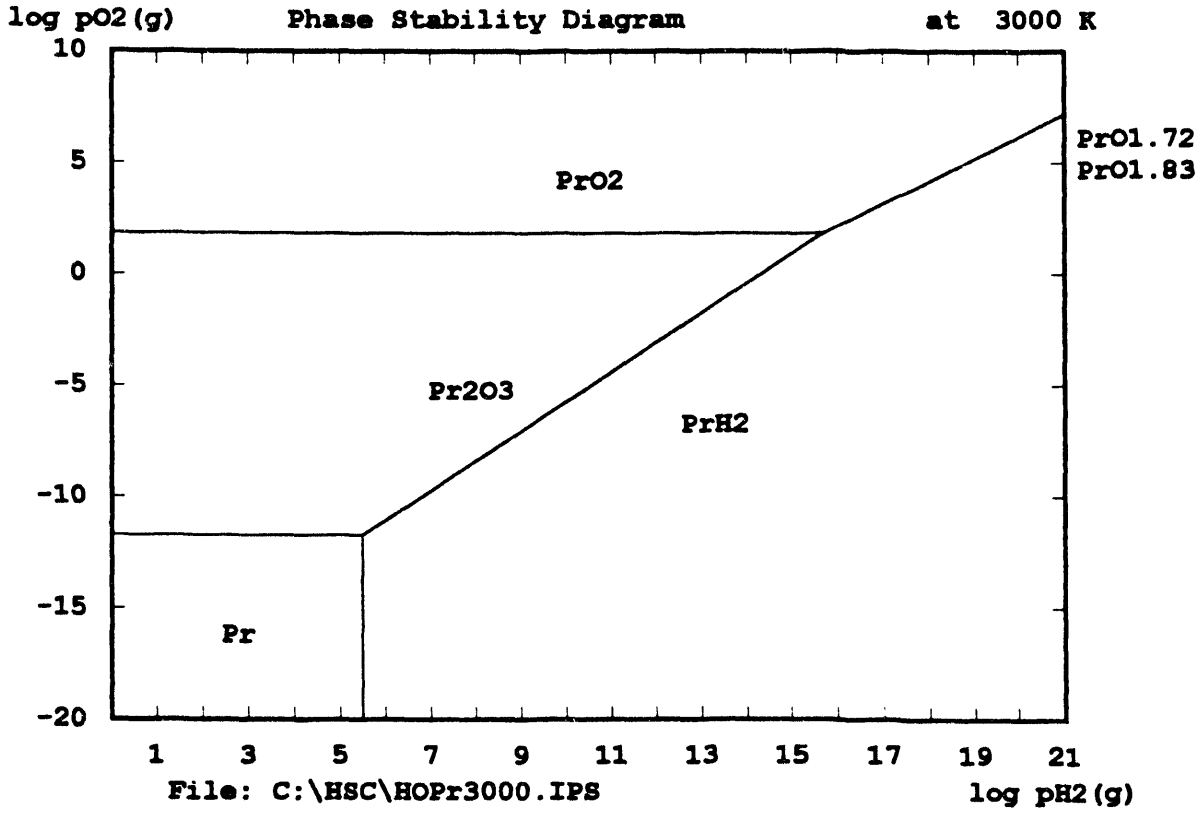

Fig. 14c. Phase stability diagram for praseodymium-oxygen-hydrogen at 3000 K.

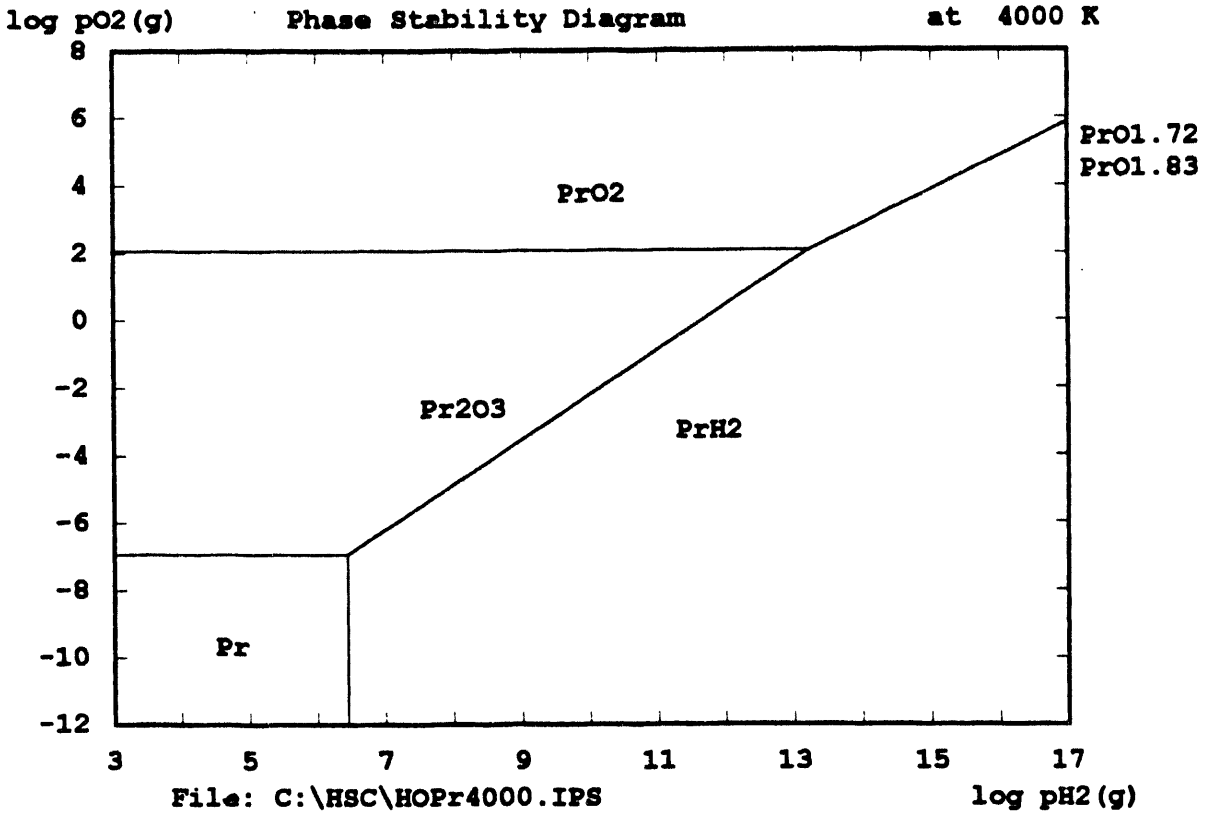

Fig. 14d. Phase stability diagram for praseodymium-oxygen-hydrogen at 4000 K.

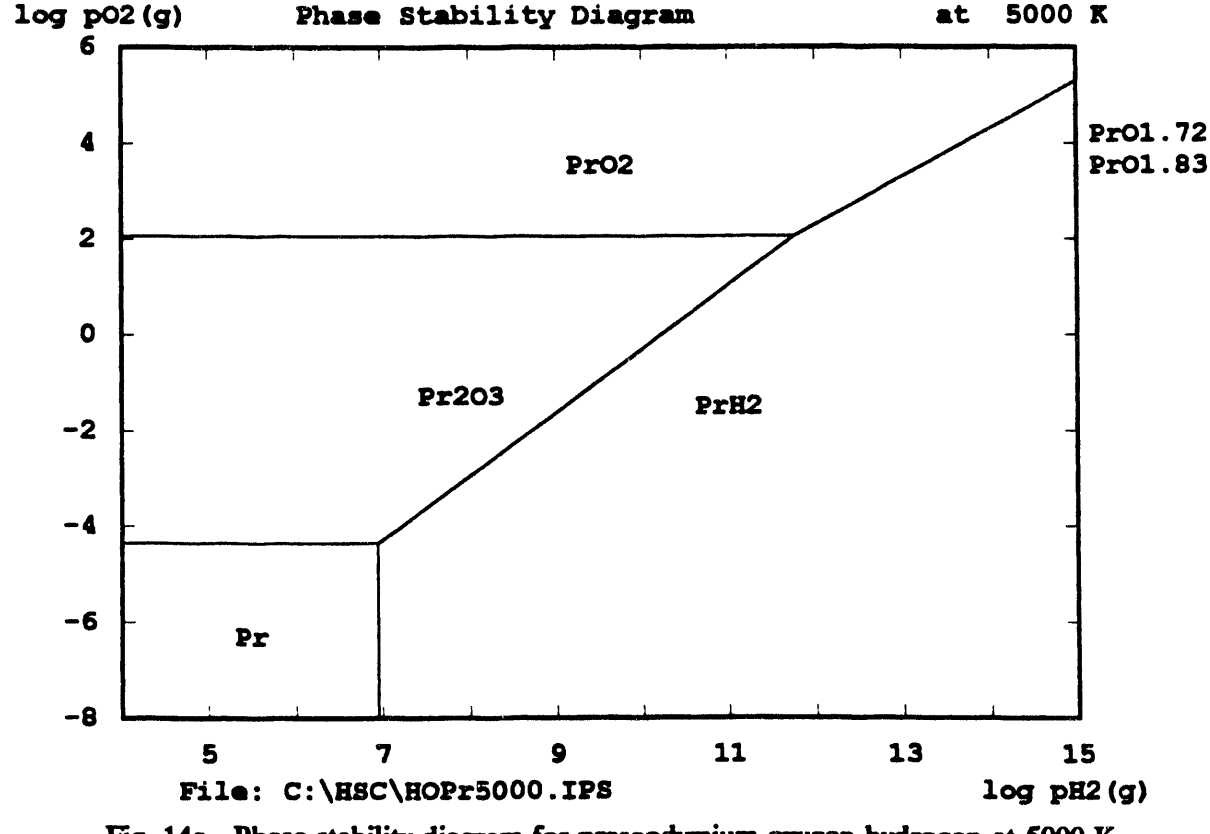

Fig. 14e. Phase stability diagram for praseodymium-oxygen-hydrogen at 5000 K.

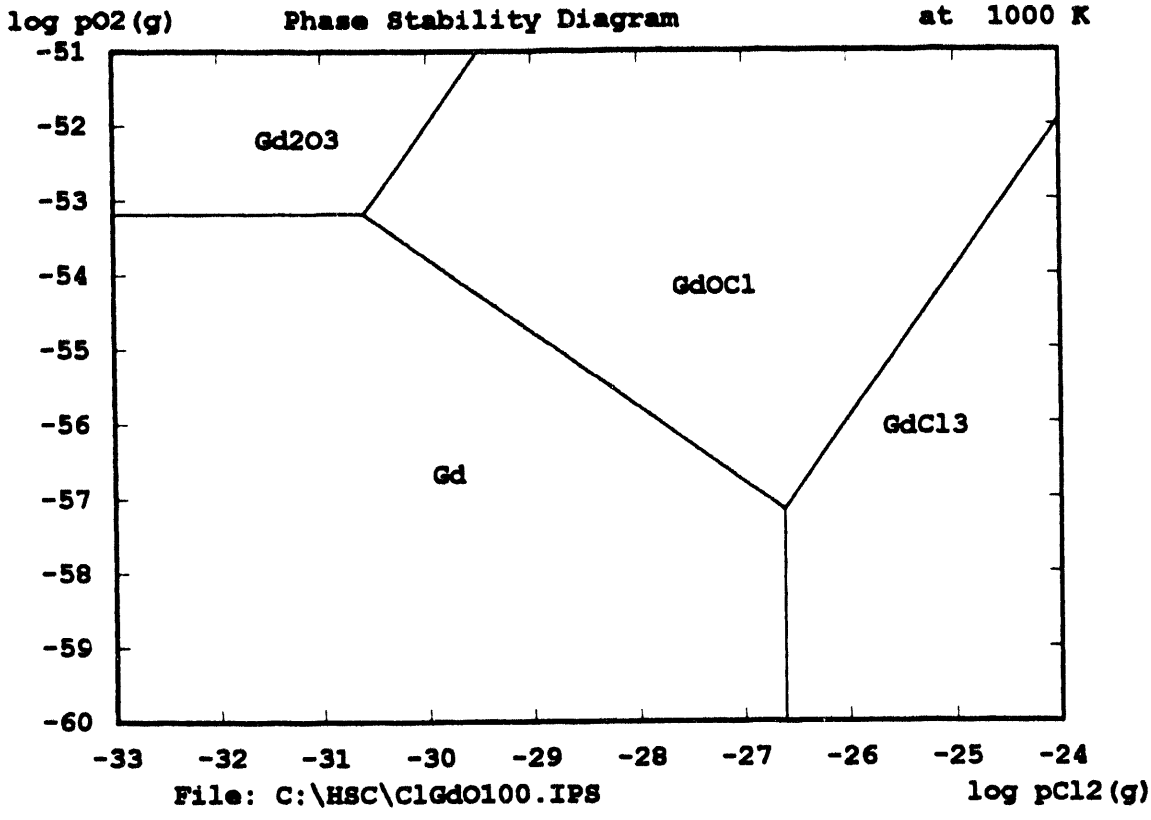

Fig. 15a. Phase stability diagram for gadolinium-oxygen-chlorine at 1000 K.

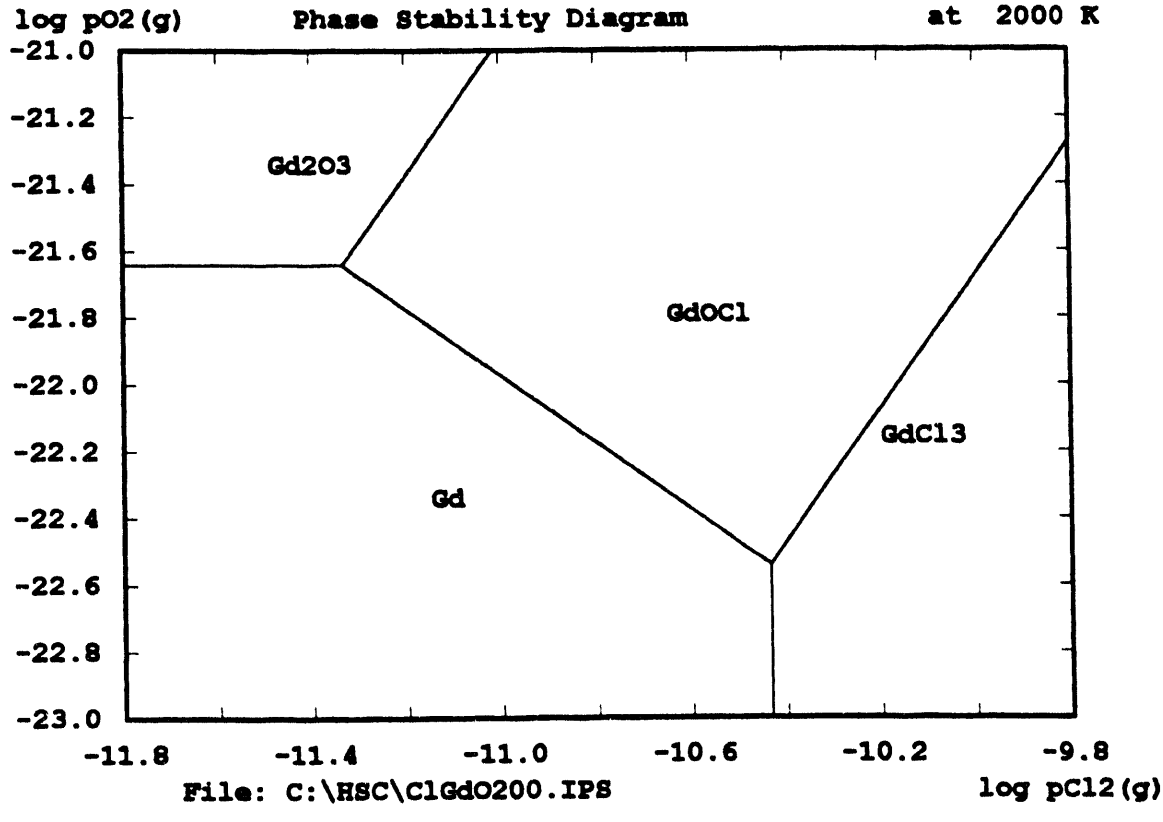

Fig. 15b. Phase stability diagram for gadolinium-oxygen-chlorine at 2000 K.

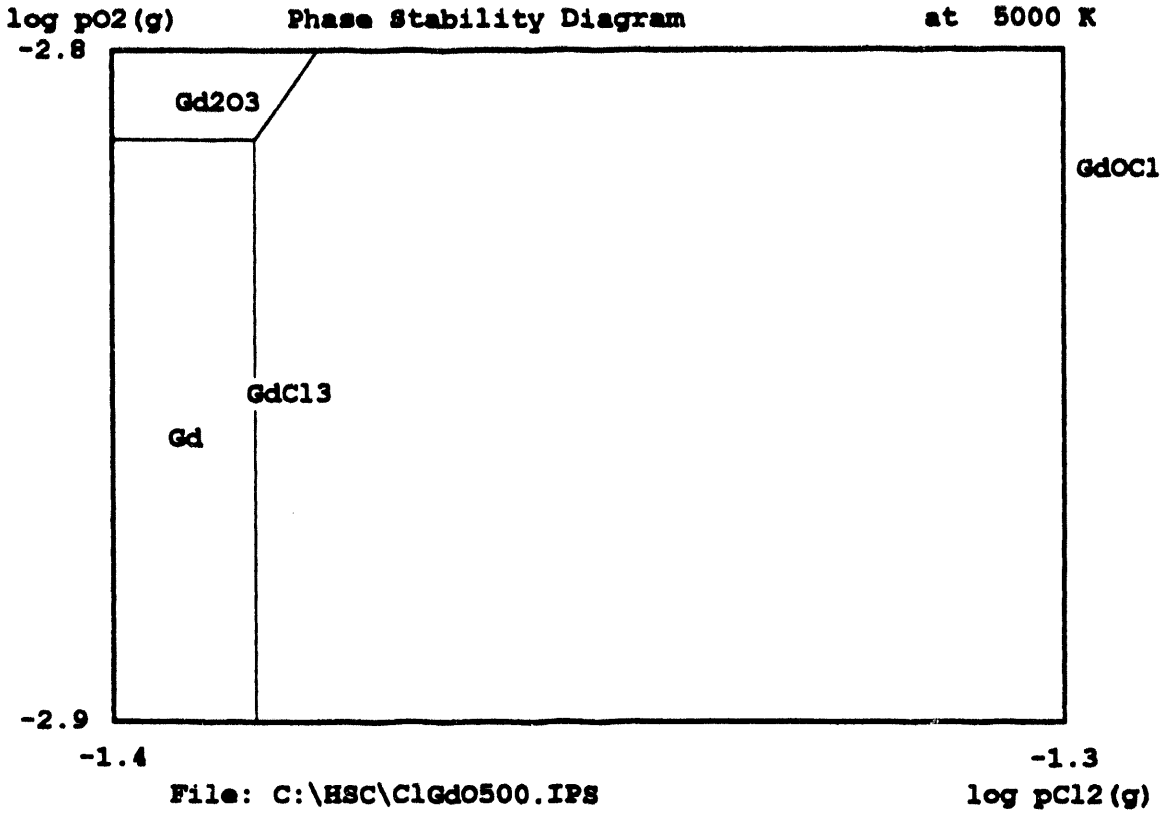

Fig. 15c. Phase stability diagram for gadolinium-oxygen-chlorine at 5000 K.

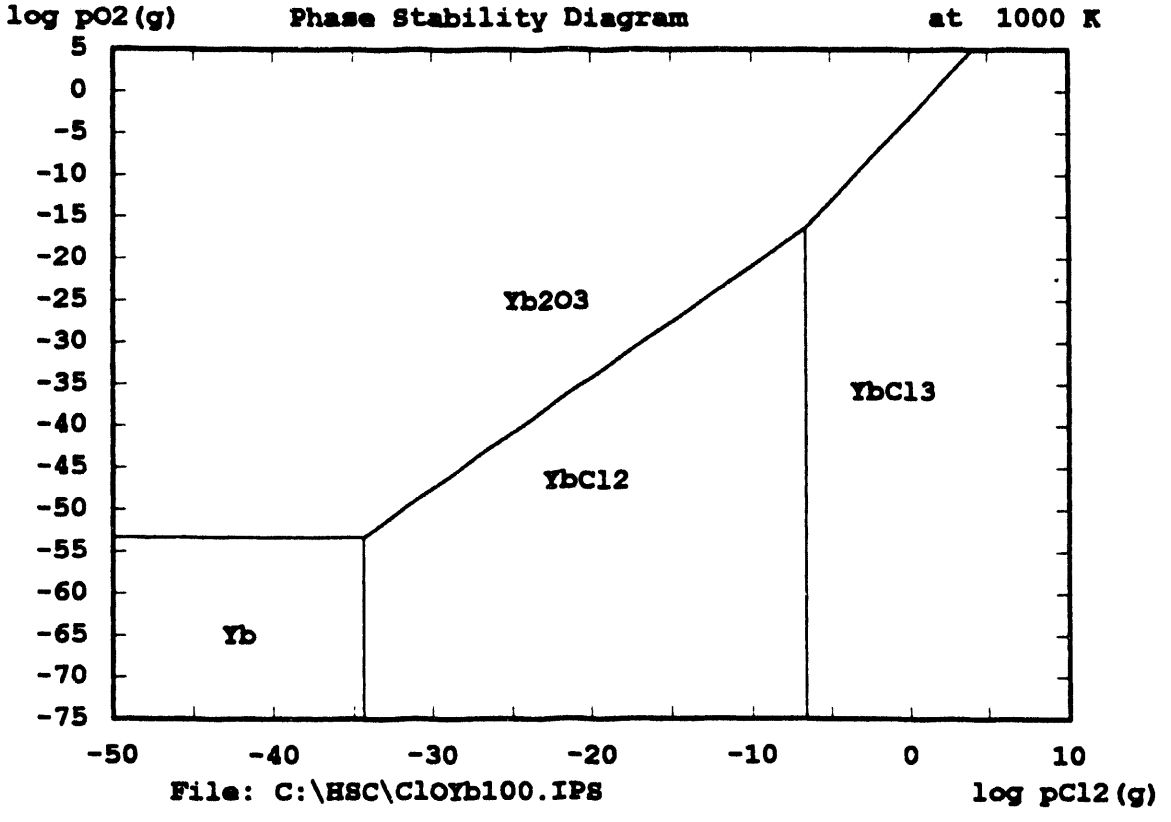

Fig. 16a. Phase stability diagram for ytterbium-oxygen-chlorine at 1000 K.

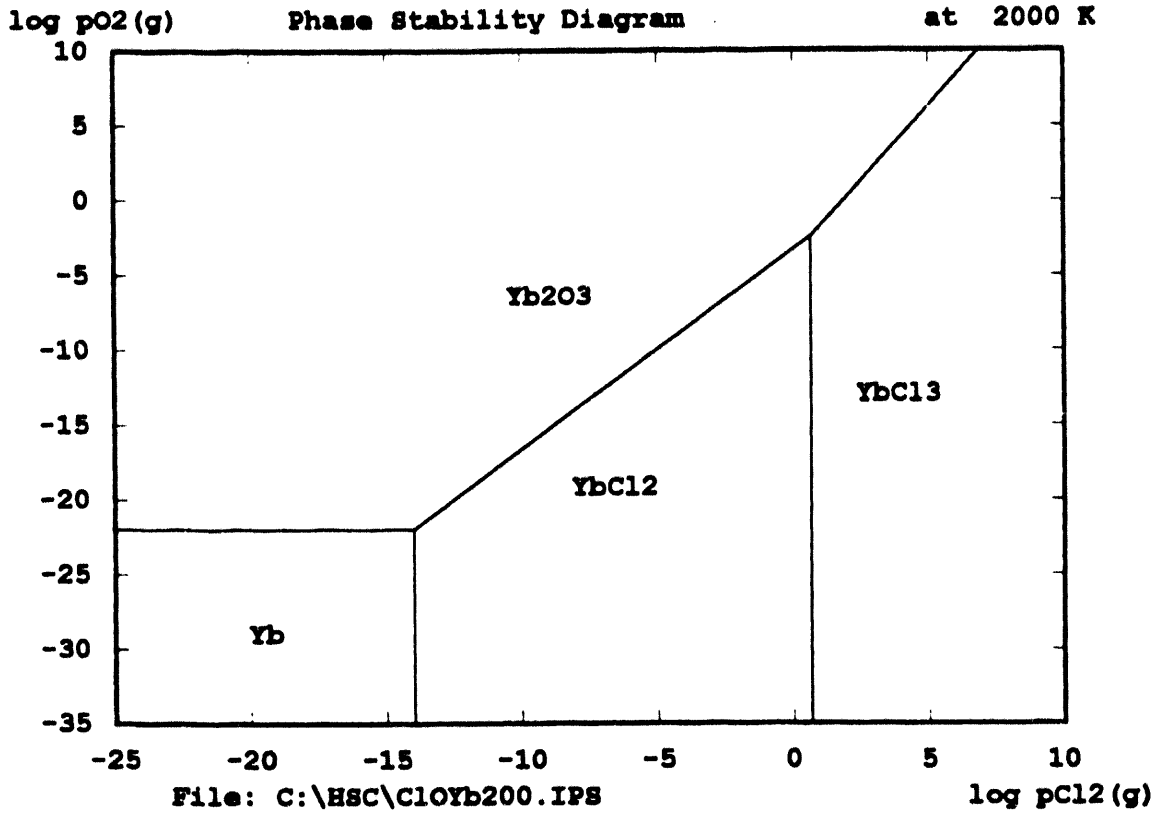

Fig. 16b. Phase stability diagram for ytterbium-oxygen-chlorine at 2000 K.

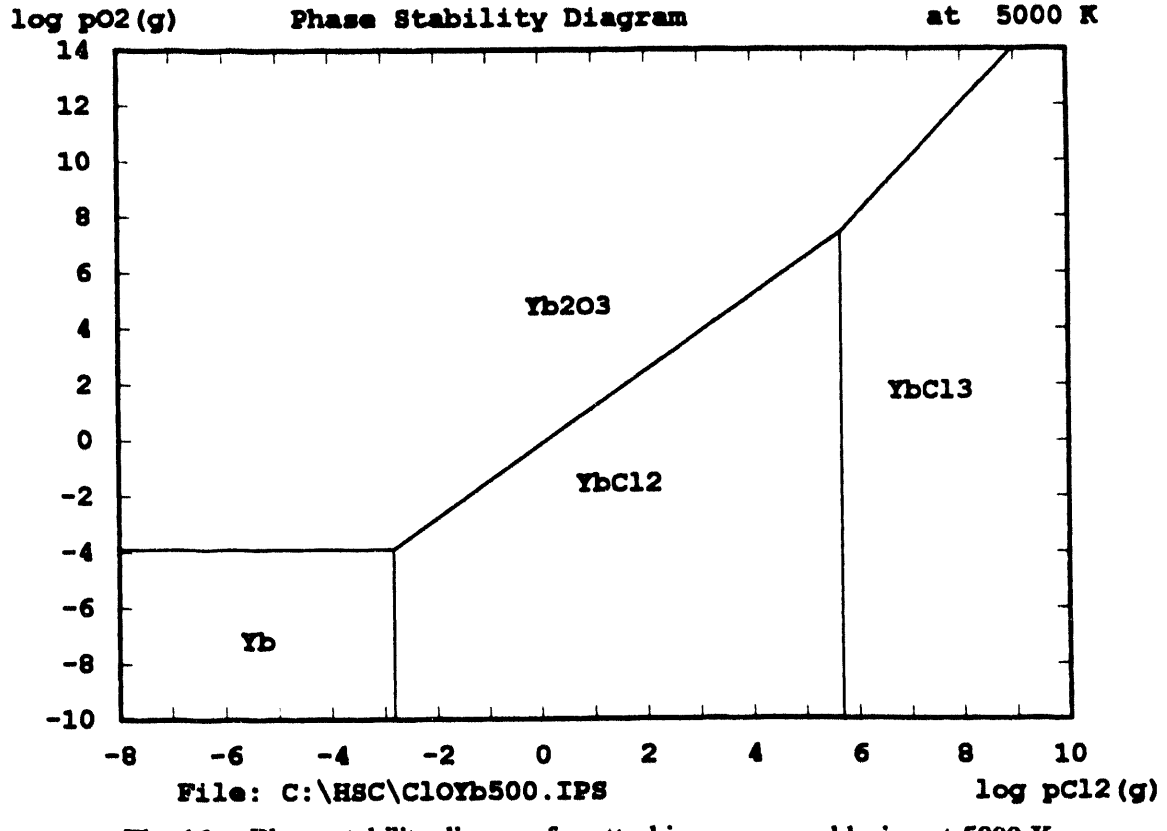

Fig. 16c. Phase stability diagram for ytterbium-oxygen-chlorine at 5000 K.

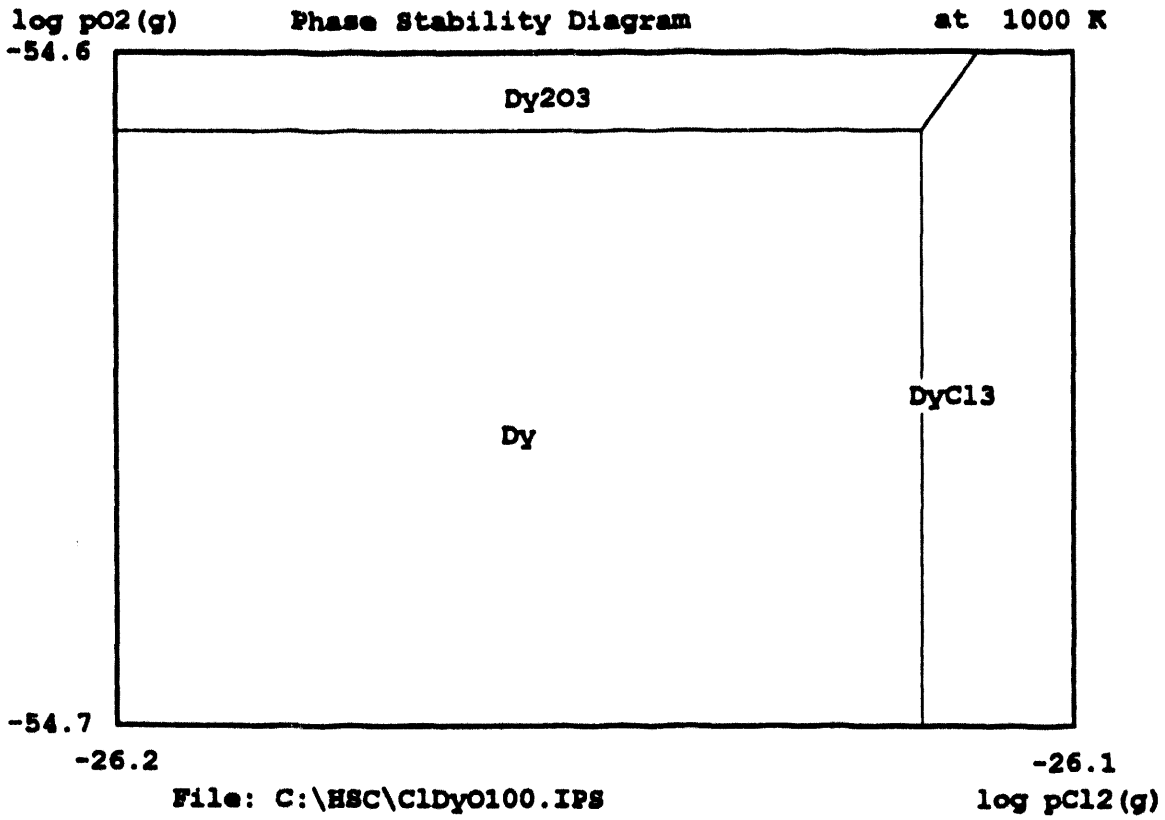

Fig. 17a. Phase stability diagram for dysprosium-oxygen-chlorine at 1000 K.

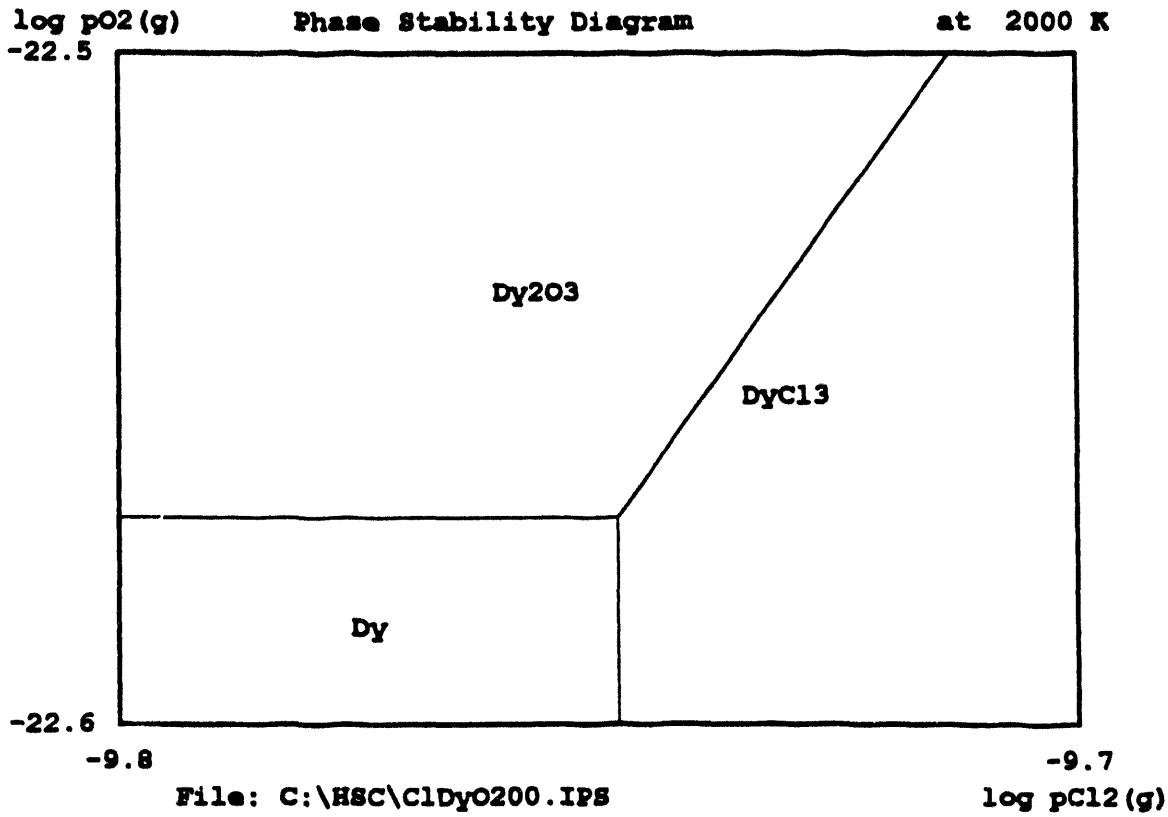

Fig. 17b. Phase stability diagram for dysprosium-oxygen-chlorine at 2000 K.

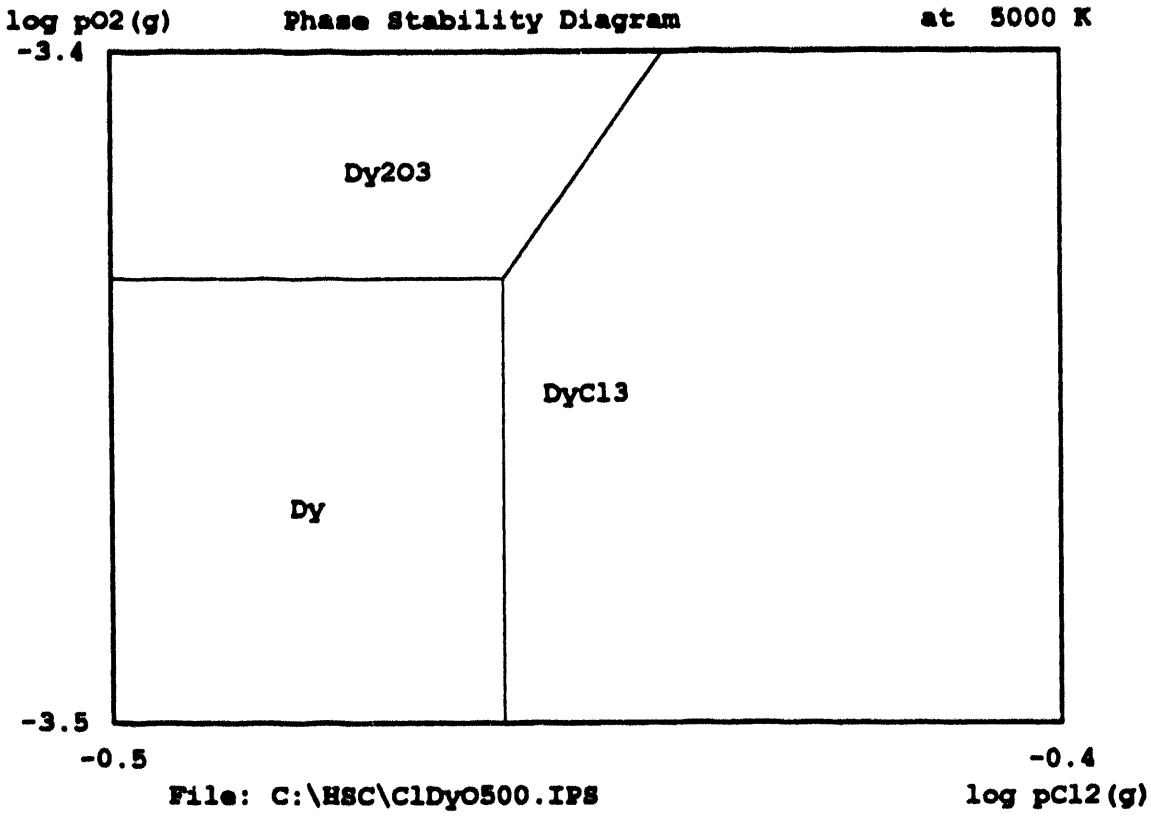

Fig. 17c. Phase stability diagram for dysprosium-oxygen-chlorine at 5000 K.

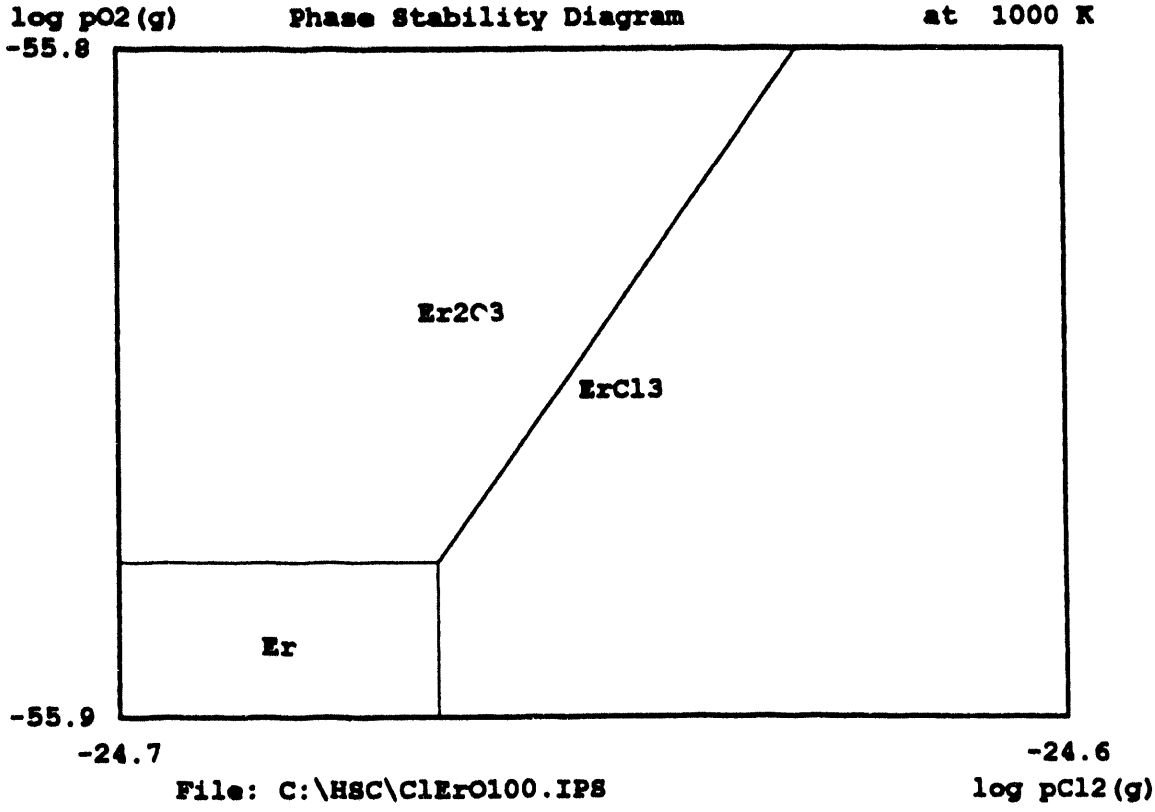

Fig. 18a. Phase stability diagram for erbium-oxygen-chlorine at 1000 K.

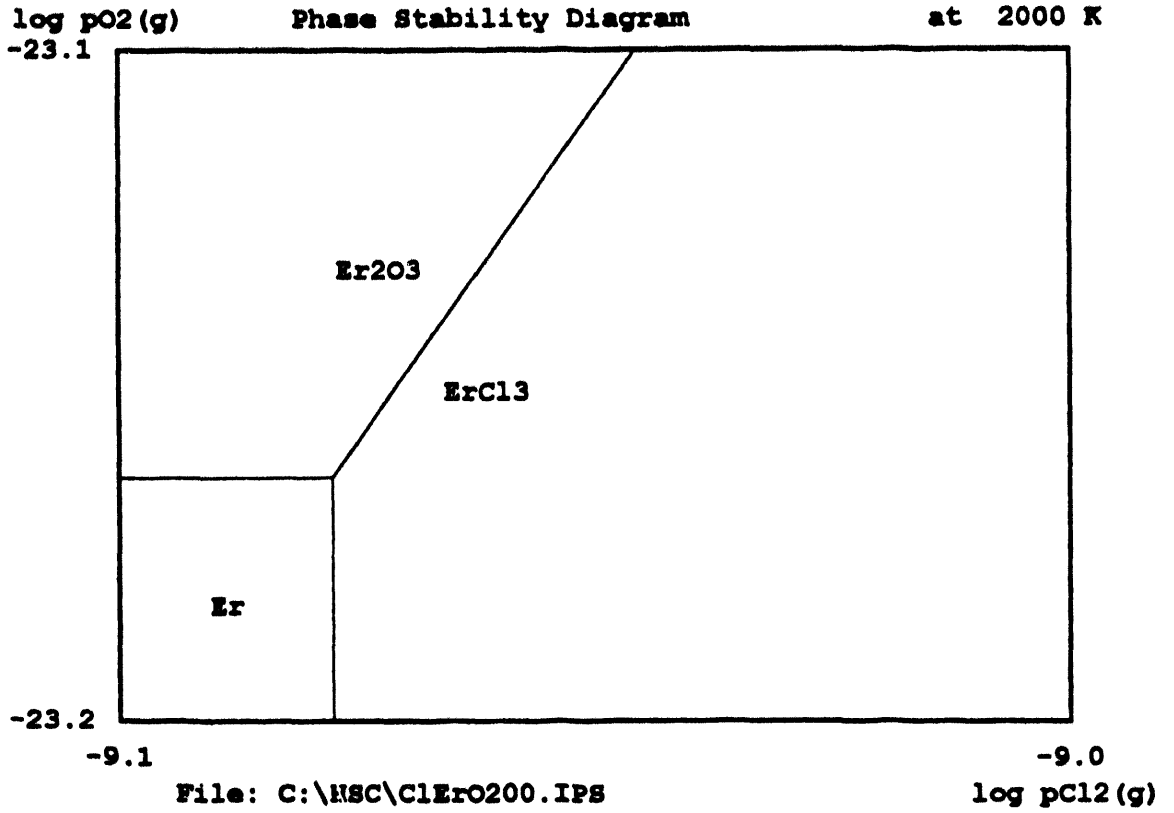

Fig. 18b. Phase stability diagram for erbium-oxygen-chlorine at 2000 K.

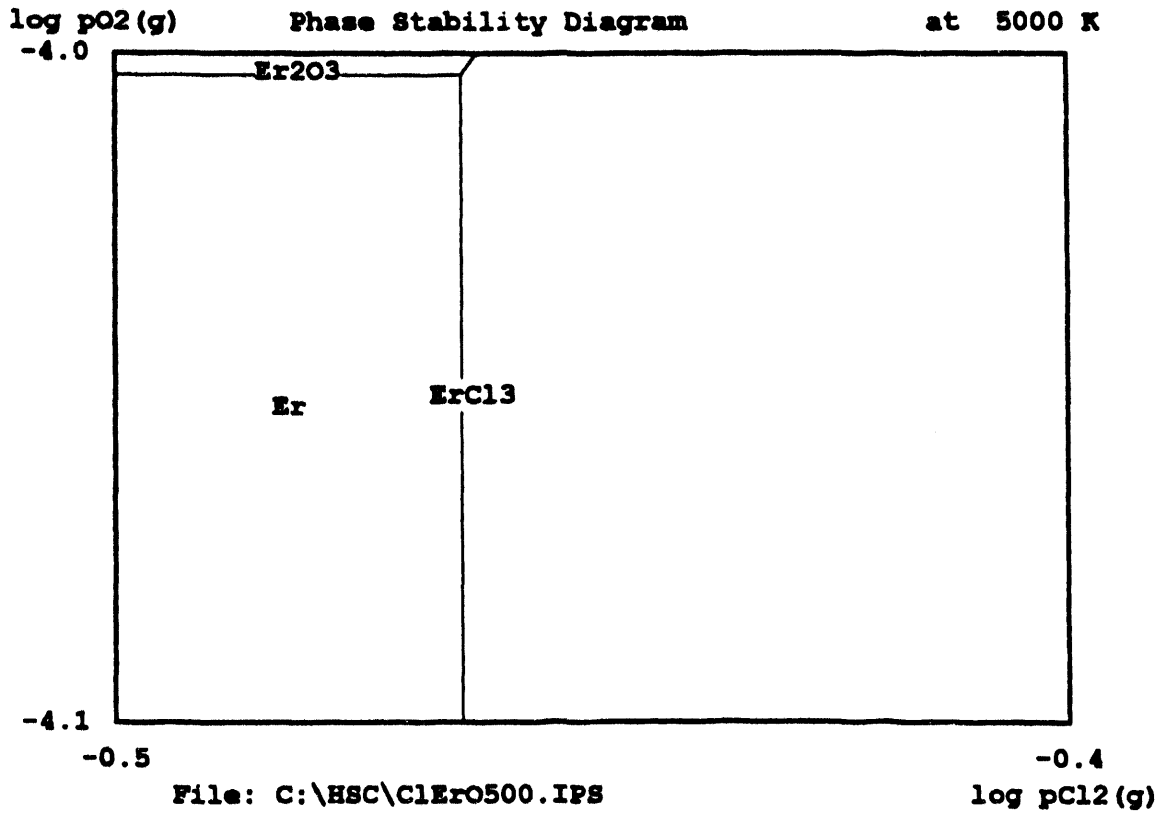

Fig. 18c. Phase stability diagram for erbium-oxygen-chlorine at 5000 K.

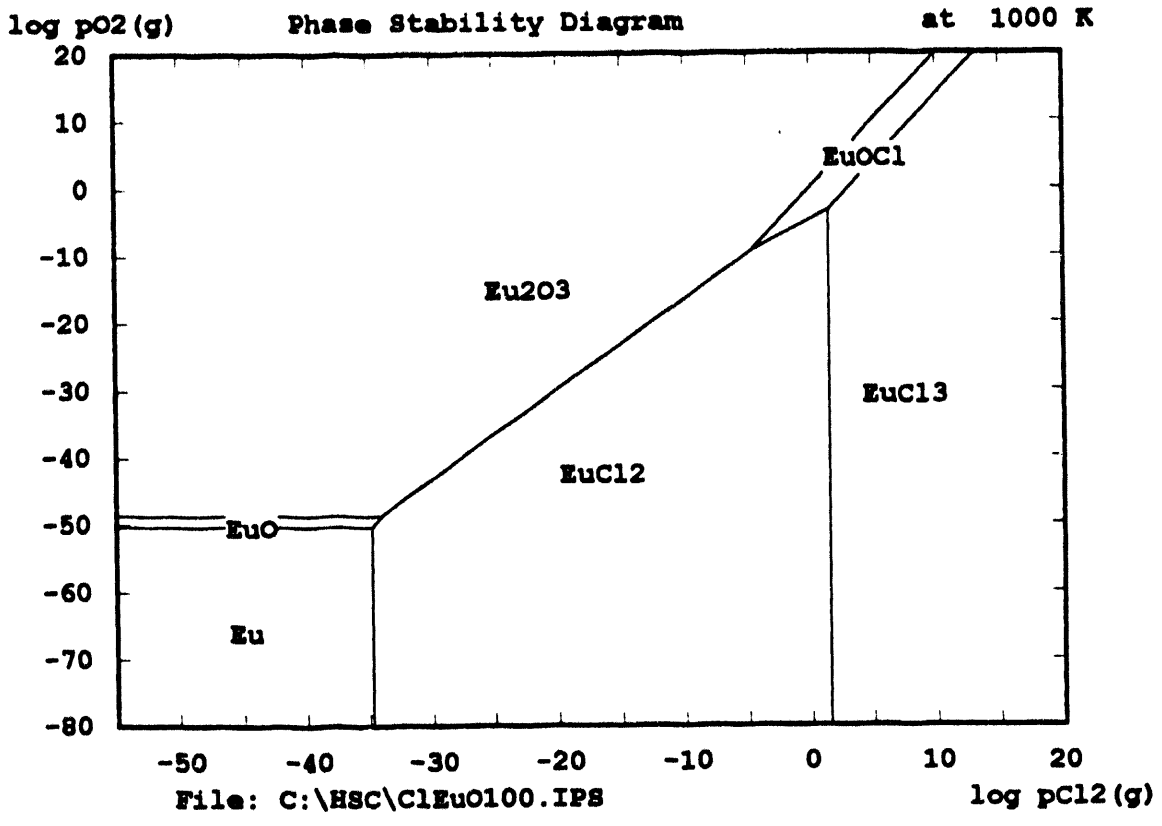

Fig. 19a. Phase stability diagram for europium-oxygen-chlorine at 1000 K.

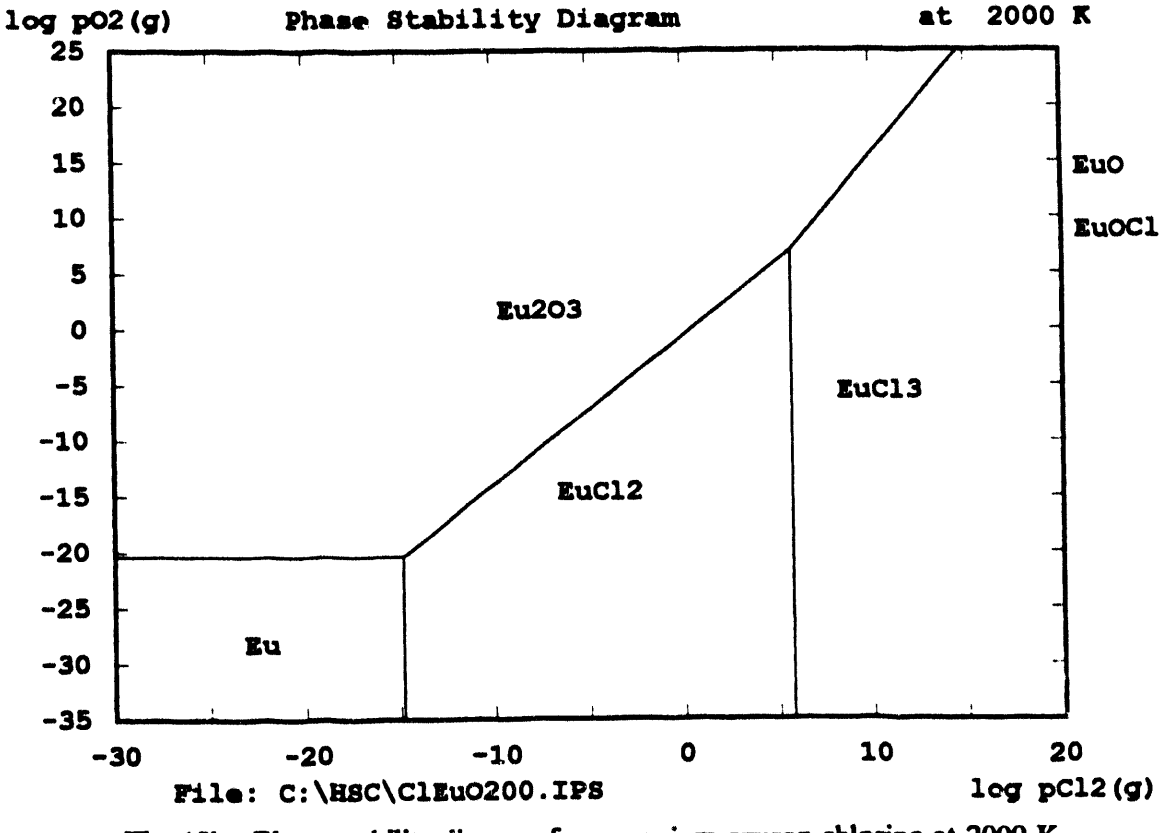

Fig. 19b. Phase stability diagram for europium-oxygen-chlorine at 2000 K.

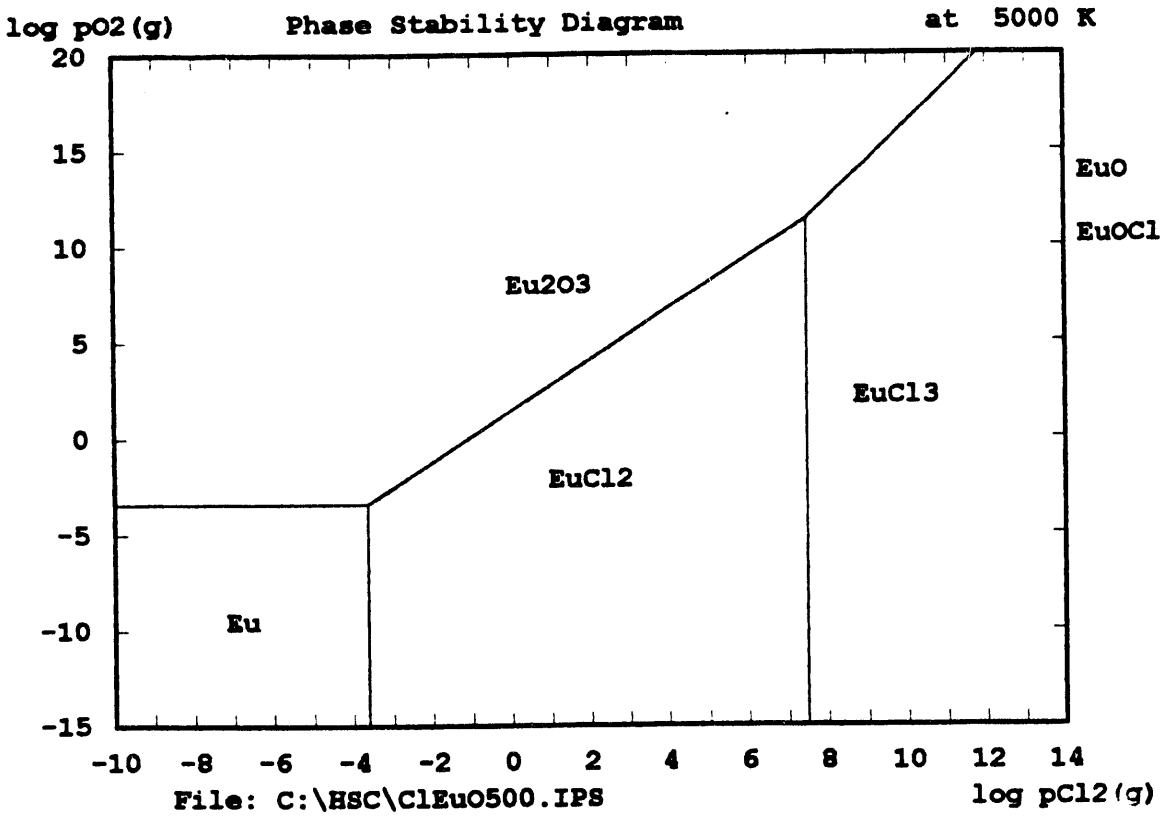

Fig. 19c. Phase stability diagram for europium-oxygen-chlorine at 5000 K.

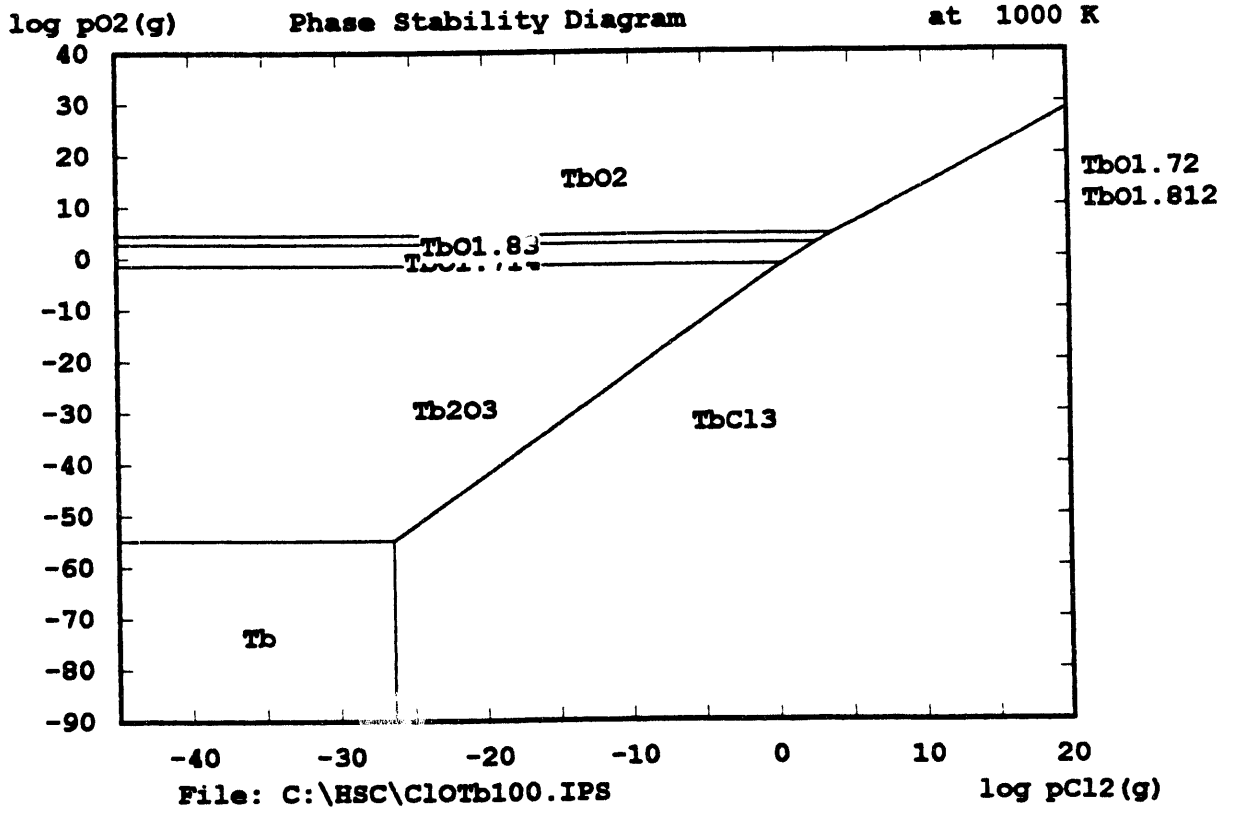

Fig. 20a. Phase stability diagram for terbium-oxygen-chlorine at 1000 K.

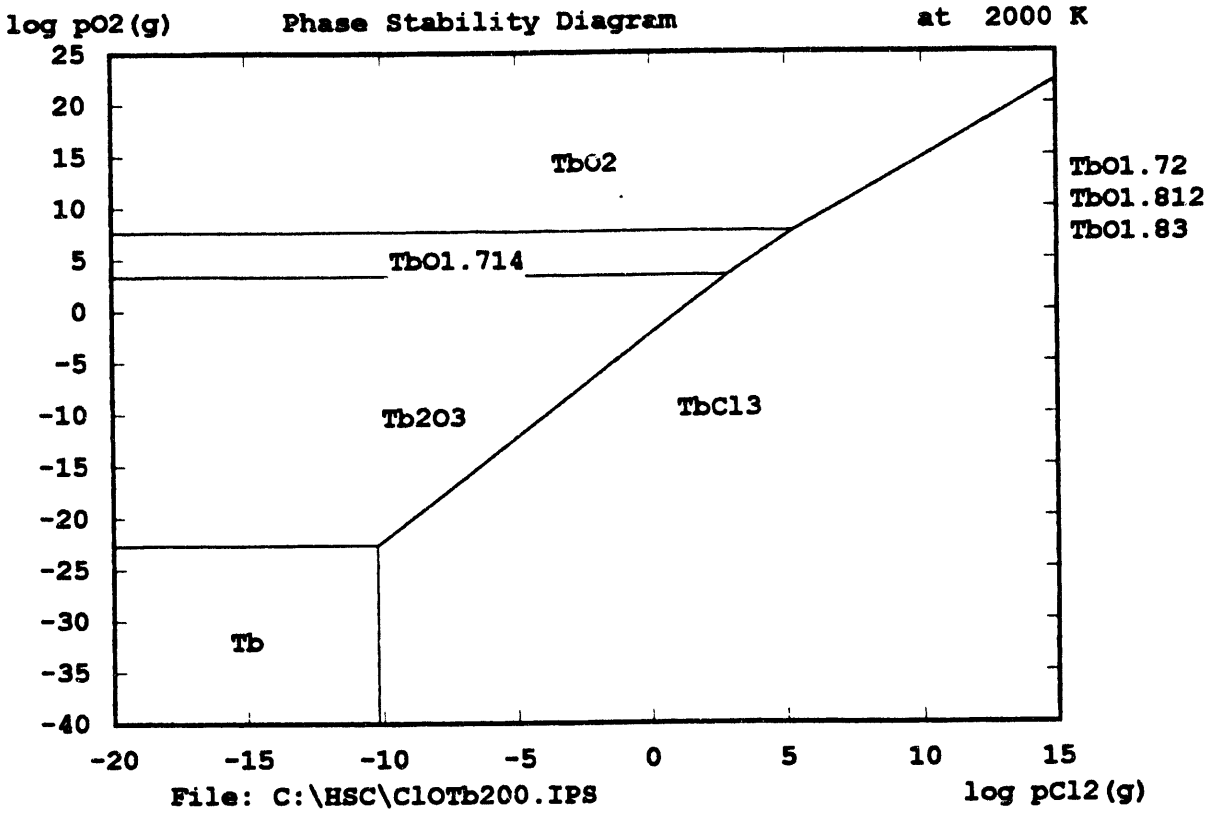

Fig. 20b. Phase stability diagram for terbium-oxygen-chlorine at 2000 K.

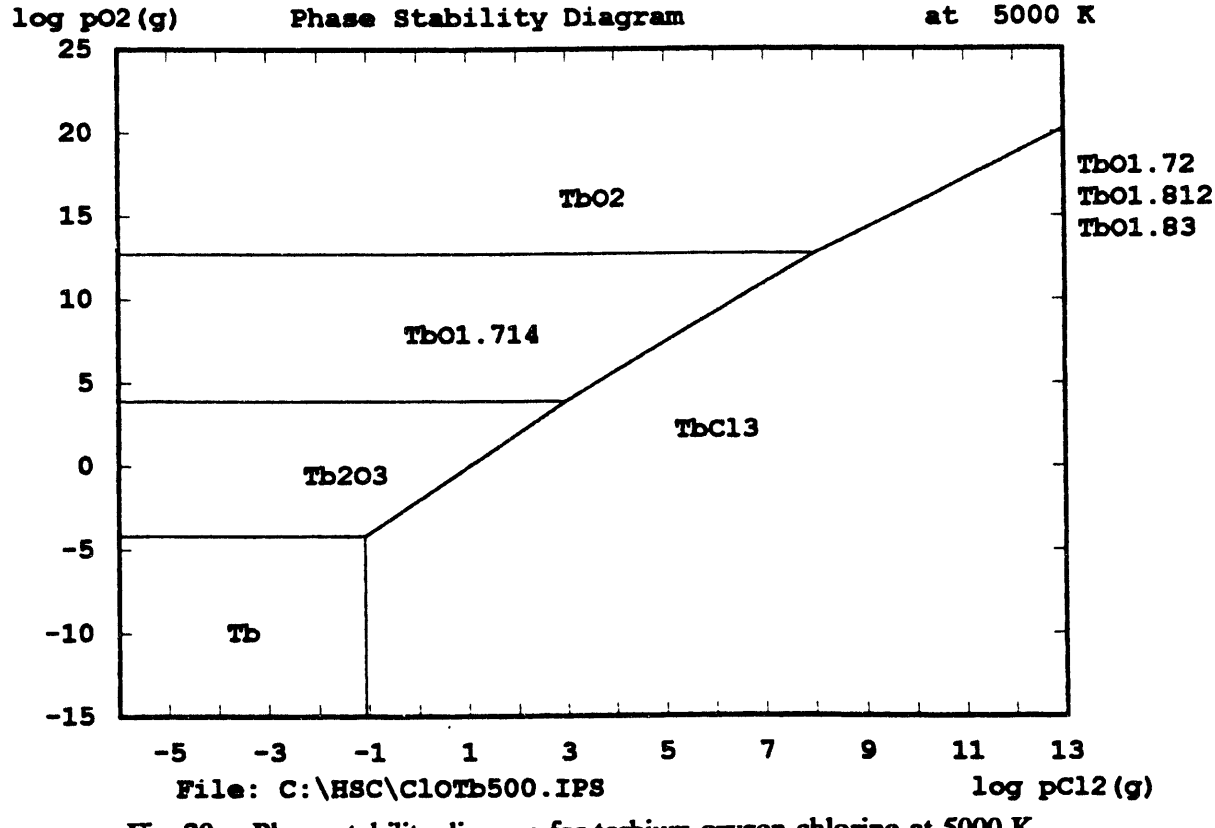

Fig. 20c. Phase stability diagram for terbium-oxygen-chlorine at 5000 K.

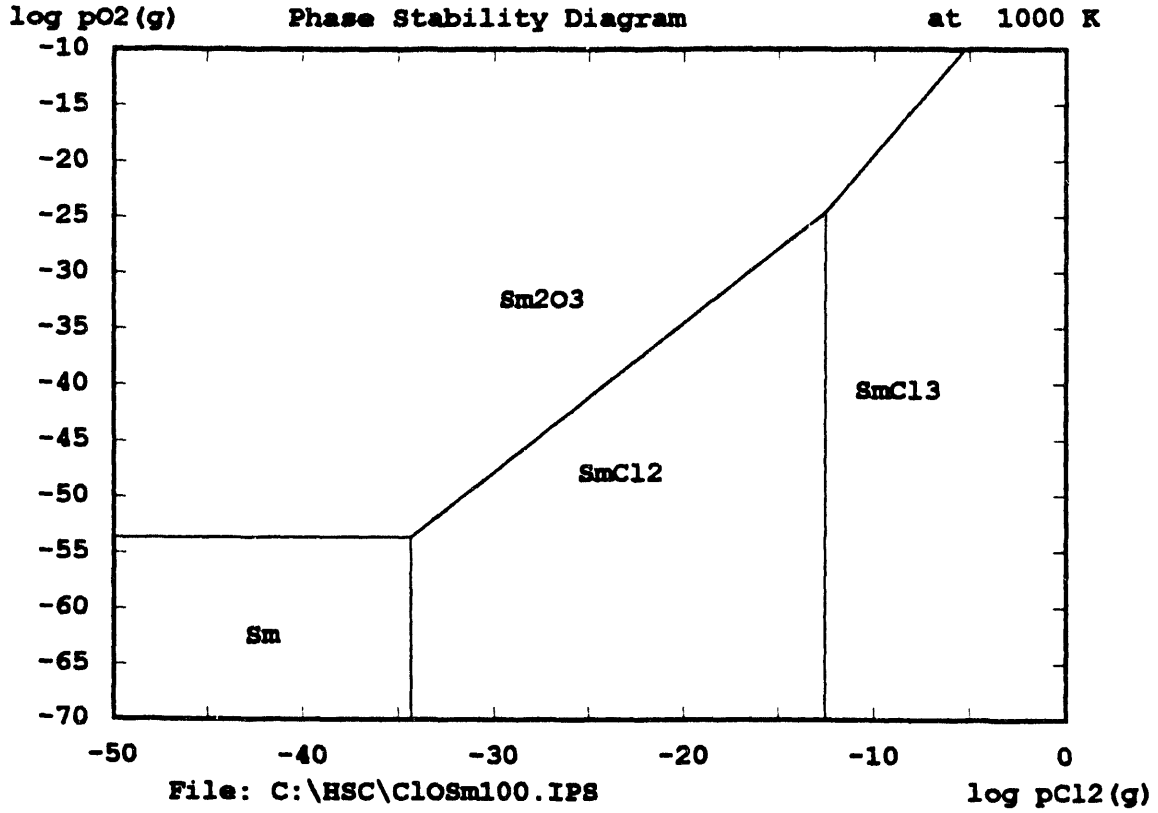

Fig. 21a. Phase stability diagram for samarium-oxygen-chlorine at 1000 K.

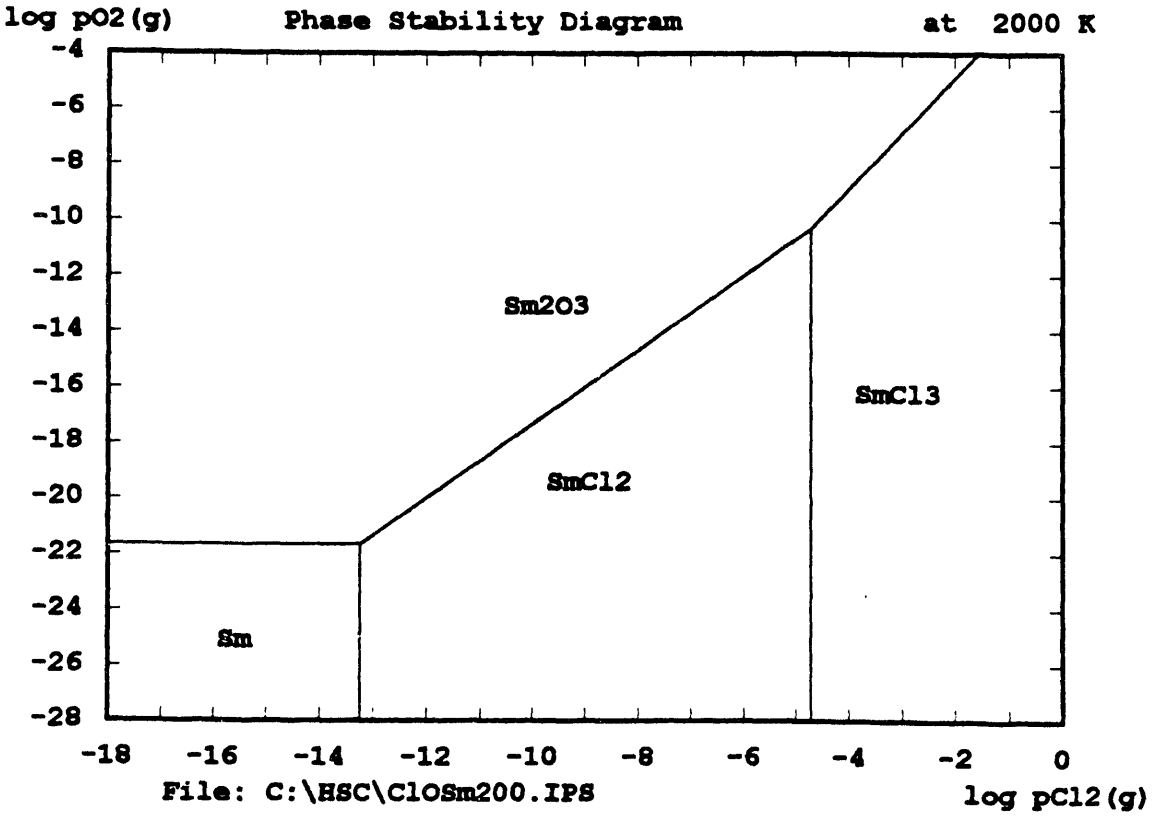

Fig. 21b. Phase stability diagram for samarium-oxygen-chlorine at 2000 K.

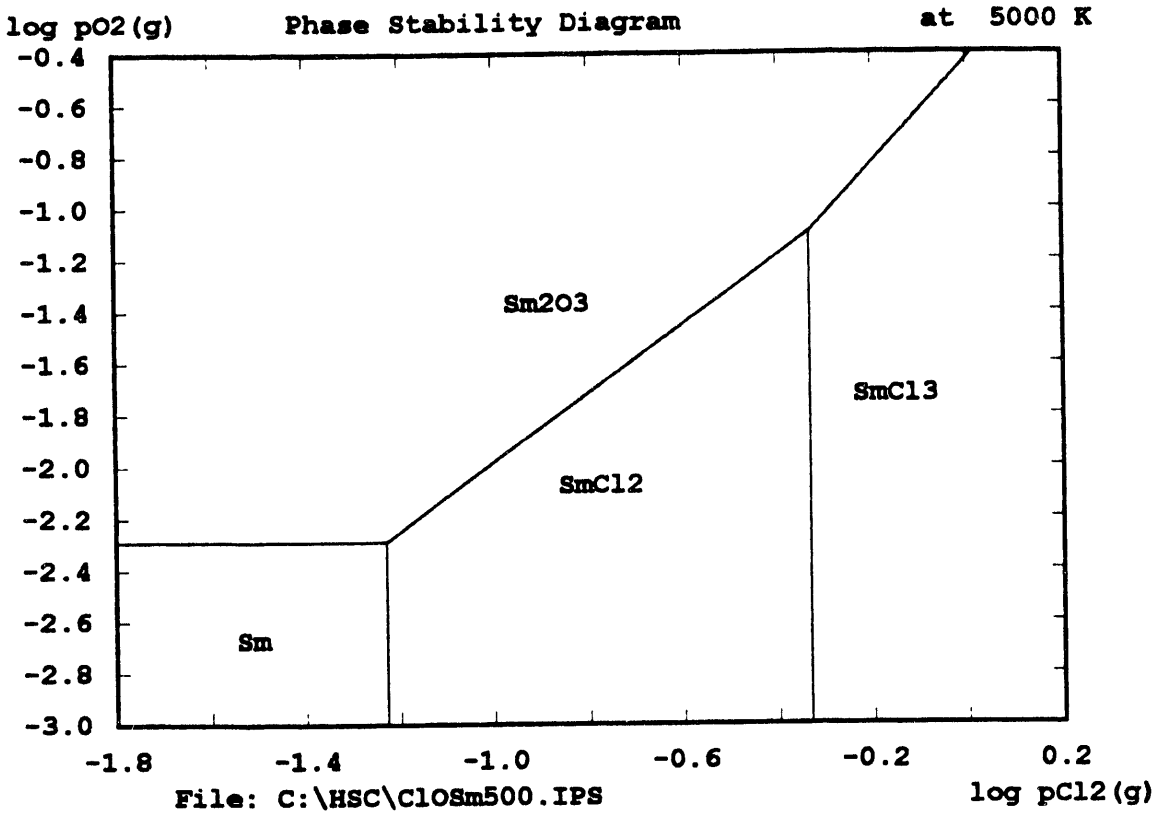

Fig. 21c. Phase stability diagram for samarium-oxygen-chlorine at 5000 K.

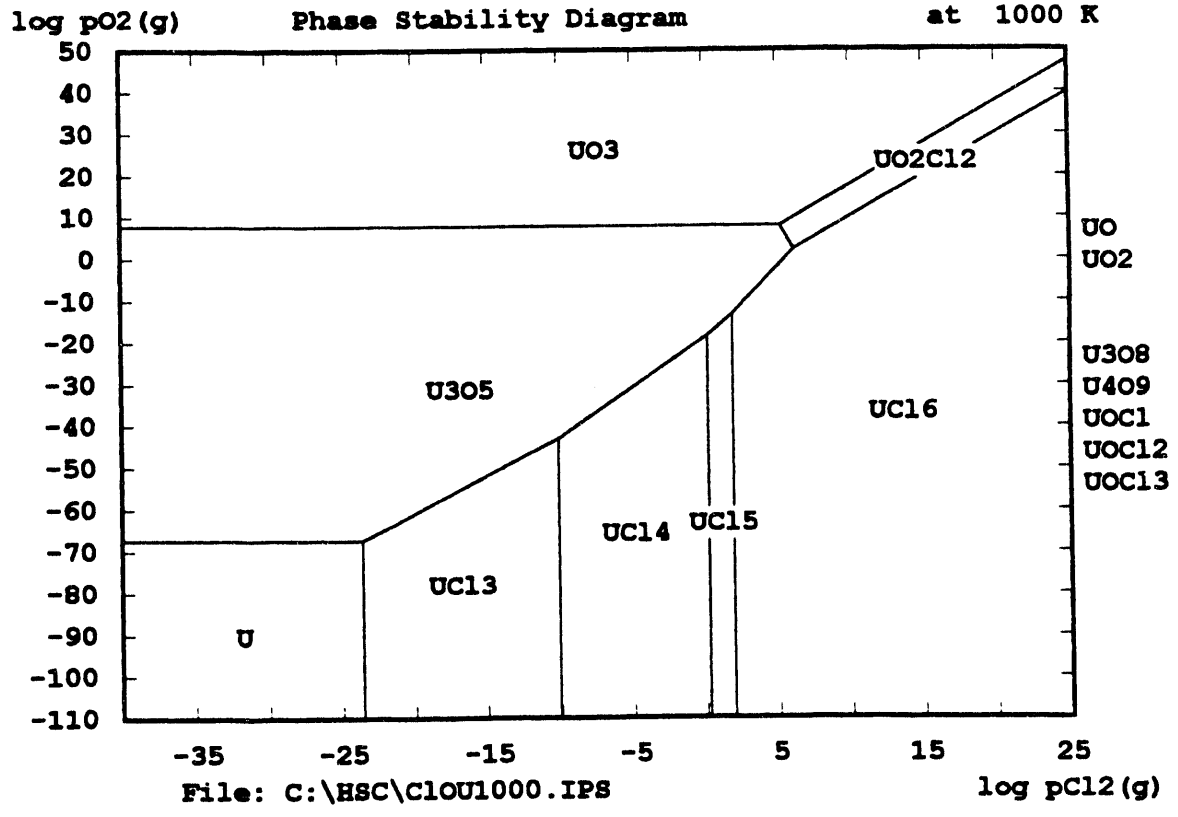

Fig. 22a. Phase stability diagram for uranium-oxygen-chlorine at 1000 K.

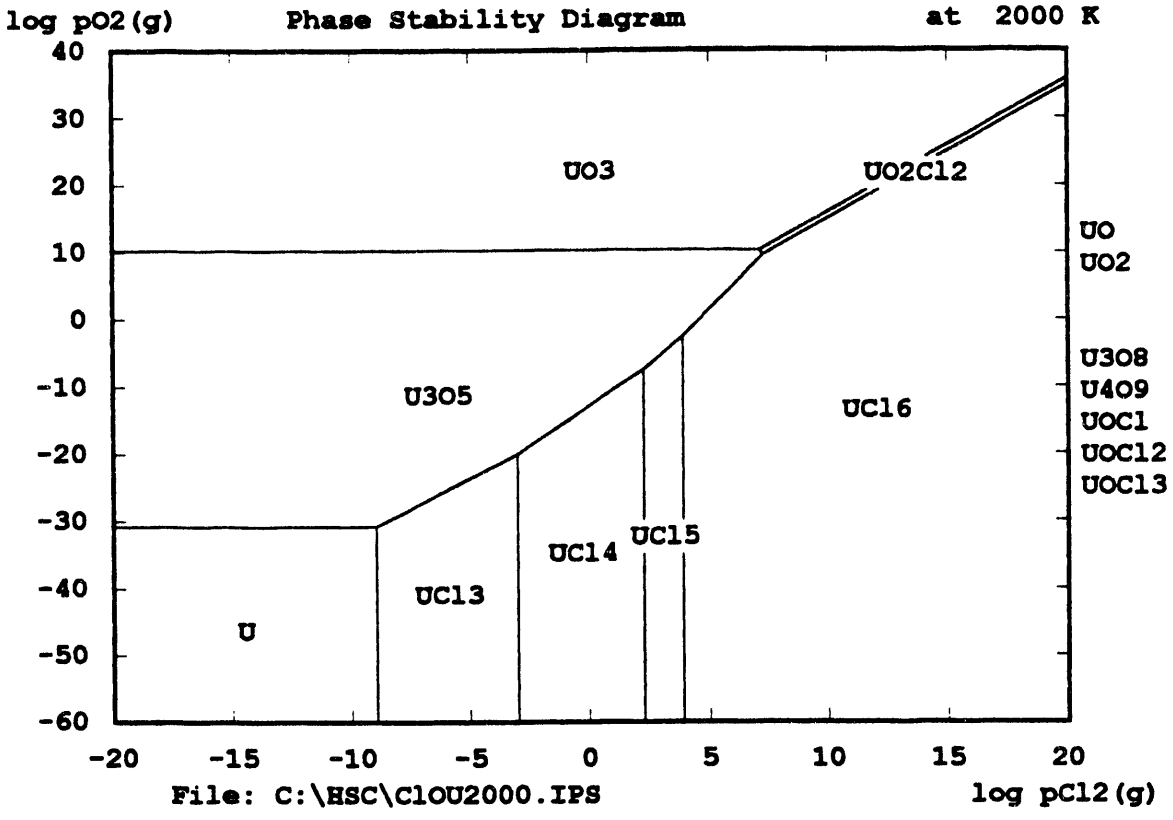

Fig. 22b. Phase stability diagram for uranium-oxygen-chlorine at 2000 K.

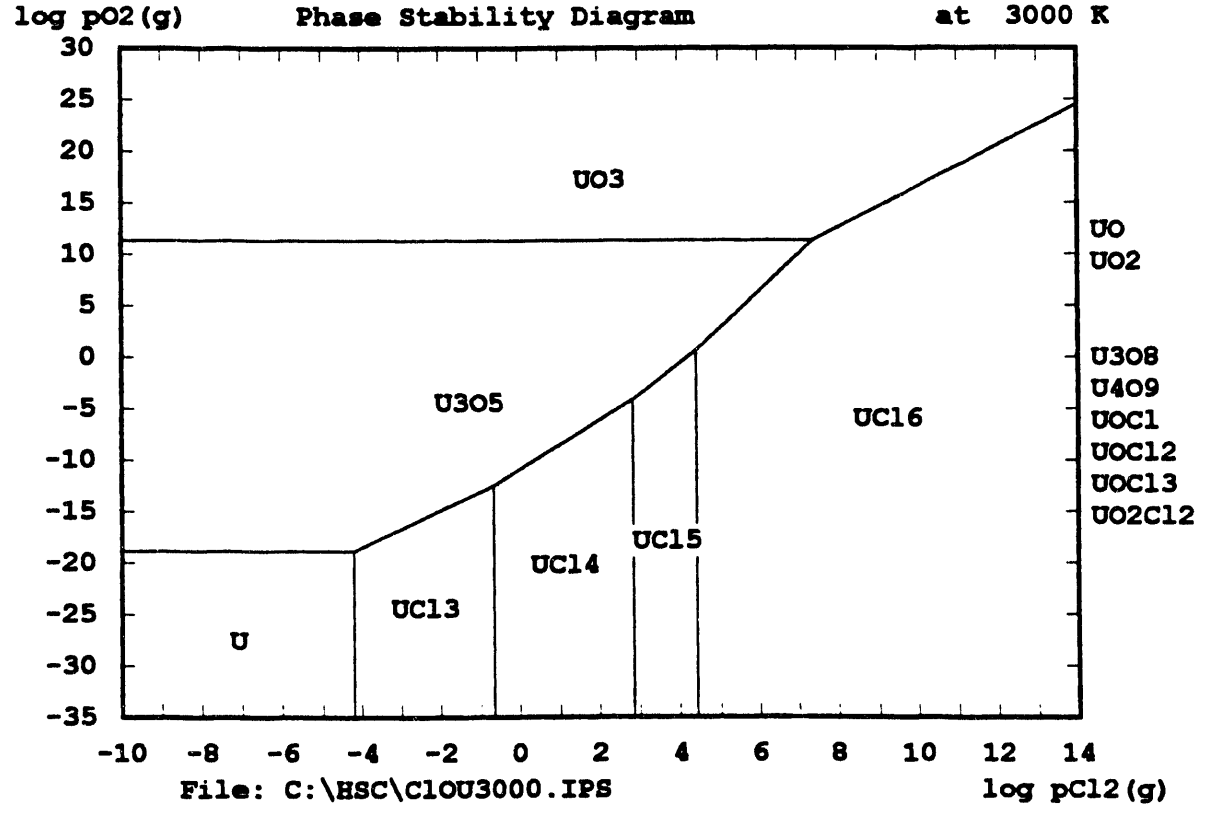

Fig. 22c. Phase stability diagram for uranium-oxygen-chlorine at 3000 K.

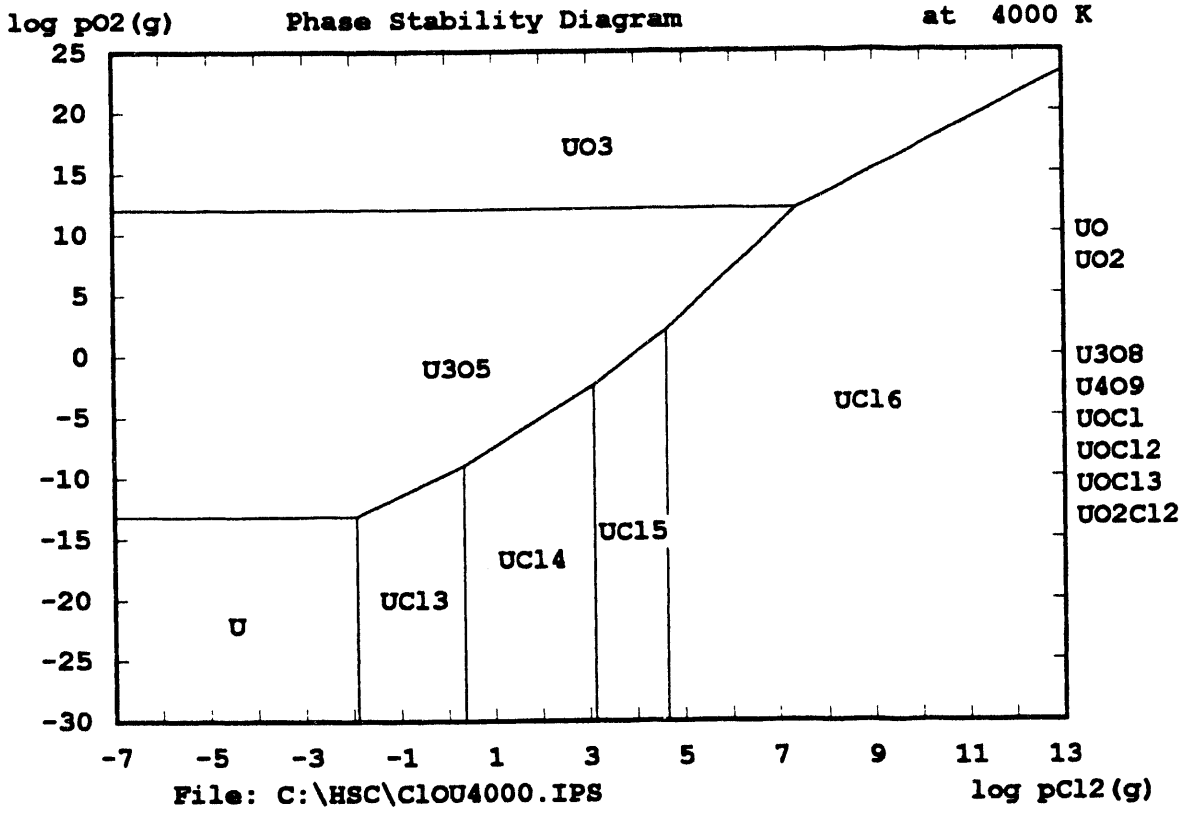

Fig. 22d. Phase stability diagram for uranium-oxygen-chlorine at 4000 K.

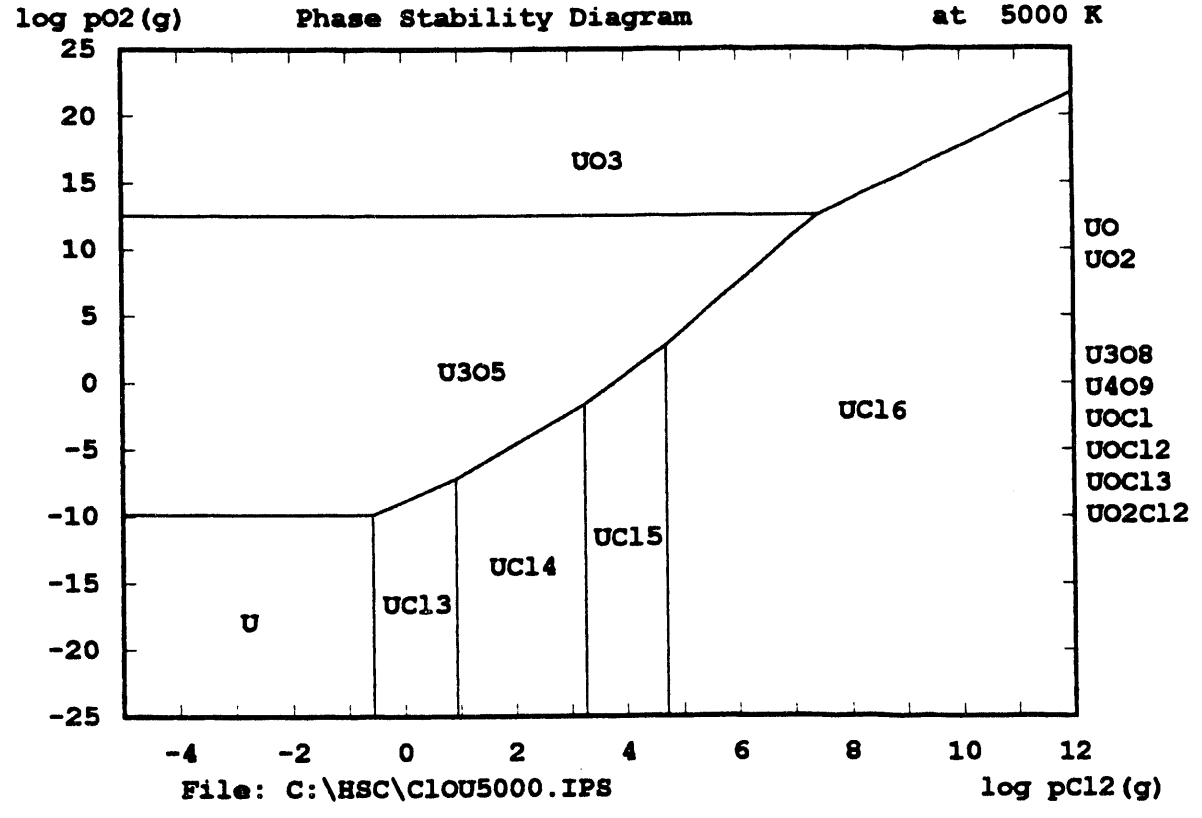

Fig. 22e. Phase stability diagram for uranium-oxygen-chlorine at 5000 K.

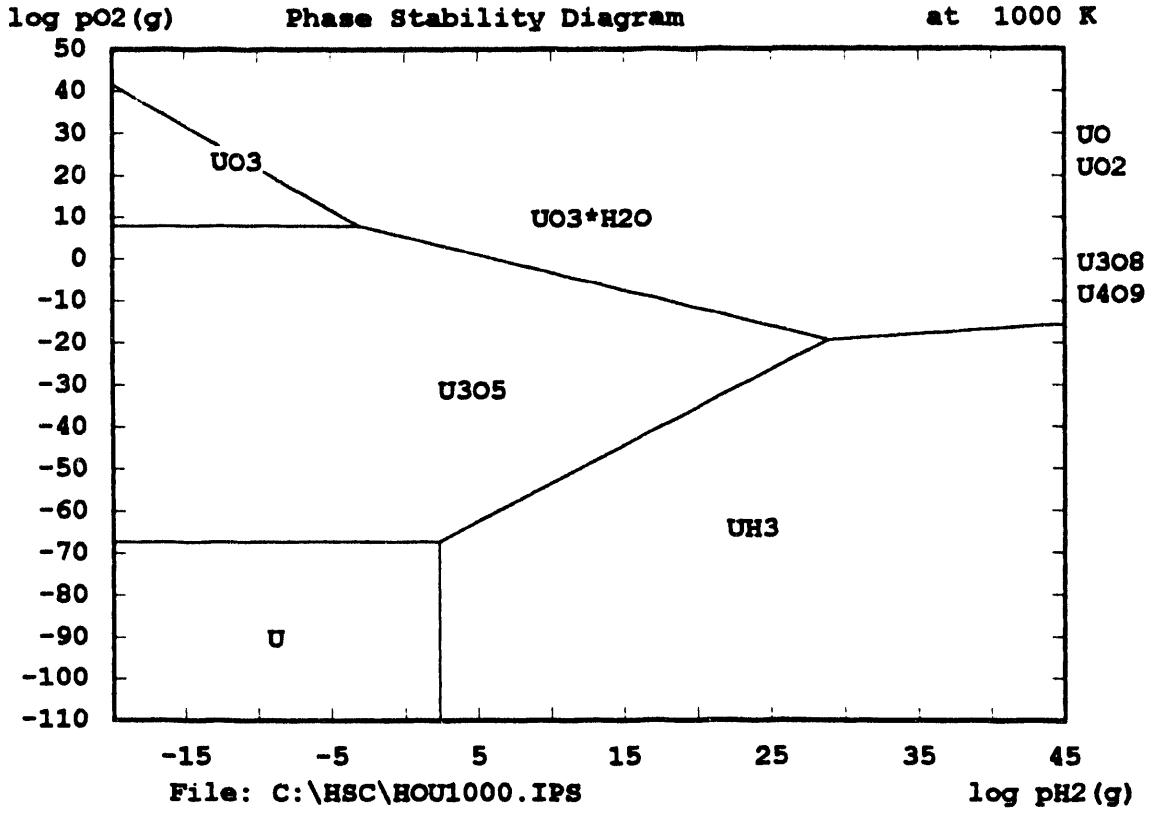

Fig. 23a. Phase stability diagram for uranium-oxygen-hydrogen at 1000 K.

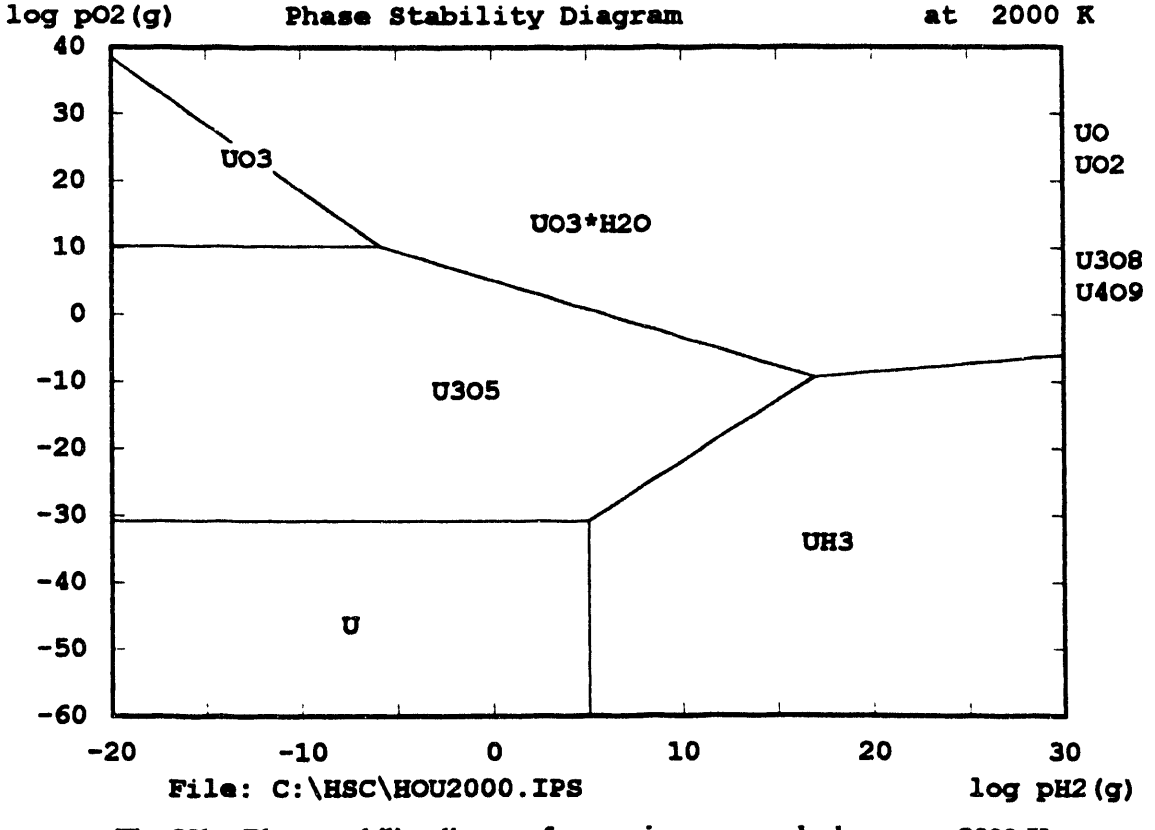

Fig. 23b. Phase stability diagram for uranium-oxygen-hydrogen at 2000 K.

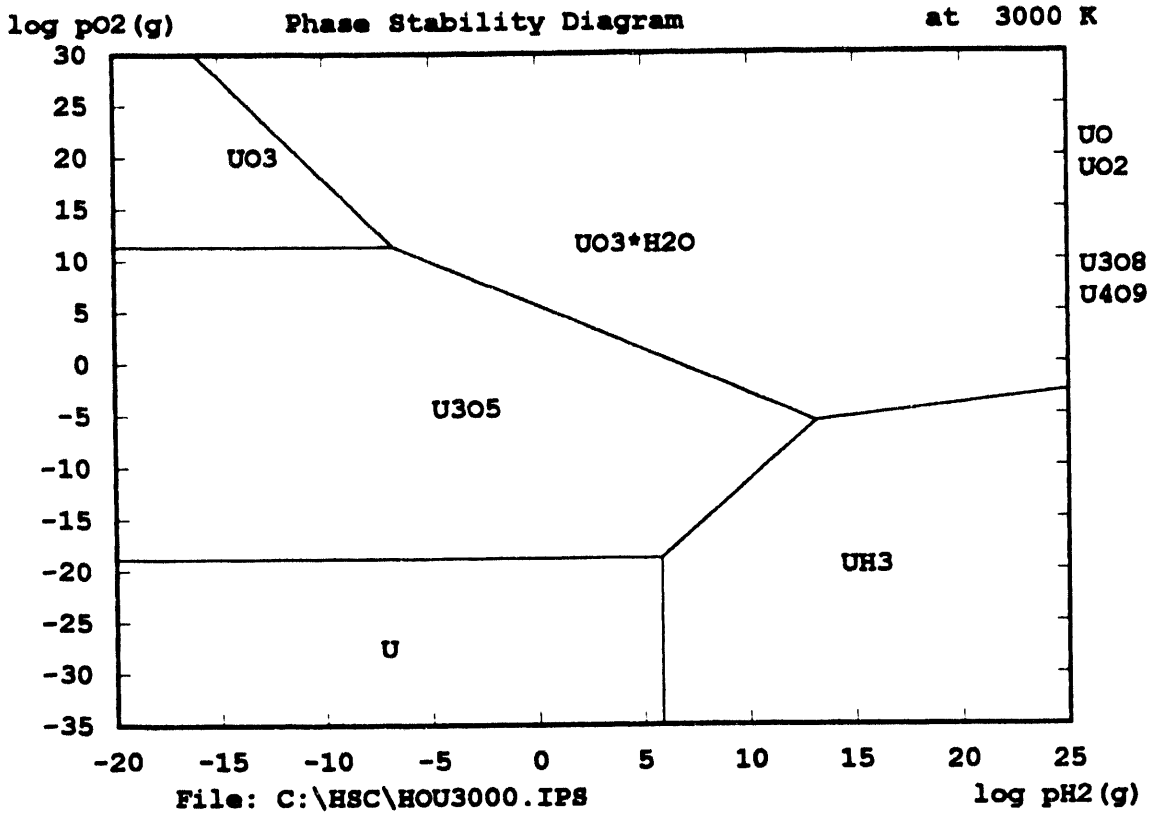

Fig. 23c. Phase stability diagram for uranium-oxygen-hydrogen at 3000 K.

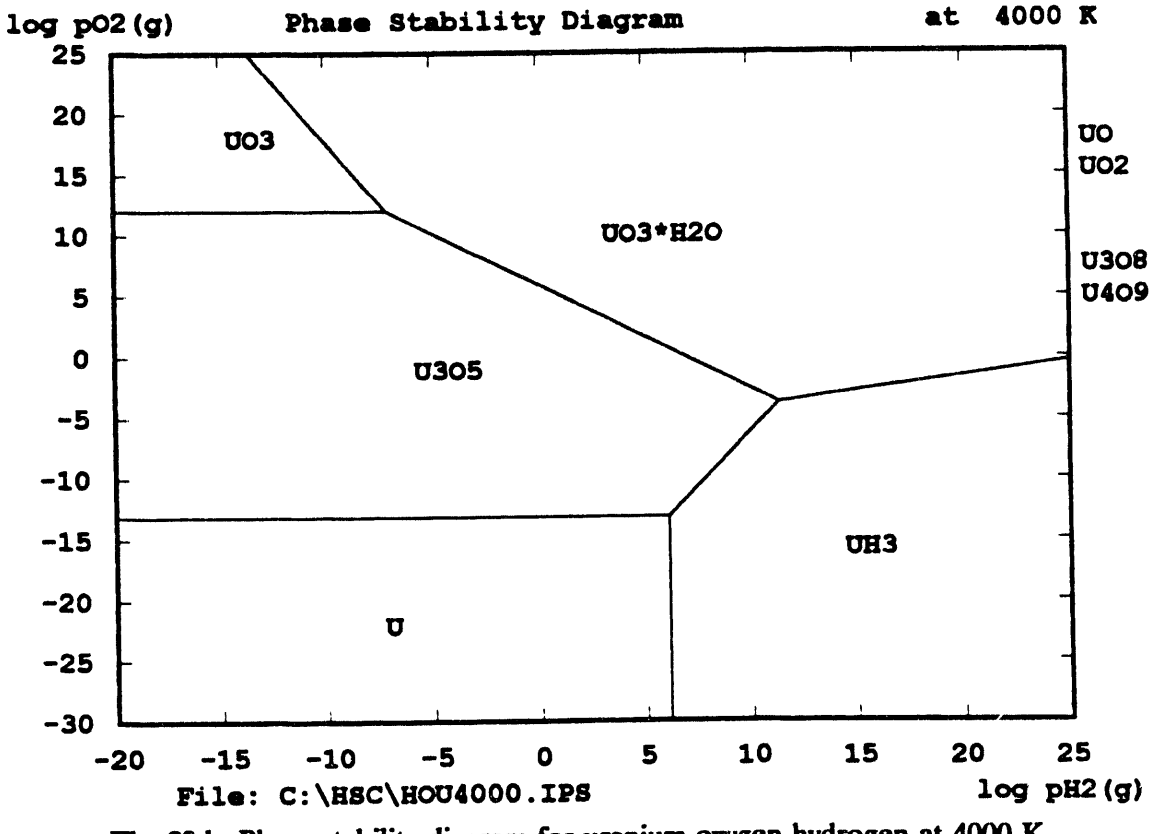

Fig. 23d. Phase stability diagram for uranium-oxygen-hydrogen at 4000 K.

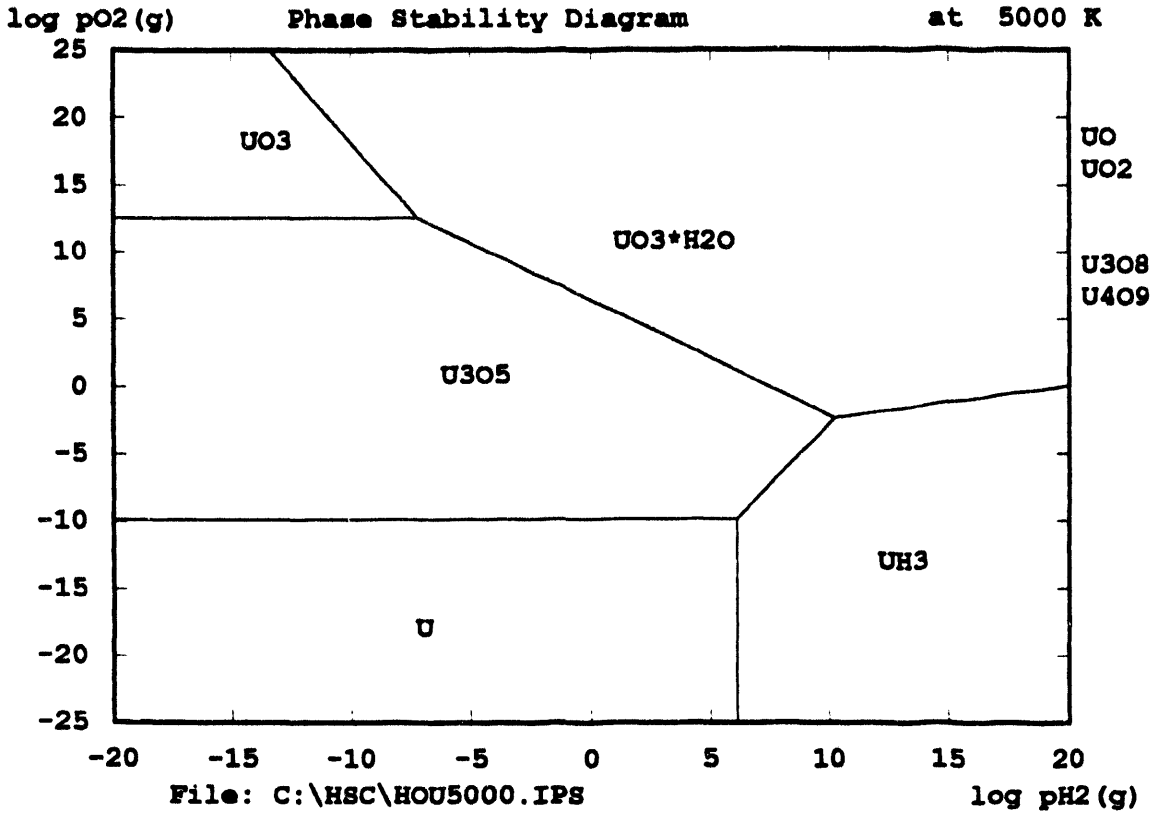

Fig. 23e. Phase stability diagram for uranium-oxygen-hydrogen at 5000 K.

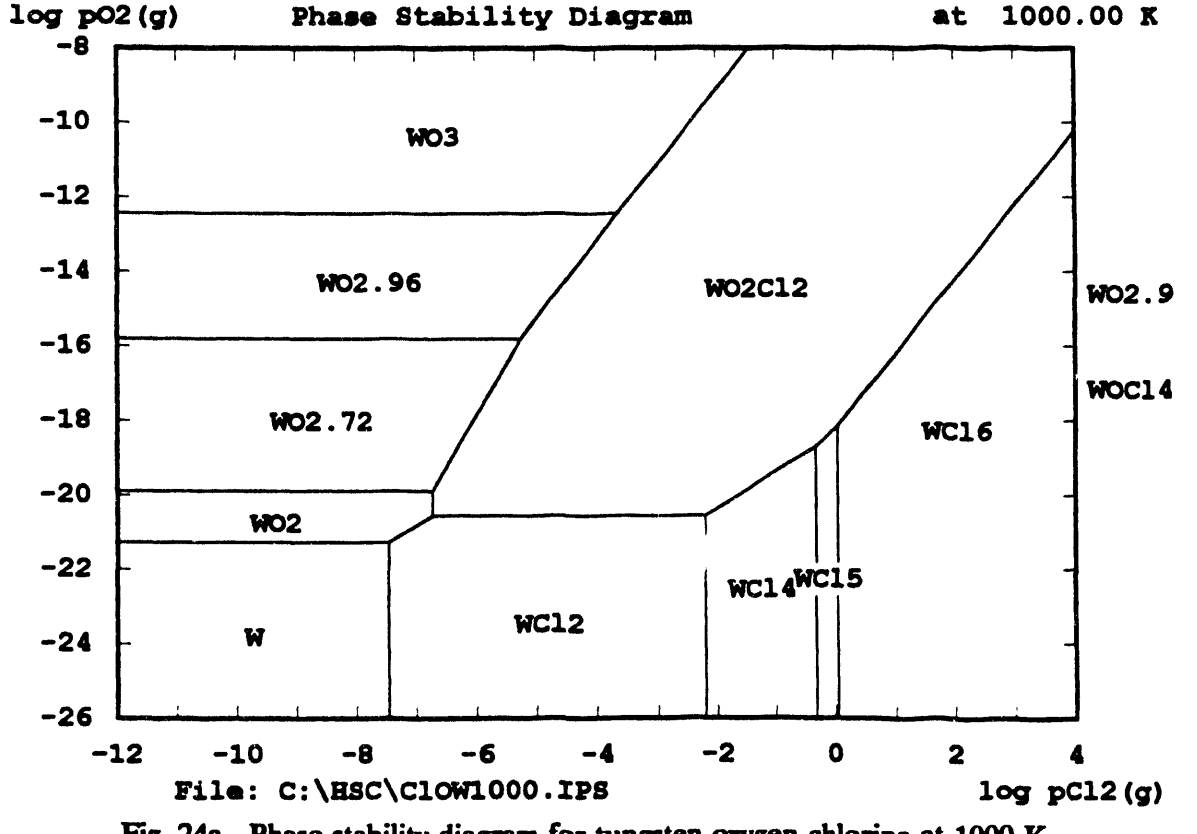

Fig. 24a. Phase stability diagram for tungsten-oxygen-chlorine at 1000 K.

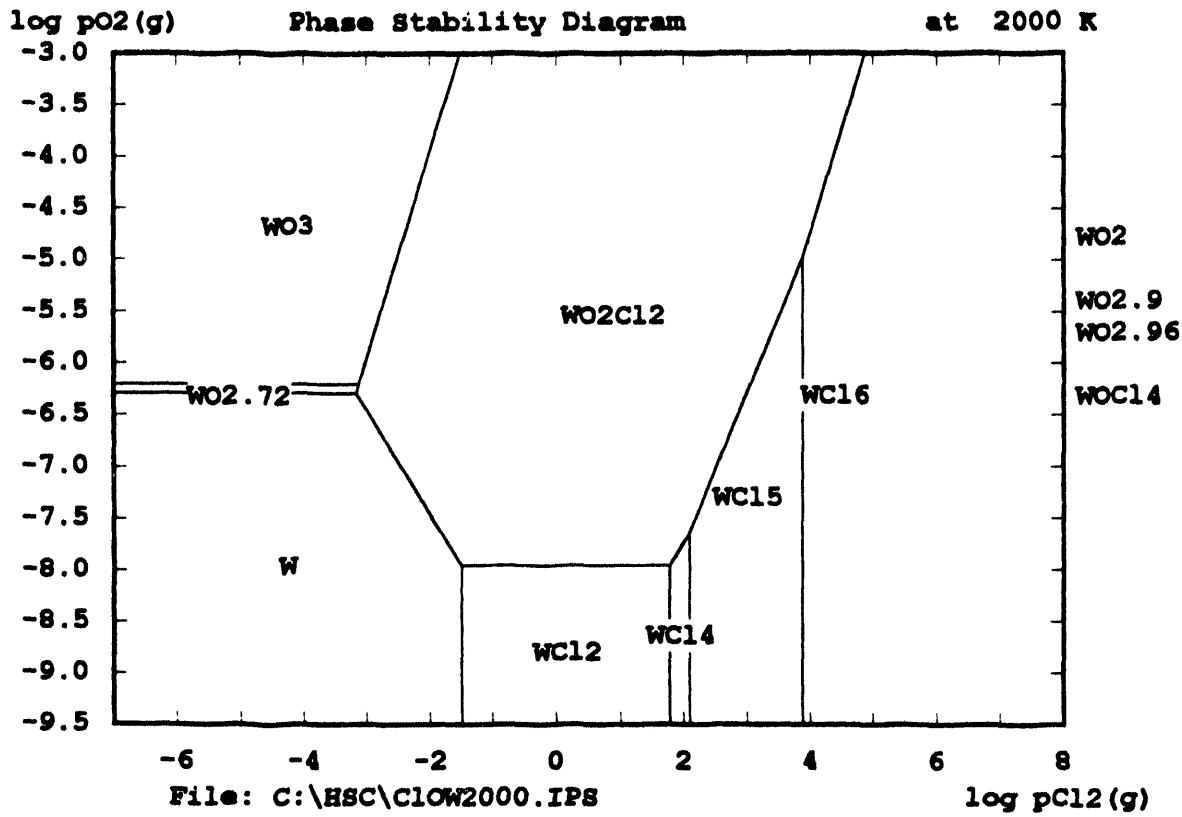

Fig. 24b. Phase stability diagram for tungsten-oxygen-chlorine at 2000 K.

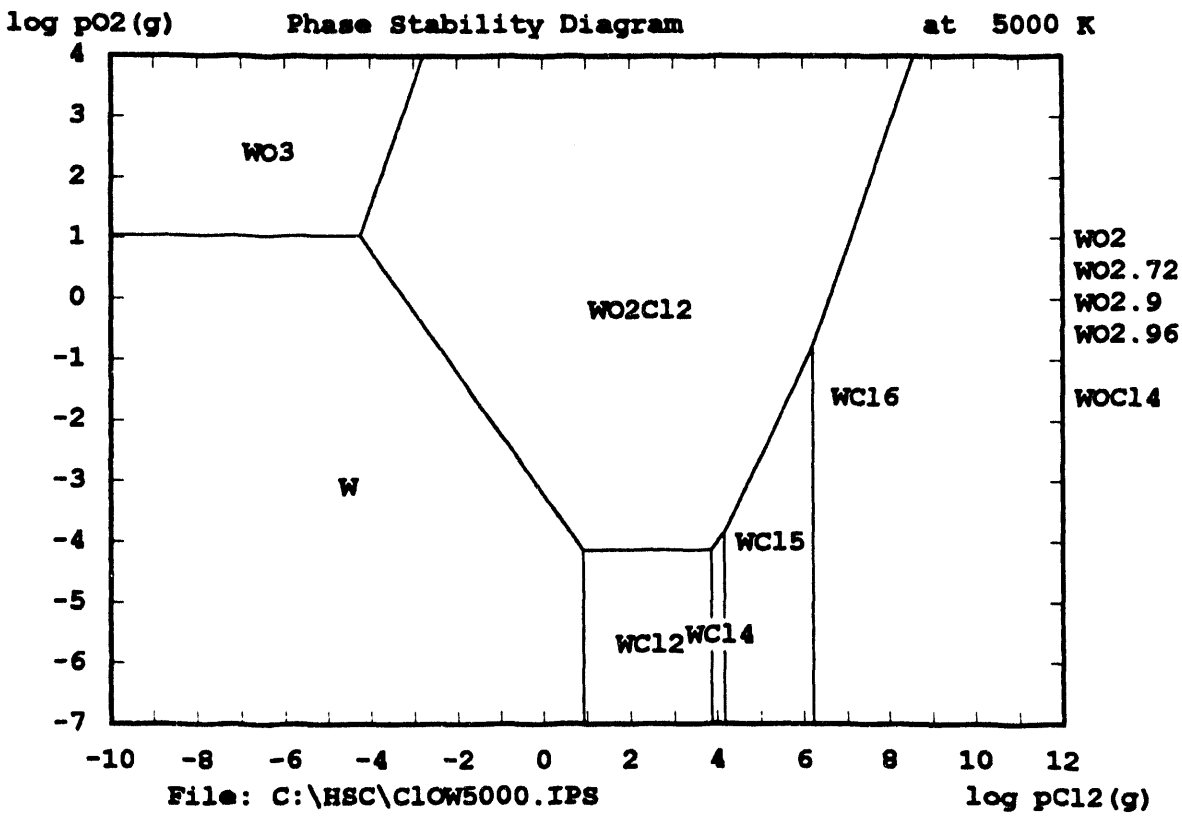

Fig. 24c. Phase stability diagram for tungsten-oxygen-chlorine at 5000 K.

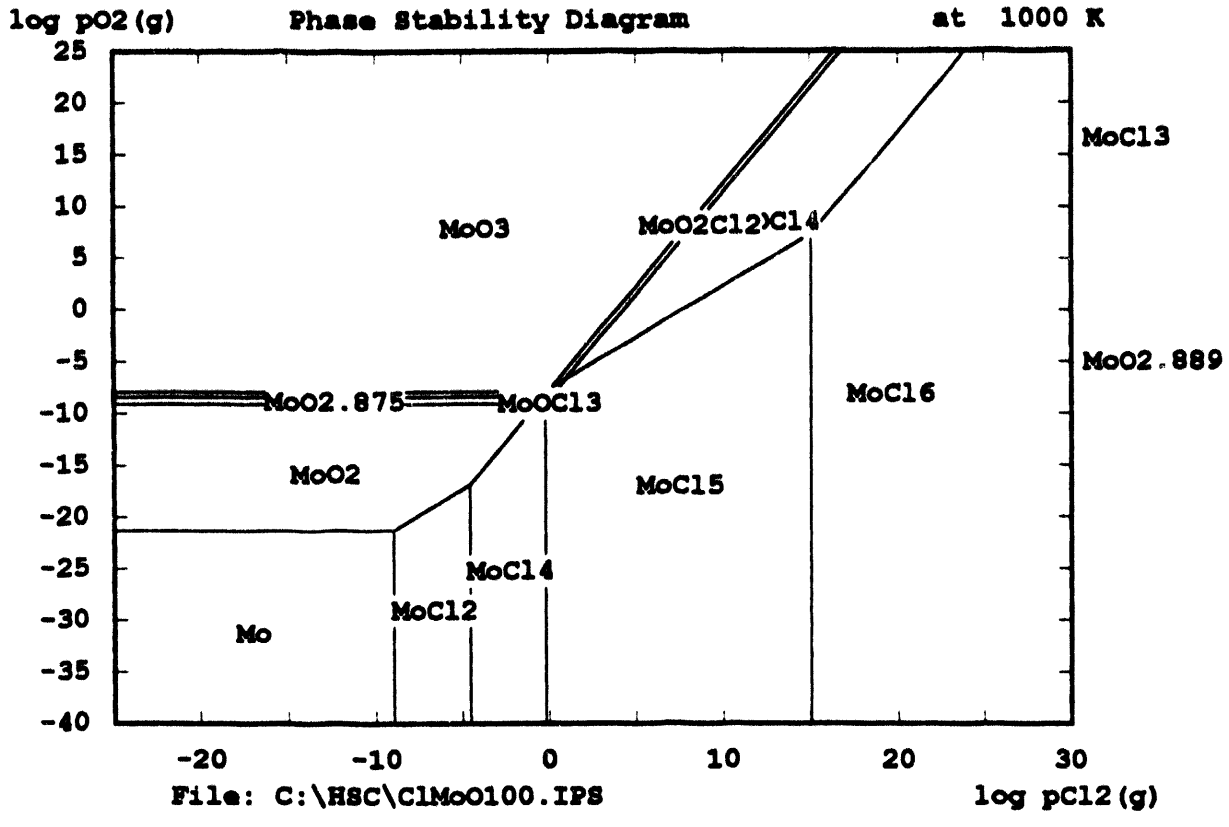

Fig. 25a. Phase stability diagram for molybdenum-oxygen-chlorine at 1000 K.

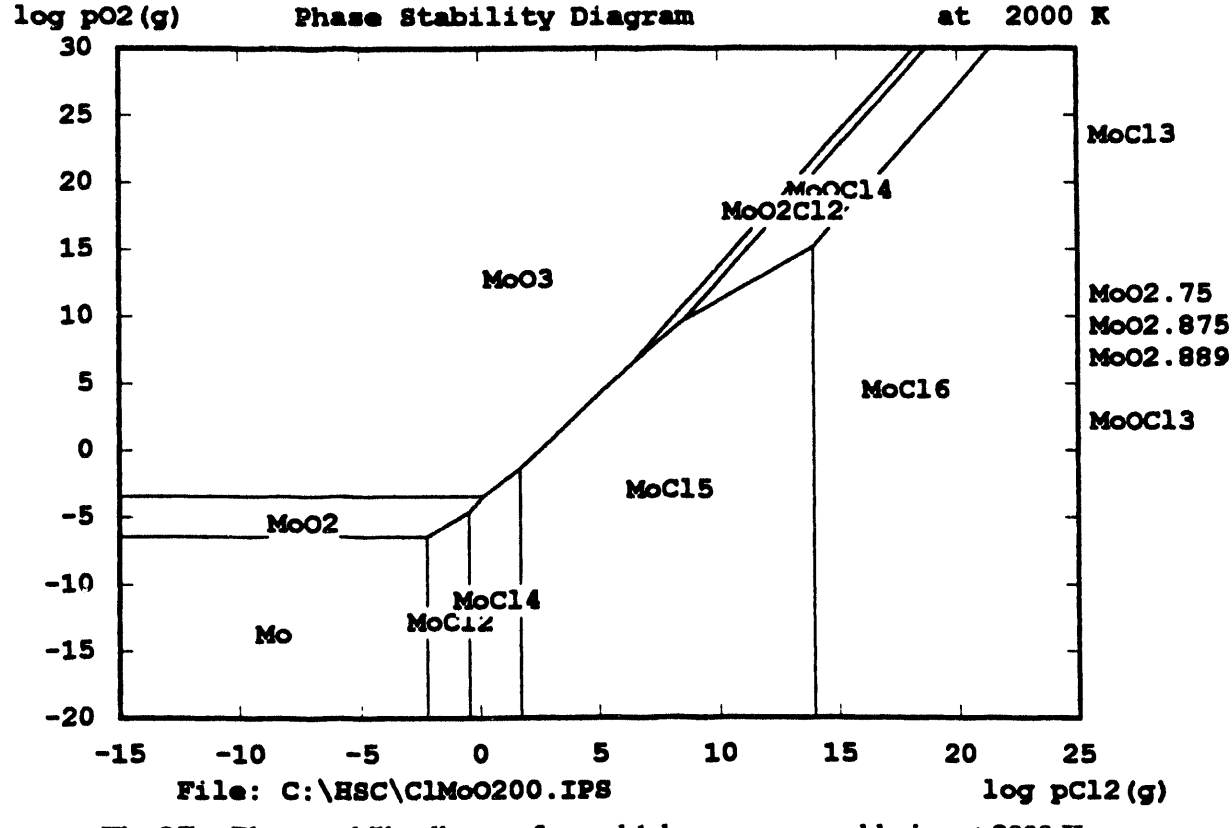

Fig. 25b. Phase stability diagram for molybdenum-oxygen-chlorine at 2000 K.

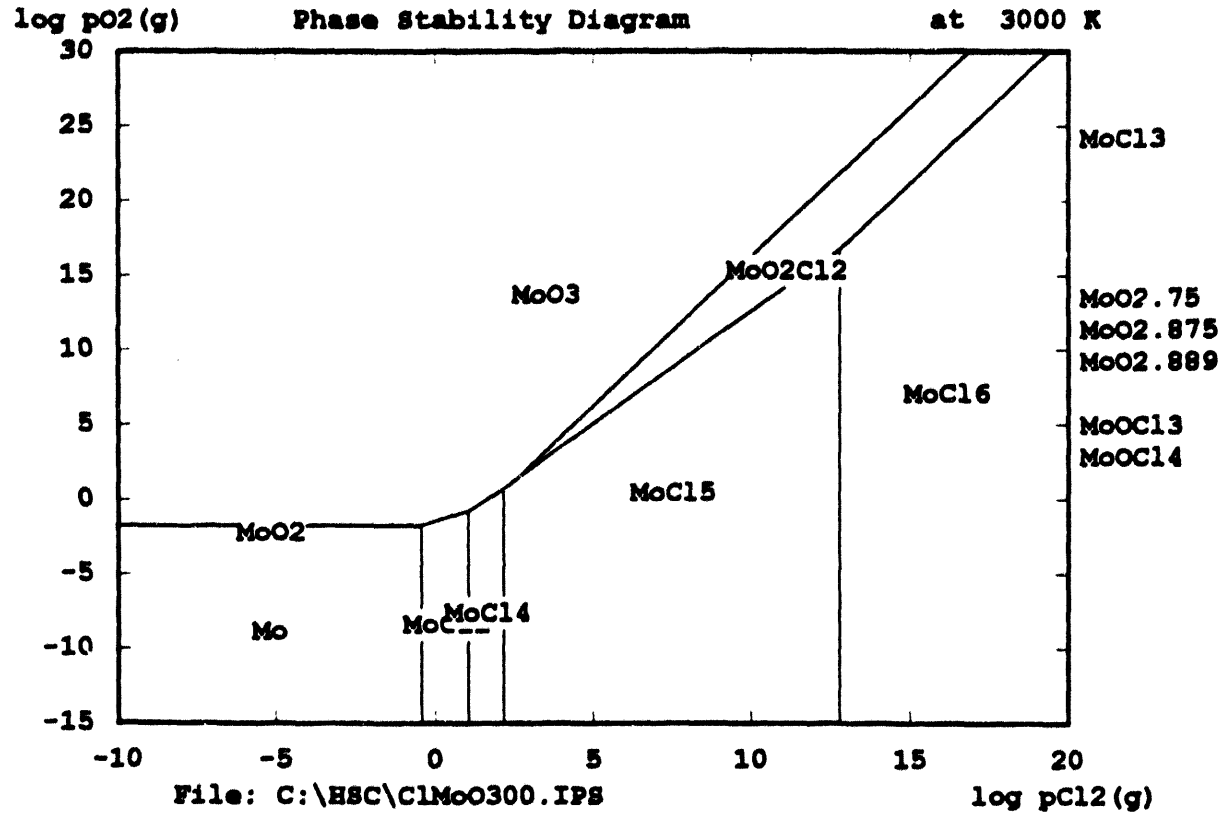

Fig. 25c. Phase stability diagram for molybdenum-oxygen-chlorine at 3000 K.

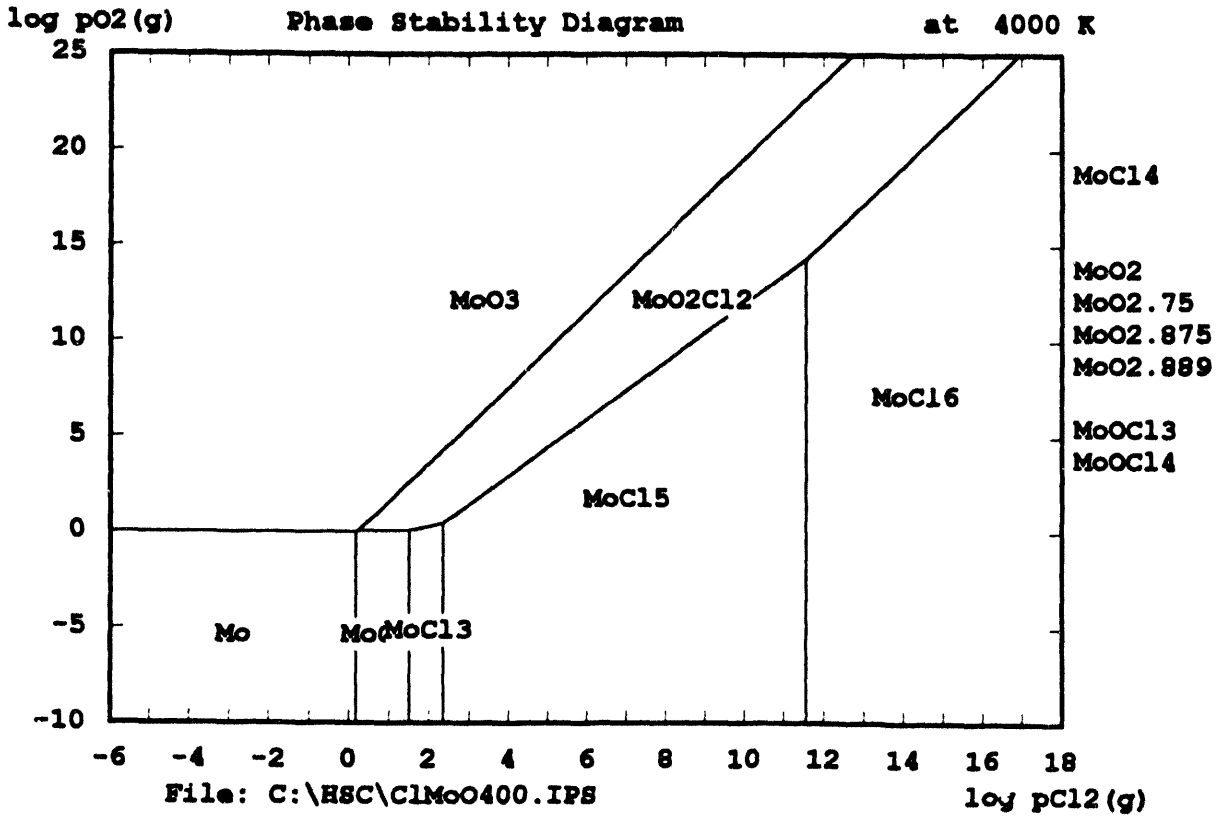

Fig. 25d. Phase stability diagram for molybdenum-oxygen-chlorine at 4000 K.

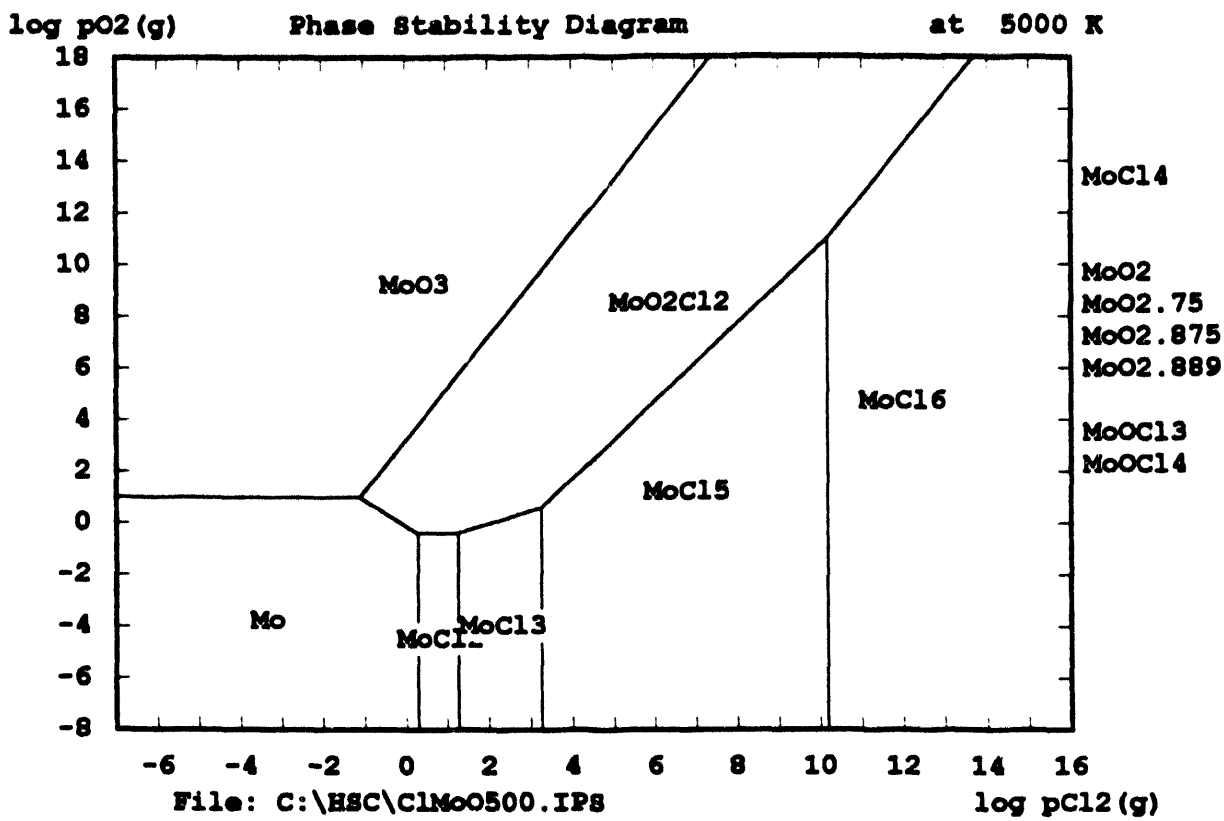

Fig. 25e. Phase stability diagram for molybdenum-oxygen-chlorine at 5000 K.

$T := 500,510 \ldots 5000$

$$\log P_T := 8.38 - \frac{30970}{T}$$

$$\log Q_T := 8.16 - \frac{28770}{T}$$

$$\log R_T := 4.36 - \frac{20790}{T}$$

Comparison of PuO1.82 and CeO2 vapor pressures.
P(atm) vs T(K).
(1) Graph P is PuO1.82:- D.R. Messier, JACS 51, 710 (1968).
Knudsen cell data, 2070-2380K.
(2) Graph Q is CeO2 over congruently evaporating Ce2O3 R.J. Ackermann and E.G. Rauh, J. Chem Thermodynam. 3, 609 (1971).
(3) Graph R is CeO2 over Ce2O3.04. ibid.

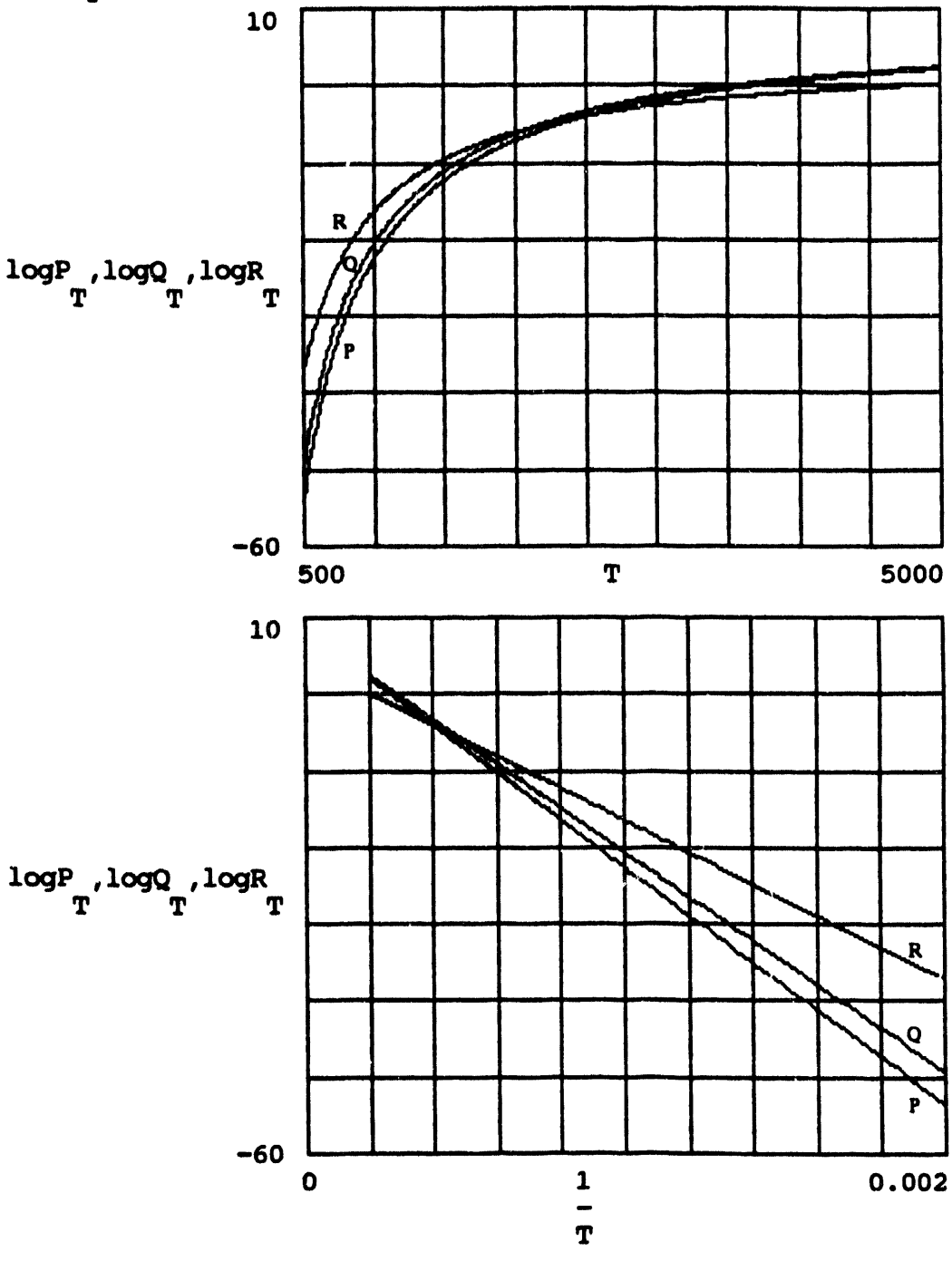

Fig. 26. Comparison of $PuO_{1.82}$ and CeO_2 vapor pressures.

$T := 500,510 \ldots 5000$

$$\log P_T := 29.65 - \frac{34933}{T} - 5.64 \cdot \log(T)$$

$$\log Q_T := 8.846 - \frac{34933}{T}$$

$$\log R_T := 10.057 - \frac{31910}{T}$$

UO2 vapor pressure (atm) vs T (K).
P is IWGFR recommendation.
Q is OK to MP.
Gmelin Handbook of Inorganic Chemistry
Supplement C5 (1986).
R is fit to Katz and Rabinowitch,
1873-2273K effusion data.
Chemistry of Uranium (1951).

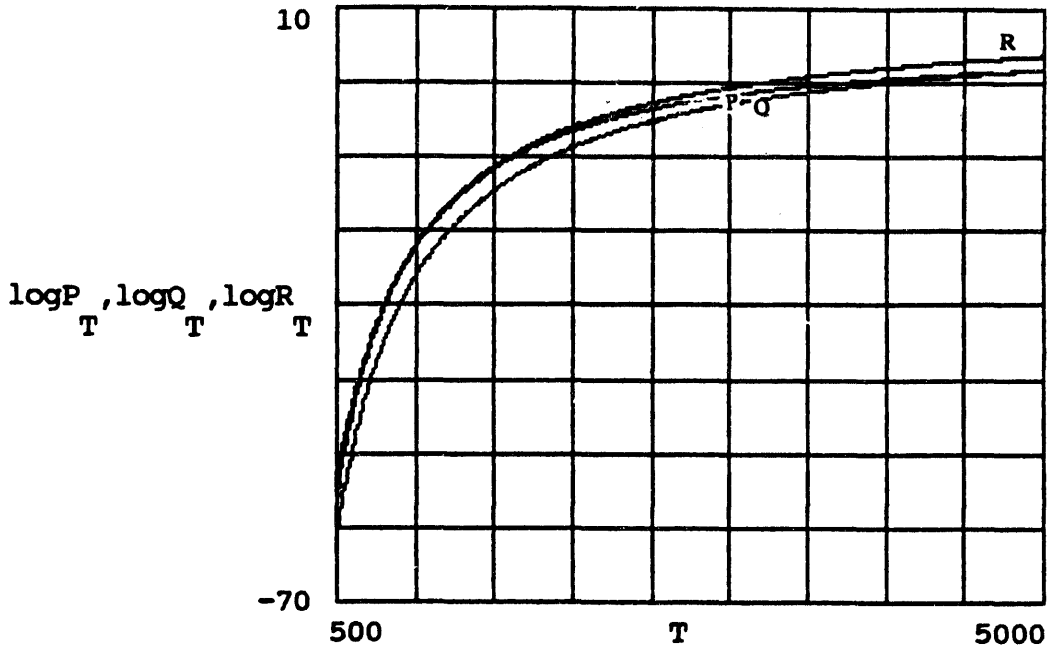

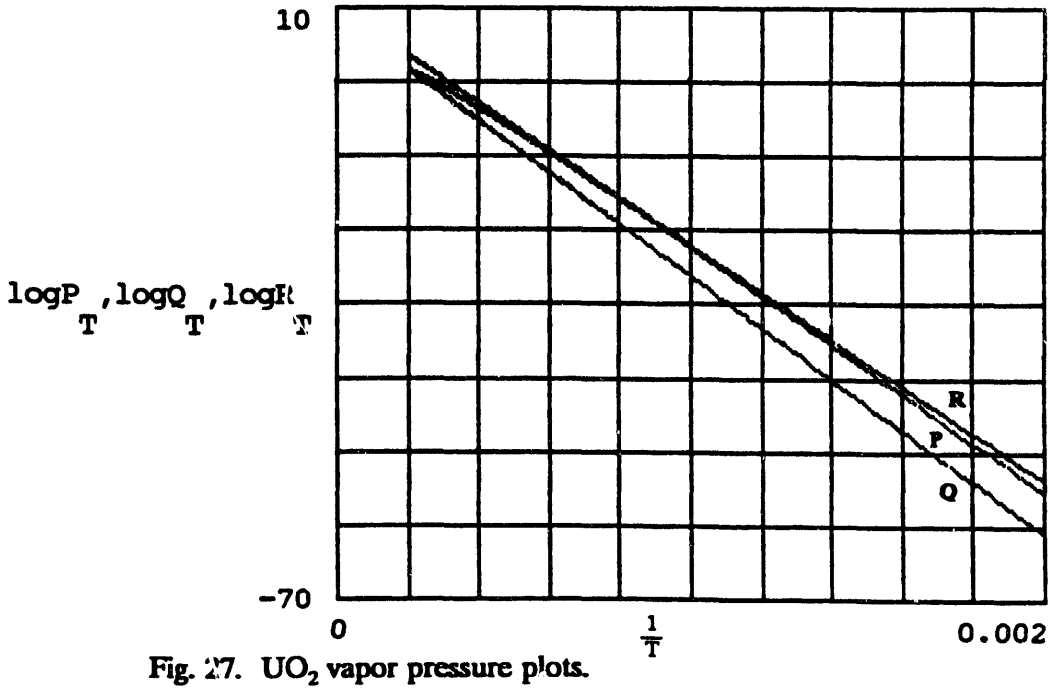

Fig. 27. UO_2 vapor pressure plots.

```
r := corr(x,y)
m := slope(x,y)

b := intercept(x,y)

linear(x) := m·x + b
```

r = -0.999

$m = -3.191 \cdot 10^{4}$

b = 10.057

logP(UO2)(atm)
=10.057-3.191E4/T(K).
Katz and Rabinowitch,
Chem of Uranium (1951)
1873-2273K.

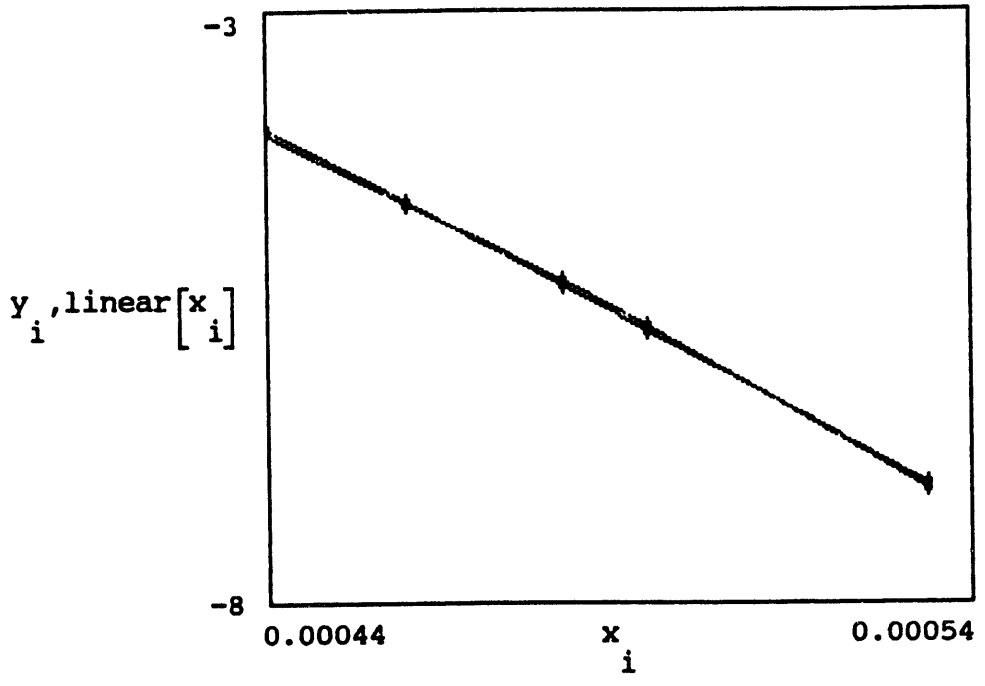

Fig. 28. Fit to Katz and Rabinowitch (1951) UO_2 vapor pressure data.

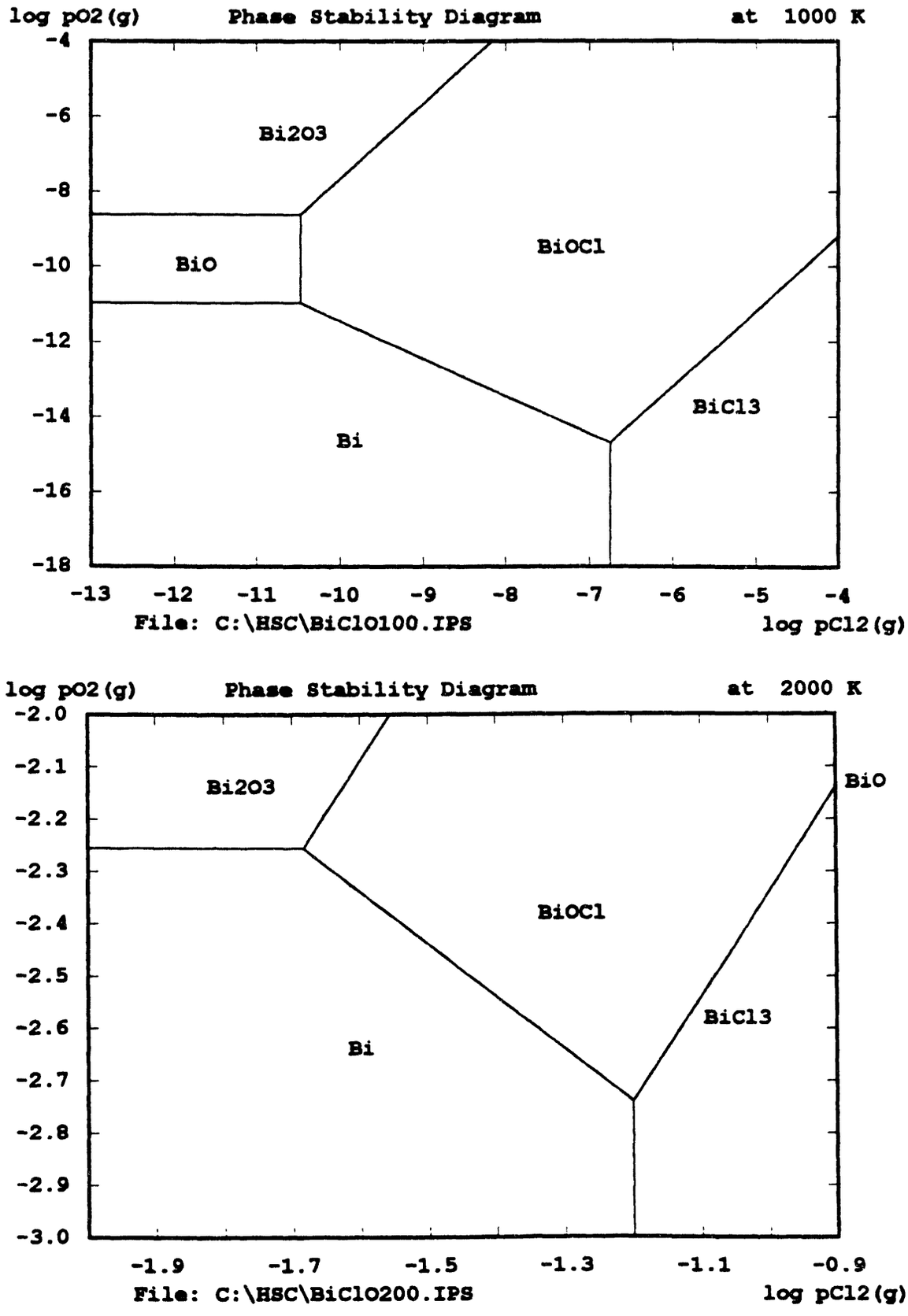

Fig. 29. Phase stability diagrams for bismuth-oxygen-chlorine. (*a*) At 1000 K, (*b*) at 2000 K.

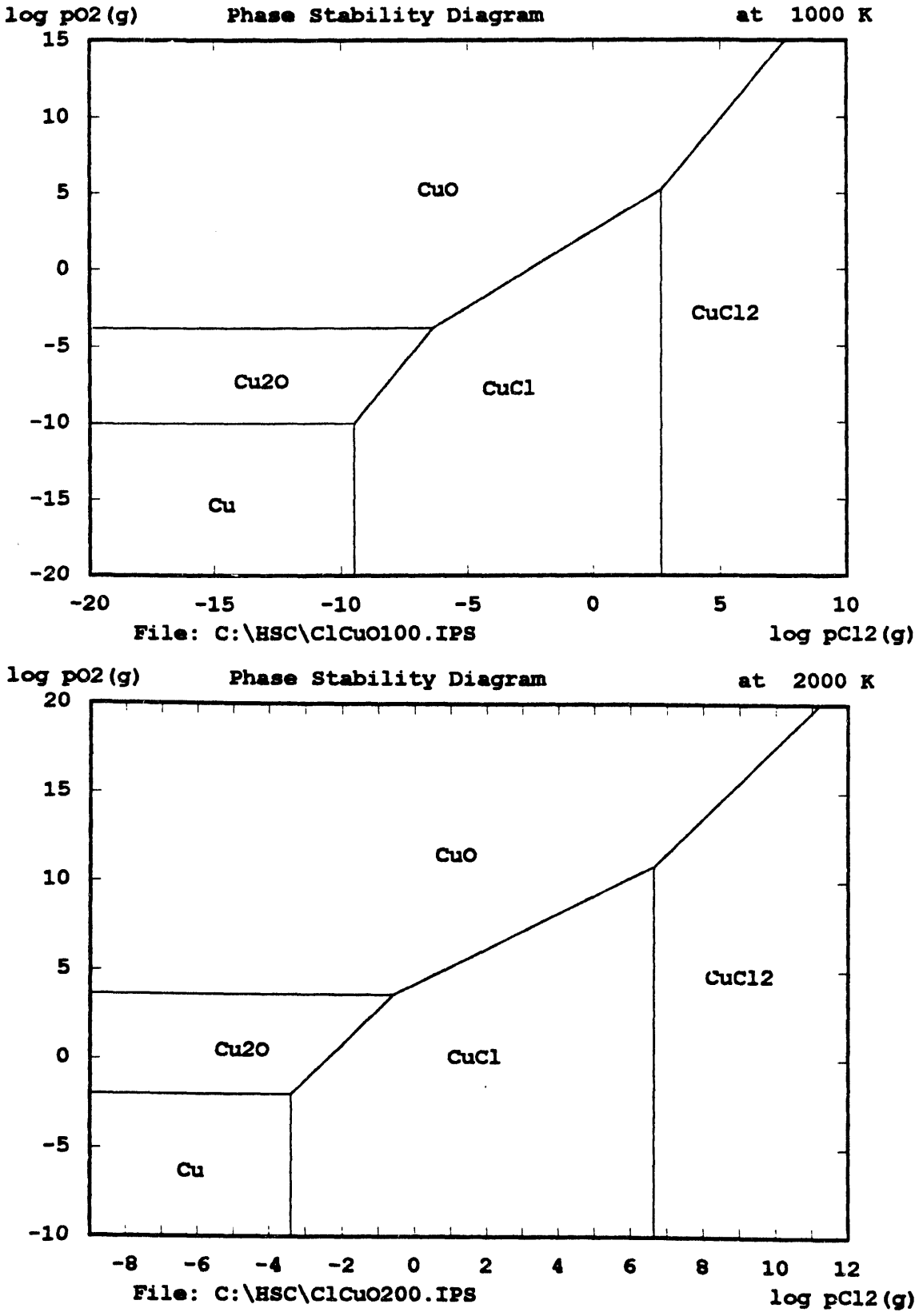

Fig. 30. Phase stability diagrams for copper-oxygen-chlorine. (*a*) At 1000 K, (*b*) at 2000 K.

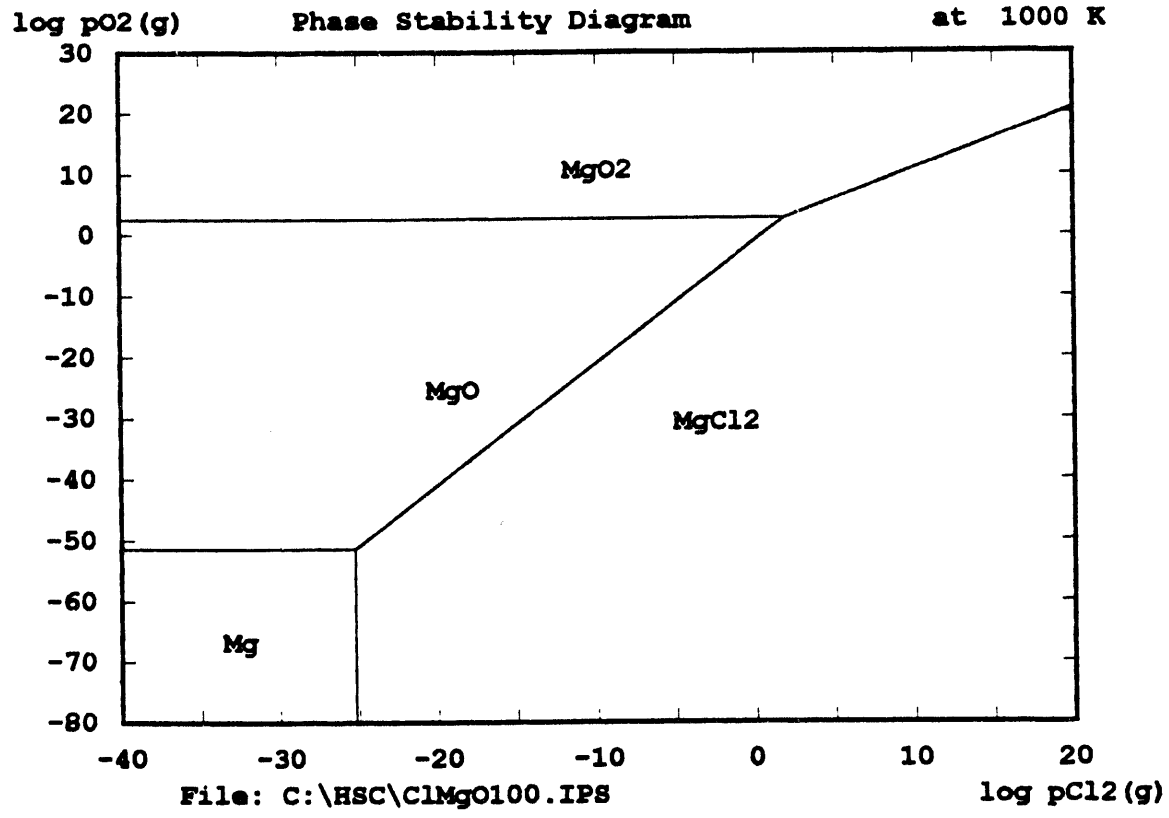

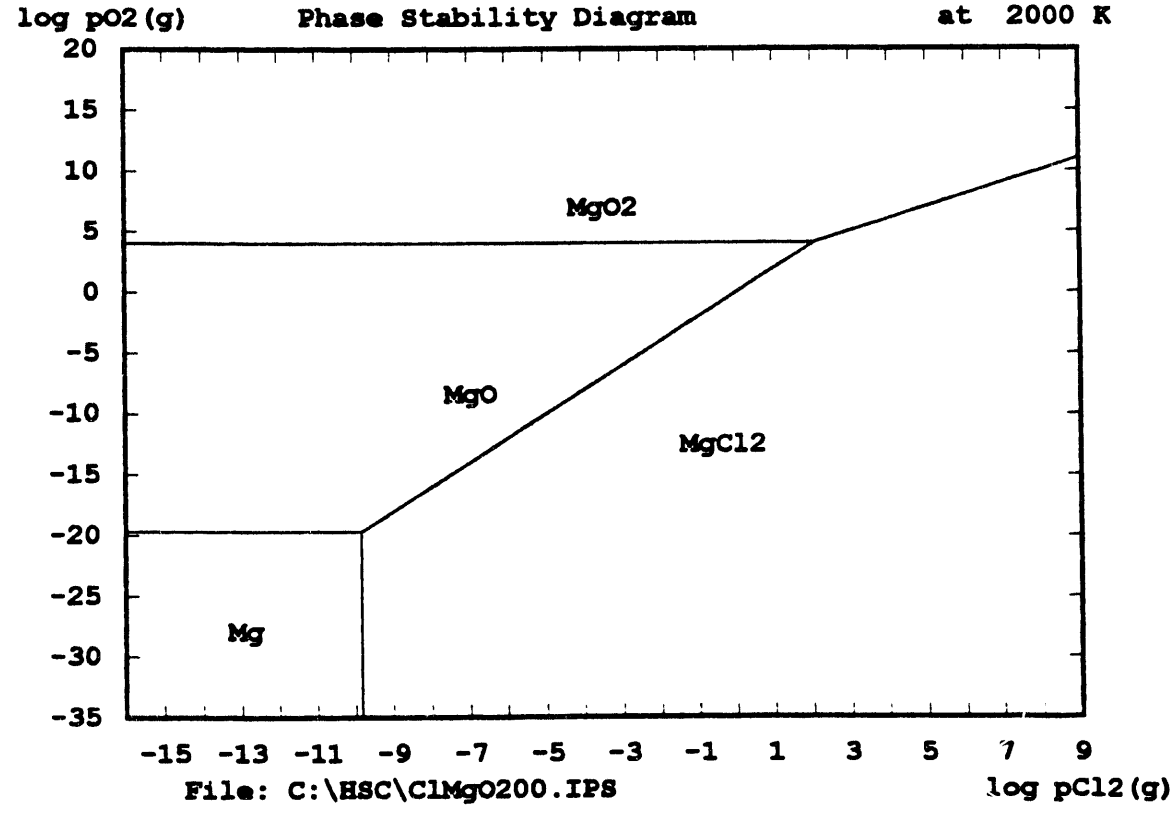

Fig. 31. Phase stability diagrams for magnesium-oxygen-chlorine. (*a*) At 1000 K, (*b*) at 2000 K.

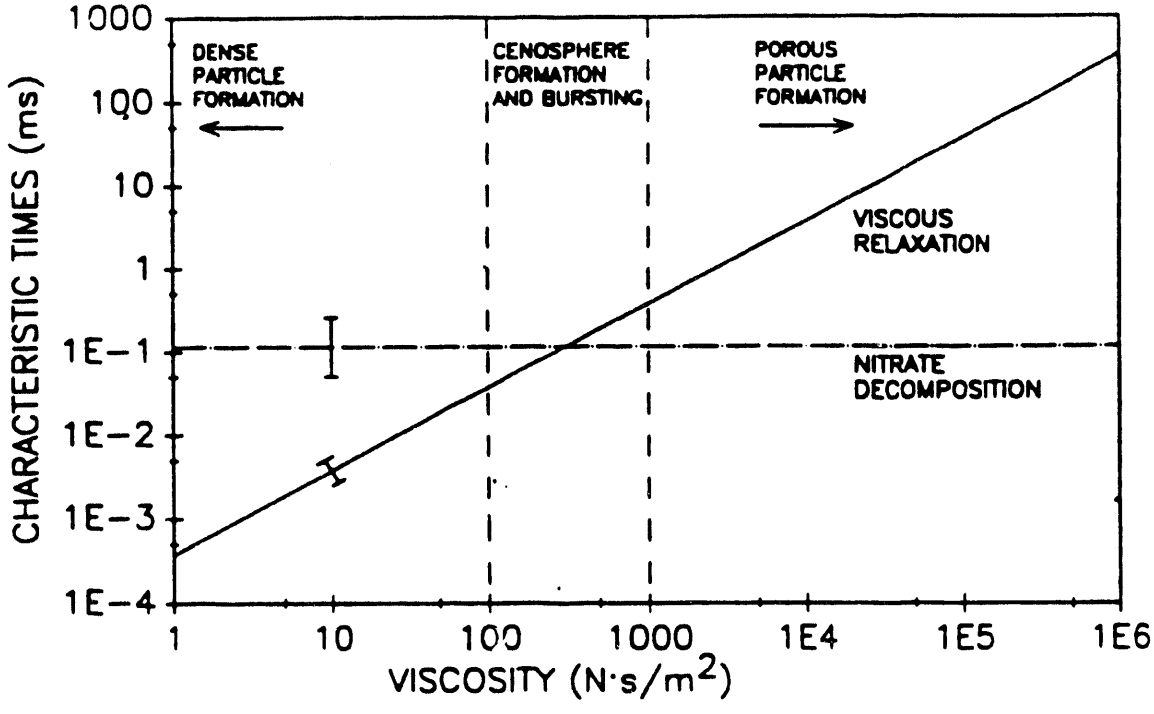

Fig. 32. Characteristic viscous relaxation time for a 4-μm particle expanding to 10 μm. Also shown is the characteristic time for nitrate decomposition (dashed-dotted line) for a 4 μm particle at a furnace temperature of 1200 K. Variations in the results of calculations using a wide range of metal nitrate properties are indicated by error bars. This diagram is Fig. 7 of ref. 32 (Mulholland and Sarofim), reproduced by permission of copyright holder.

INTERNAL DISTRIBUTION

1. T. Abraham
2. W. Anderson
3. W. Altman
4. P. Backus
5. M. Baer
6. M. Baker
7. R. Bastion
8. H. Beeson
9–13. J. Berry
14. G. Bloom
15. G. Boris
16. W. Bostick
17. C. Brown
18. C. Buttram
19. R. Cannon
20. J. Chiang
21. A. Croff
22. T. Conley
23. S. Crosley
24. C. Daugherty
25. J. Dunn
26. M. Elmore
27. R. Fellows
28. C. Frye
29. R. Genung
30. R. Glass
31. L. Gibson
32. M. Gilliam
33. E. Harrington
34. H. Haselton
35. H. Hayden
36. W. Hermes
37. B. Hightower
38. D. Hoffman
39. D. Hutchins
40. G. Kamp
41. J. Kennerly
42. R. R. Kimmett
43. D. Kucsmas
44. H. Lee
45. D. Lennon
46. A. Malinauskas
47. A. Mattus
48. C. Mattus
49. D. Milewski
50. M. Morris
51. D. Moser
52. C. Newman
53. J. Perona
54. A. Richmond
55. T. Rogers
56. R. Sams
57. L. Stinton
58. P. Wayland
59. Central Research Library
60. Document Reference Center
61. ORNL Patent Section
62–63. ORNL Laboratory Records
64. ORNL Laboratory Records, RC

EXTERNAL DISTRIBUTION

65. N. Askew, Westinghouse Savannah River Co., P.O. Box 616, Aiken, SC 29802
66. C. Baldwin, EG&G Rocky Flats, P.O. Box 464, Highway 93 & Cactus, Bldg. 881, Golden, CO 80402-0464
67. M. Ballestri, BDM Federal, 20251 Century Blvd., 4th Floor, Germantown, MD 20874
68. L. M. Barton, Jr., Vortec Corporation, 3370 Ridge Pike, Collegeville, PA 19426-3158
69. J. Bassi, EM-351, U.S. Department of Energy, 12850 Middlebrook Road, Germantown, MD 20874
70. R. Bastian, Focus Environmental, 9050 Executive Park Drive, Suite A-202, Knoxville, TN 37923
71. S. Bates, EG&G Idaho, Inc., P.O. Box 1625, MS-3930, Idaho Falls, ID 83415-3930
72. T. Bergsman, Battelle Pacific Northwest Laboratory, Battelle Boulevard, MS P7-41, Richland, WA 99352
73. P. Biswas, Environmental Engineering, University of Cincinnati, Cincinnati, OH 45221-0071
74. W. J. Bjorklund, Waste Management Section, Laboratory Safety Department, Batellee Pacific Northwest Labs, P.O. Box 999, Richland, WA 99352
75. L. Borduin, Los Alamos National Laboratory, One Bikini Road, MS K557, Los Alamos, NM 87545
76. M. Brooks, Waste Policy Institute, 555 Quince Orchard Blvd., Suite 600, Gaithersburg, MD 20879
77. D. Brooman, Belfort Engineering and Environmental Services, 275 West St., Annapolis, MD 21401
78. H. Burns, Westinghouse Savannah River Co., P.O. Box 616, Bldg. 704-61s, Aiken, SC 29808
79. G. Bryan, Pacific Northwest Lab, Battelle, Blvd., Richland, VA 99352
80. P. Castel, U.S. DOE/HQ, WINCO, 20201 Century Blvd., Rm. 408, Germantown, MD 20874
81. D. Chaiko, Argonne National Lab, CMT/Bldg. 205, 9700 S. Cass Ave., Argonne, IL 60439
82. W. Clark, Energy and Environmental Research Corporation, 18 Mason, Irvine, CA 92718
83. C. Collier, BDM Federal, 20251 Century Blvd., 4th Floor, Germantown, MD 20874
84. C. Cooley, U.S. Department of Energy, EM-50, Trevion II, Washington, D.C. 20585-0002
85. T. Cooper, Westinghouse Hanford Corp., 2355 Stevens Dr., MS N3-12, Richland, WA 99352
86. J. Cooper, Chester Environmental, 12242, S.W. Garden Place, Tigard OR 97223
87. A. Corstillo, FERMCO, 25 Merchant St., 3rd Floor Technology, Springdale, OH 45246
88. S. Couture, Lawrence Livermore National Lab, P.O. Box 808, L-591, Livermore, CA 94551
89. G. Coyle, EM-541, U.S. Department of Energy, 12800 Middlebrook Road, Trevion II, Germantown, MD 20874-1290
90. P. Coyle, EM-55, U.S. Department of Energy, 19901 Germantown Road, Germantown, MD 20874

91. J. Cudalty, Focus Environmental, 9050 Executive Park Drive, Suite A-202, Knoxville, TN 37923
92. J. Cunnane, Argonne National Lab, 9700 South Cass Ave., Bldg, 205, Argonne, IL 60439
93. J. Dancz, SAIC, Quince Diamond Executive Center, 555 Quince Orchard Rd., Suite 500, Gaithersburg, MD 20878-4137
94. W. Davis, University of Tennessee, College of Engineering, Knoxville, TN 37996-2010
95. C. Dempsey, Risk Reduction Engineering Lab, US EPA, Cincinnati, OH 45224
96. L. Dole, Environmental Remediation Consultant, 2108 Granada Blvd., Knoxville, TN 37922
97. S. Domotor, U.S. Department of Energy, EM-351, Trevion II, Washington, DC 20585
98. M. Durham, ADA Technologies, Inc., 304 Inverness Way South, Suite 110, Englewood, CO 80112
99. A. Eicher, Focus Environmental, 9050 Executive Park Drive, Suite A-202, Knoxville, TN 37923
100. P. Erickson, EPA-RREL, 5995 Center Hill Ave., Cincinnati, OH 45224
101. R. Eschenbach, Retech, Inc., P.O. Box 997, 100 Henry Station Road, Ukiah, CA 95482-0997
102. J. Fannon, U.S. DOE, HQ/EM-50, 20201 Century Blvd., Bellmeade Bldg. II, Rm. 402, Germantown, MD 20874
103. C. Frank, EM-50, U.S. Department of Energy, Forrestal Office Building, Washington, DC 20585
104. E. Franz, Brookhaven National Lab, Environmental & Waste Technology Center, North Railroad St., Bldg. 830, Upton, NY 11973
105. G. Frazier, University of Tennessee, College of Engineering, Knoxville, TN 37996-2010
106. N. French, Sandia National Laboratory-Livermore, 7011 East Avenue, Livermore, CA 94550
107. M. Fuhrmann, Brookhaven National Laboratory, Building 703, Upton, NY 11973
108. A. Gatuchette, US EPA, Risk Reduction Engineering Lab, 26 W. Martin Luther King Blvd., Cincinnati, OH 45268
109. R. Gay, Rockwell International, Canoga Park, CA 91309-7930
110. R. Gehrke, EG&G Idaho, Inc., 2151 N Blvd., MS-7111, P.O. Box 1625, Idaho Falls, ID 83415
111. R. Geimer, SAIC, 545 Shoup Ave., P.O. Box 50697, Idaho Falls, ID 83405-0697
112. J. Gill, James H. Gill & Associates, 12015 Manchester, St. Louis, MO 63131
113. R. Gillins, SAIC, 545 Shoup Ave., P.O. Box 50697, Idaho Falls, ID 83405-0697
114. K. Hain, EM-55, U.S. Department of Energy, 1000 Independence Ave., SW, Washington, DC 20585
115. P. Hart, U.S. Department of Energy, EM-542, Trevion II, 19901 Germantown Rd., Germantown, MD 20874-0002
116. J. Helt, Argonne National Laboratory, 9700 S. Cass Avenue, Bldg. 205, Argonne, IL 60439
117. D. Helton, Westinghouse Savannah River Co., P.O. Box 616, Bldg. 773-41 A., Rm. 228, Aiken, SC 29802
118. C. Henke, Focus Environmental, 9050 Executive Park Drive, Suite A-202, Knoxville, TN 37923
119. J. Hillary, EG&G Idaho, Inc. P.O. Box 1625, Idaho Falls, ID 83415

120. G. Hinshaw, Midwest Research Institute, 425 Volker Blvd., Kansas City, MO 64110
121. D. Hjeresen, AET, MS-P641, Bikini Road, Los Alamos, NM 87545
122. J. Hnat, Vortec Corporation, 3770 Ridge Pike, Collegeville, PA 19426
123. T. Ho, Lamar University, P.O. Box 10053, Beaumont, TX 77710
124. J. Hunter, Westinghouse Hanford Co., P.O. Box 1970, MS L531, Bldg. 3766, Rm. 14, Richland, WA 99352
125. J. Jacquin, SAIC, 555 Quince Orchard Road, Suite 500, Gaithersburg, MD 20878
126. P. Jones, BDM Federal, 555 Quince Orchard Road, Suite 400, Gaithersburg, MD 20878-1437
127. P. Kalb, Brookhaven National Lab, Environmental & Waste Technology Center, North Railroad Street, Bldg. 830, Upton, NY 11973
128. T. Kan, LLNL, MS-1467, P. O. Box 808, Livermore, CA 94550
129. R. Koenig, Merlin Co./Boulder, Inc., 395 Ridgeview Lane, Boulder CO 80302
130. K. Kostelnik, EG&G Idaho, Inc., P.O. Box 1625, MS-3930, Idaho Falls, ID 83415-3930
131. D. Kried, Battelle Pacific NW Lab, Battelle Blvd., Richland, WA 99352
132-134. O. Krikorian, L-369, LLNL, P.O. Box 808, Livermore, CA 94550
135. O. Kruger, Westinghouse Hanford Company, 2355 Stevens Dr., Richland, WA 99352
136. D. Kuchynka, U.S. Department of Energy,
137. M. Lankford, EM-552, U.S. Department of Energy, 12800 Middlebrook Road, Trevion II, Germantown, MD 20874
138. C. Lee, EPA Risk Reduction Engineering Laboratory, Cincinnati, OH 45268
139. S. Lein, EM-54, U.S. Department of Energy, 12800 Middlebrook Road, Trevion II, Germantown, MD 20874-1290
140. J. Lightly, University of Utah, Salt Lake City, UT 84112
141. J. Lippold, BDM Federal, 20251 Century Blvd., 4th Floor, Germantown, MD 20874
142. J. Mayberry, SAIC, P.O. Box 50697, Idaho Falls, ID 83405-0697
143. J. McCray, WINCO, P.O. Box 4000, MS-5218, Idaho Falls, ID 83415-4000
144. W. McCulla, Los Alamos National Laboratory, SM 30 Warehouse, Bikini Road, S J-563, Los Alamos, NM 87545
145. J. McFee, IT Corporation, 5301 Central Ave., NE, Albuquerque, NM 87108
146. X. Meng, Center for Environmental Engineering, Stevens Institute of Technology, Hoboken, NJ 07030
147. T. Miller, University of Tennessee, College of Engineering, Knoxville, TN 37996-2010
148. T. Moberg, WHC, P.O. Box 1970, MS-425, Richland, WA 99352-1970
149. J. O. Moore, U.S. Department of Energy, P.O. Box 2001, Oak Ridge, TN 37830-8620
150. C. Nagel, Molten Metal Technology, 25 First St., Cambridge, MH 02141
151. R. Nakaoka, Los Alamos National Laboratory, P.O. Box 1663, MS-6517, Los Alamos, NM 87545
152. M. Nawar, Office Of Radiation Programs, 401 N. Street, S.W. (ANR-461) Washington, DC 20460
153. J. Newburn, Thermatrix Inc., 3590 N. First Street, Suite 310, San Jose, CA 95134
154. G. Ordaz, EM-541, U.S. Department of Energy, 12800 Middlebrook Road, Trevion II, Germantown, MD 20874
155. T. Overcamp, Clemson Universtiy, 342 Computer Ct., Anderson, SC 29625

156. C. Owens, EG&G Idaho, P.O. Box 1625, Idaho Falls, ID 83415-3960
157. R. Peters, Battelle-Pacific Northwest Lab, P.O. Box 999, MS P7-41, Richland, WA 99352
158. H. Pham, Air Products and Chemicals, Inc., 7201 Hamilton Boulevard, Allentown, PA 18195-1501
159. B. Place, Westinghouse Hanford Co., P.O. Box 1970, MS-H5-33, Richland, WA 99352
160. R. Price, Duratek, 8955 Guilford Rd., Suite 200, Columbia, MD 21046
161. G. Reed, University of Tennessee, College of Engineering, Knoxville, TN 37996-2010
162. W. Ross, Battelle-Pacific Northwest Lab, P.O. Box 999, MS P7-41, Richland, WA 99352
163. A. F. Sarofim, Department of Chemical Engineering, 66-153, MIT Cambridge, MS 02139
164. R. Schumacker, Westinghouse Savannah River Co., SRTC, P.O. Box 616, Bldg. 773-42A, Aiken, SC 29808
165. B. Schutte, EM-54, U.S. Department of Energy, 12800 Middlebrook Road, Trevion II, Germantown, MD 20874-1290
166. B. Schwinkendorf, BDM Federal, 1801 Randolph Rd., SE, Albuquerque, NM 87106
167. W. Searles, Associated Technical Consultants, 2375 Dorr St., Suite I, Toledo, OH 43607-3406
168. R. Seeker, EER Corp., 18 Mason, Irvine, CA 92718
169. G. Sevigny, Battelle-Pacific Northwest Lab, P.O. Box 999, MSIN P7-42A, Aiken, SC 29808
170. M. Shupe, EM-541, U.S. Department of Energy, Trevion II, Room 440, 19901 Germantown Road, Germantown, MD 20874-1290
171. D. Singh, Argonne National Lab, 9700 South Cass Ave., Bldg. 212, Rm. G-233, Argonne, IL 60439
172. S. Slate, Battelle Pacific Northwest Laboratory, 902 Battelle Blvd., P.O. Box 999, KI-25, Richland, WA 99352
173. E. F. Snow, Plasma Energy Applied Technology, Inc., 4914 Moores Mill Road, Chase Industrial Park, Huntsville, AL 35811
174. G. Sprenger, Waste Project, EG&G-Rocky Flats Plant, P.O. Box 464, Bldg. 750, Golden, CO 80402-0464
175. M. Springer, Plasma Energy Applied Technology Inc., 4914 Moores Mill Road, Chase Industrial Park, Huntsville, Al 35811
176. S. Stein, Battelle, Seattle Research Center, 4000 NE 41st, Seattle, WA 98105-5428
177. M. Stevenson, SAIC, 545 Shoup Ave., Idaho Falls, ID 83402-3575
178. P. Sydenticker, BDM Federal, 20251 Century Blvd., 4th Floor, Germantown, MD 20874
179. T. Timmerman, Mason & Hanger, Bldg. 11-2, P.O. Box 50697, Idaho Falls, ID 83405-0697
180. T. Uhlmeyer, MD-Ferguson Co., 7295 Highway 94 South, St Charles, MO 63304
181. R. VanKonynenburg, Lawrence Livermore National Laboratory, P.O. Box 808 L352, Livermore, CA 94550
182. J. Vavruska, Equinox, Ltd., 872 Don Cubero Ave., Santa Fe, NM 87501
183. C. Ward, Westinghouse Savannah River, Building 773-A, D-1134, Aiken, SC 29808
184. S. Warren, EM-442, U.S. Department of Energy, 12800 Middlebrook Road, Trevion II, Germantown, MD 20874-1290

185. L. Waterland, Accurex Environmental Corp., 555 Clyde Ave., P.O. Box 7044, Mountain View, CA 94039
186. K. Whittle, Electropyrolysis, Inc., 996 Old Eagel School Road, Wayne, PA 19087
187. J. Witzeman, P.O. Box 398704, 7400 Willley Road, Fernald, OH 45030
188. S. Wolf, U.S. Department of Energy, Trevion II, 19901 Germantown Road, Germantown, MD 20874
189. W. Wolfe, SAIC, 545 Shoup Ave., P.O. Box 50697, Idaho Falls, ID 83405-0697
190. R. Womack, Retech, Inc., P.O. Box 997, 100 Henry Station Road, Ukiah, CA 95482-0997
191. M. Zenkowich, EM-323, U.S. Department of Energy, 12800 Middlebrook Road, Germantown, MD 20874
192. Office of Assistant Manager, Energy Research and Development, DOE-OR, P.O. Box 2001, Oak Ridge, TN, 37831
193-194. Office of Scientific and Technical Information, P.O. Box 62, Oak Ridge, TN 37831

DATE
FILMED
6/30/94
END